SEMI-ANALYTICAL COMPLEX VARIABLE BASED STOCHASTIC FINITE ELEMENT METHOD

by

WEIYA JIN

Presented to the Faculty of the Graduate School of

The University of Texas at Arlington in Partial Fulfillment

of the Requirements

for the Degree of

DOCTOR OF PHILOSOPHY

THE UNIVERSITY OF TEXAS AT ARLINGTON

December 2008

ACKNOWLEDGEMENTS

I cannot fully express my gratitude to my advisor, Dr. Brian H. Dennis, for his constant support throughout my graduate studies at the University of Texas at Arlington. His expert advice as a teacher and researcher, guidance and assistance as a friend, and his example of patience, generosity and selfless concern for his students will always be a source of inspiration in my personal and professional life. I am so fortunate to be counted as one of his students. Thank you Dr. Dennis.

I would like to acknowledge Professor Bo ping Wang, Professor Wen Chan, Professor Kent Lawrence and Professor Seiichi Nomura for serving on my PhD committee. Their advice and assistance is greatly appreciated.

It is also a pleasure to acknowledge the support of the many wonderful friends who cheered me up during difficult times: Rajeev Kumar, Takahiro Sonoda, Wei Han, Chinmay Adhvaryu, Ai Ueno, Tao heng Pan and Xiaohong Fan.

Deepest appreciation to my parents and my brothers for their love, support and encouragement throughout my graduate study.

Many thanks to my dearest son, Juntao Xu, for always filling my life with so much happiness. You are my treasure and my fountain of joy!

Special thanks to the most wonderful and understanding person in my life, my lovely husband, Diping Xu, for persistent support, patience and love that enabled me to walk this journey.

November 20, 2008

ABSTRACT

SEMI-ANALYTICAL COMPLEX VARIABLE BASED STOCHASTIC FINITE ELEMENT METHOD

Weiya Jin, PhD.

The University of Texas at Arlington, 2008

Supervising Professor: Brian H. Dennis

The stochastic finite element method (SFEM) is an approach that allows an analyst to define material, load, and geometry parameters as random variables to represent uncertainty in an engineering problem. The method is then used to estimate the probability of exceeding specified performance thresholds. A necessary ingredient for this analysis is consistent, accurate and efficient algorithms for computing finite element response sensitivities.

In this work, the semi-analytical complex variable method (SACVM) is introduced as a method for computing accurate response sensitivities of stochastic models. The SACVM incorporates the complex variable method (CVM) with the semi-analytical method (SAM). It takes advantage of the CVM and the SAM to compute response sensitivities consistently, accurately and efficiently. To date, this approach has not been reported or published in the context of the stochastic finite element method.

The SACVM combined with the first-order reliability method (FORM) algorithm becomes the semi-analytical complex variable based stochastic finite element method (SACV-SFEM) and is then applied to various benchmark problems. Specifically, the method is used to evaluate the reliability index of the beam and plate bending problems, steady-state heat conduction problems, linear elastic fracture mechanics problems, material and geometric nonlinear problems. The accuracy and efficiency achieved by the SACV-SFEM approach are compared with the semi-

analytical finite difference based stochastic finite element method (SAFD-SFEM), the finite difference based stochastic finite element method (FD-SFEM) and the complex variable based stochastic finite element method (CV-SFEM).

The results show that the SACV-SEFM obtains the reliability index in a consistent, accurate, and efficient manner for all the benchmark problems. In the application of heat conduction in electronic packaging problems, the SACV-SFEM can always use one perturbation size to obtain accurate reliability index for all the thermal conductivities whose values may have a large difference. The SAFD-SFEM produces inaccurate shape sensitivities in linear beam and thin plate bending problems, whereas the SACV-SFEM produces accurate shape sensitivities. The FD-SFEM produces inaccurate sensitivities in linear fracture mechanics problems due to the ill-conditioned global stiffness matrix that is used twice in the algorithm. However, the SAFD-SFEM achieves higher accuracy by using the global stiffness matrix only once. In the material and geometrically nonlinear problems, the SACV-SFEM shows higher efficiency than the FD-SFEM and the CV-SFEM, and is more consistent and accurate than the FD-SEFM and the SAFD-SFEM.

TABLE OF CONTENTS

LIST OF ILLUSTRATIONS

LIST OF TABLES

CHAPTER 1

INTRODUCTION

The finite element method (FEM) is nowadays the most advanced and powerful approach for the analysis of complex structures. With the rapid increase in computational power, FEM has found applications in many different fields. However, many of those applications are deterministic, that is, they do not incorporate the uncertainties that exist in the models of real world problems. These uncertainties are usually intrinsic to the parameters of the model which, due to our lack of knowledge, are not known exactly. The traditional finite element method is deterministic; it only can deal with the uncertainties as average characteristics at best, and will lead to rough representations of the reality. The ability to incorporate uncertainty into the analysis is critical for the design of reliable and robust engineering systems. Thus, research involving the extension of the finite element method for analysis under uncertainty is expected to grow in the coming years. Much of that work will focus on improving the accuracy and efficiency of non-deterministic finite element methods.

The stochastic finite element method (SFEM) combines uncertainty in input variables and the finite element method into a tool for reliability assessment of structures. The first order reliability method (FORM) and the Second order reliability method (SORM) provide the basis for analyzing uncertainties and computing probabilities, while the finite element method provides the spatial discretization for analyzing complicated structures.

Structural performance criteria are specified in terms of limit state functions, and failure probabilities are obtained as complementary probabilities of achieving the predefined limit state. The algorithms of SFEM need to determine the design point on the limit state surface that separates the safe domain from the failure domain. A necessary requirement for finding the

design point is the availability of the gradient vector of the performance function taken with respect to the random variables. In the context of SFEM, this implies the need for computing finite element response sensitivity with respect to the random variables.

The consistency, accuracy and efficiency of the reliability index obtained from SFEM significantly depend directly on the consistency, accuracy and efficiency of the method used to calculate the sensitivities.

1.1 Methods for Computing Sensitivity

There are several methods to compute response sensitivities with respect to random variables, including the finite difference method (FDM), the analytical method (AM), the semi-analytical method (SAM) and the complex variable method (CVM).

The FDM is the most common and simple method and is independent of the type of finite elements used. But it is computationally expensive as a full deterministic analysis is required for each random variable in the problem. Furthermore, FDM faces the dilemma of choosing the appropriate step size. The small finite difference perturbation should be chosen to minimize the truncation error while avoiding the subtractive cancellation error that occurs when the step size becomes to small. Therefore, there is an optimal step size that will minimize the total error. The step size will vary from one parameter to the next and is rarely known a priori. For highly non-linear responses, the error resulting from a poor choice of step size can be significant.

The AM is efficient and reliable. However, its formulation and implementation are more difficult and depend on the particular problem and finite element type. Its application to complicated problems can be very cumbersome.

The SAM shows the efficiency of the analytical method with the simplicity of the global finite difference method. Compared to the FD method, it is slightly more complicated to program, but far easier and more general than AM. However, a number of papers have been

reported that the SAM exhibits serious shape sensitivity inaccuracies in structures modeled by beam, frame, plate, and shell elements.

To date, the CVM has not been widely exploited in finite element analysis. Some researchers employ CVM in the computational fluid dynamics as a way to calculate sensitivities for design optimization. In structural analysis field, very few people use it. The CVM is attractive because it does not involve a subtraction operation and is applicable to any simulation code using real-valued variables. It can provide the same accuracy as automatic differentiation (AD), but is far less intrusive on the source code. A step size can be chose as small as possible with no loss of accuracy due to subtractive cancellation. On the other hand, the sensitivity computation using complex variable does come at a price, namely more computation time and memory.

After considering the advantages and disadvantages of the four sensitivity methods, the semi-analytical complex variable method (SACVM) is proposed. First, it is noted that the SACVM is a novel approach that does not appear in the open literature. The SACVM avoids the inaccuracies that plague the SAM, which stem from the inaccuracies of the FDM, and eliminates the computational cost of CVM. The CVSAM can always calculate accurate response sensitivity without increasing computer time and memory requirements.

The semi-analytical complex variable stochastic finite element method (SACV-SFEM) incorporates SAM, CVM into FORM based SFEM. The SACV-SFEM can readily compute the reliability of the system whether the limit state function is explicit or implicit. It computes first-order derivative of the limit state function with respect to the input random variables accurately without any subtractive cancellation errors that occur with the finite difference method. The algorithm of SACV-SFEM comes from the SAM which makes the whole analysis more efficient. The requirement in SACV-SFEM for combining the SACVM with an existing FEM code is simple and easy for programming.

1.2 Present Work

The proposed research involves the application of the proposed SACVM to stochastic finite element analysis, thus creating the SACV-SFEM. Compared to other methods, the SACV-SFEM is more attractive because it can acquire the reliability index of the structure very accurately without any subtraction error or extra computational cost, and it can be applied to any finite element code with a few modifications. Other methods might fail to get the correct result (SA), need numerous computer resources (FD), or require substantial source code modifications (SA, AD).

The consistency, accuracy, efficiency, and versatility of the SACV-SFEM are demonstrated with results for several benchmark problems. So far, the proposed approach has not been reported in the open literature.

Chapter 2 contains theory and literature review of stochastic finite element method. It introduces the limit state function, algorithm of first order reliability method (FORM), computing response sensitivity by different methods, as well as the corresponding research work done by others. The concept of the SACV-SFEM is introduced.

Chapter 3 Applies the SACV-SFEM to beam and thin plate structures,. The response sensitivity and reliability index obtained from the SACV-SFEM are compared with the finite difference based stochastic finite element method (FD-SFEM), the semi-analytical finite difference based stochastic finite element method (SAFD-SFEM) and the complex variable based stochastic finite element method (CV-SFEM). The failure probabilities obtained from the SACV-SFEM are compared with the traditional Monte Carlo method.

Chapter 4 contains the verification and application of the SACV-SFEM to benchmark problems and electronic packaging problems in steady-state heat conduction. The results obtained from the SACV-SFEM are compared with the FD-SFEM, the SAFD-SFEM and the CV-SFEM.

Chapter 5 employs the SACV-SFEM to linear elastic fracture mechanics problems. Three geometries are considered: a center cracked tension (CCT) specimen, a single edge notched tension (SENT) specimen and double edge notched tension (DENT) specimen. The results obtained from the SACV-SFEM are compared with the FD-SFEM, the SAFD-SFEM and the CV-SFEM.

Chapter 6 contains the application of SACV-SFEM to material and geometric nonlinear problems. The benchmark heat conduction problem with temperature dependent thermal conductivity is considered as a nonlinear material example. The classic nonlinear Euler-Bernoulli beam is considered as a geometric nonlinear example. The results obtained from the SACV-SFEM are compared with the FD-SFEM, the SAFD-SFEM and the CV-SFEM.

Chapter 7 presents the conclusions of the dissertation.

CHAPTER 2

THEORY AND LITERATURE REVIEW

2.1 Stochastic Finite Element Method

The traditional finite element method (FEM) ignores the uncertainty of the input parameters, and gives the realistic response which are implicit functions of the input variables. The stochastic finite element method (SFFM), which combines the desired features of FEM with randomness and spatial variability of the system, has developed quickly in last twenty years. The existing theories for the SFEM approaches can be classified into three branches.

2.1.1 Perturbation method

The perturbation method (Handa [1], Hisada [2, 3], Baecher [4] and Phoon [5]) focuses on computing the first two statistical moments of the response quantities. It supposes each random input variable be the sum of its mean value and a zero-mean random variable α_i. In finite element analysis, it aims to evaluate the statistics of the nodal displacements, strains, and stresses from the mean values of the input variables and the covariance of matrix α. Since it is based on Taylor series expansion, results obtained from perturbation method are expected to be accurate only in case of small variability of the parameters.

2.1.2 Spectral approach

The spectral approach (Ghanem [6, 7, 8, 9]) focuses on computing the global probabilistic structure of the response quantities considered as random processes. It represents the mechanical response of a system through its coefficients over a basis of the space of random variables. For example a nodal displacement, if it is considered a random variable, can be expressed as

$$\boldsymbol{u}(\theta) = \sum_{\boldsymbol{j}=0}^{\boldsymbol{P}-1} \boldsymbol{u_j} \Psi_{\boldsymbol{j}}\left(\{\zeta_{\boldsymbol{k}}(\theta)\}_{\boldsymbol{k}=1}^{\boldsymbol{M}}\right) \tag{2-1}$$

where $\Psi_{\boldsymbol{j}}\left(\{\zeta_{\boldsymbol{k}}(\theta)\}_{\boldsymbol{k}=1}^{\boldsymbol{M}}\right)$ is the polynomial chaos basis defined by means of $\boldsymbol{M}$ standard normal variables $\{\zeta_{\boldsymbol{k}}(\theta)\}_{\boldsymbol{k}=1}^{\boldsymbol{M}}$.

Due to its complexity, the spectral approach is only practical for linear problems. The current implementation is limited to linear elastic 2-D mechanical problems, and 1-D dynamic problems.

2.1.3 Probabilistic finite element method

The probabilistic finite element method focuses on computing the probability of failure of the system, which is based on the definition of a limit state function. The classical reliability analysis applied in the probabilistic finite element method is first order reliability method (FORM) and second order reliability method (SORM). And FORM has been employed widely because of its efficiency and simplicity.

This proposal focuses on the third branch, the probabilistic finite element method, and aims at improving its accuracy and efficiency. In the following context, without any special declaration, we refer to the probabilistic finite element method as stochastic finite element method (SFEM).

2.2 Probabilistic Finite Element Method (SFEM)

The stochastic finite element method combines a traditional reliability method and the deterministic analysis to capture the desirable features of both. It represents the structure as realistically as possible while considering the uncertainties in the input variables. It can be used for both explicit and implicit limit state functions and can estimate risk associated with any structure that can be represented with a finite element model.

2.2.1 Limit state function

The limit state function decides the limit state criteria related with two vectors, the load $\boldsymbol{S}$ and resistance $\boldsymbol{R}$. The vectors $\boldsymbol{S}$ and $\boldsymbol{R}$ are associated with random input variables $\boldsymbol{X} = (\mathrm{X}_1, \mathrm{X}_2, \Lambda\ , \mathrm{X}_{\boldsymbol{n}})$ by a transformation. Mathematically, limit state function can be described as $\mathrm{g}(\boldsymbol{R}, \boldsymbol{S})$. The expression $\mathrm{g}(\boldsymbol{R}, \boldsymbol{S}) > 0$ defines the safe state of the structure, and the expression $\mathrm{g}(\boldsymbol{R}, \boldsymbol{S}) \leq 0$ defines the failure state of the structure. It represents the limit state criteria has been reached or exceeded, as shown in Figure 2.1.

A limit state can be an explicit or implicit function of the basic random variables and it can be in a simple or complicated form.

The probability of failure is then given by:

$$\mathrm{P_f} = \int_{\boldsymbol{g}(\boldsymbol{R},\boldsymbol{S})<0} \boldsymbol{f}(\boldsymbol{R}, \boldsymbol{S})\mathrm{dRdS} \qquad (2\text{-}2)$$

where $\boldsymbol{f}(\boldsymbol{R},\boldsymbol{S})$ is the joint probability density function for $\boldsymbol{R}$ and $\boldsymbol{S}$, which are related to basic random variables $\boldsymbol{X}$.

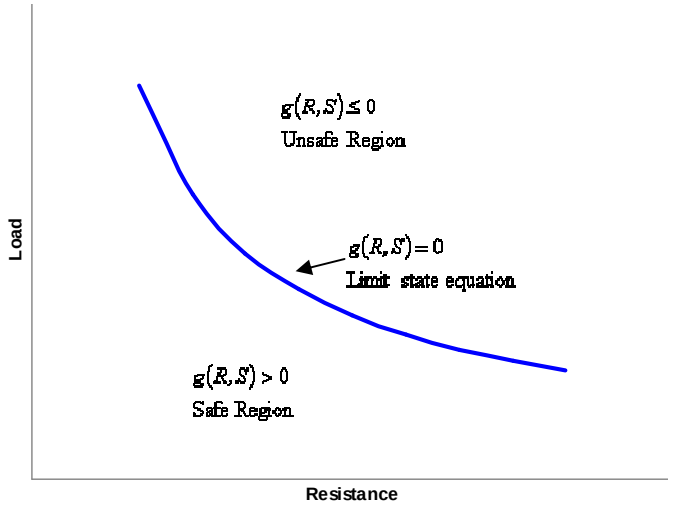

Figure 2.1 Limit state criteria

Equation (2-2) exhibits two difficulties. First, the joint probability density function is usually unknown in general. Second, even if the joint probability density function is known,

evaluating the integral over the failure domain is extremely complicated. Therefore, some approximate methods have been developed to make this integral easier to compute. These methods can be divided into two groups: first order reliability methods (FORM) and second order reliability methods (SORM).

2.2.2 First Order Reliability Method (FORM)

FORM is developed from second moment method, which uses the information on first and second moments of the random variables. Second moment methods include first order second moment method (FOSM) and advanced first order second moment method (AFOSM).

2.2.2.1 First Order Second Moment Method (FOSM)

In 1969, Cornell [10] developed FOSM by using the simple two-variable approach to get the reliability index β and then calculated the failure probability according to β.

The limit state function is defined as

$$\boldsymbol{Z} = \boldsymbol{R} - \boldsymbol{S} \tag{2-3}$$

Where $\boldsymbol{R}$ and $\boldsymbol{S}$ are statistically independent normally distributed random variables, $N(\mu_{\boldsymbol{R}}, \sigma_{\boldsymbol{R}})$ and $N(\mu_{\boldsymbol{S}}, \sigma_{\boldsymbol{S}})$. Then the variable $\boldsymbol{Z}$ is also a normal random variable, $\boldsymbol{N}\left(\mu_{\boldsymbol{R}} - \mu_{\boldsymbol{S}}, \sqrt{\sigma_{\boldsymbol{R}}^2 + \sigma_{\boldsymbol{S}}^2}\right)$. The failure surface is then defined as $\boldsymbol{Z} = \boldsymbol{R} - \boldsymbol{S} < 0$.

The probability of failure can be evaluated as

$$\boldsymbol{p_f} = \boldsymbol{p}(\boldsymbol{Z} < 0) = \Phi\left(\frac{0 - (\mu_{\boldsymbol{R}} - \mu_{\boldsymbol{S}})}{\sqrt{\sigma_{\boldsymbol{R}}^2 + \sigma_{\boldsymbol{S}}^2}}\right) = 1 - \Phi\left(\frac{\mu_{\boldsymbol{R}} - \mu_{\boldsymbol{S}}}{\sqrt{\sigma_{\boldsymbol{R}}^2 + \sigma_{\boldsymbol{S}}^2}}\right) \tag{2-4}$$

where $\Phi(\ )$ is the cumulative density function of the standard normal variable.

The reliability index is denoted as

$$\beta = \frac{\mu_{\boldsymbol{Z}}}{\sigma_{\boldsymbol{Z}}} = \frac{\mu_{\boldsymbol{R}} - \mu_{\boldsymbol{S}}}{\sqrt{\sigma_{\boldsymbol{R}}^2 + \sigma_{\boldsymbol{S}}^2}} \tag{2-5}$$

The main problem with FOSM is the obtained reliability index is not invariant with respect to changes in the limit state function form. Also, FOSM considers only the mean values of the random variables and not their distribution.

2.2.2.2 First Order Reliability Method (FORM)

On the basis of FOSM, Hasofer et al. [11] developed the advanced first order second moment method (AFOSM) to solve the invariant problem in FOSM. A linear transformation is introduced to recast the variables in standard normal distribution space. However, it is only applicable for normal random variables. Rackwitz et al. [12] and Chen et al. [13] developed the equivalent normalization for the non-normal distributions of random variables in the AFOSM algorithm. After combining the work of various other researchers, the AFOSM evolved into the method now known as First Order Reliability Method (FORM). FORM can calculate the safety index of the limit state function with random variables with any kind of density distributions, including correlated or uncorrelated non-normal distributions. Before searching the design points, probabilistic transformations (Der Kiureghian et al. [14, 15], Ditlevsen et al. [16]) are applied for those variables do not have normal distributions.

After all random variables are transformed into normal distributed random variables, these variables can be linear transformed to standard normal space by [17]

$$\boldsymbol{Y} = \frac{\boldsymbol{X} - \mu_{\boldsymbol{X}}}{\sigma_{\boldsymbol{X}}} \quad \left(\boldsymbol{i} = 1,2,\Lambda\ ,\boldsymbol{n}\right) \tag{2-6}$$

and the probability of failure can be written as

$$\boldsymbol{p}_{\boldsymbol{f}} = \int_{\boldsymbol{g}(\boldsymbol{Y})<0} \phi(\boldsymbol{Y})\,\boldsymbol{dY} \tag{2-7}$$

where $\phi(\boldsymbol{Y})$ is the standard normal probability density function of $\boldsymbol{Y}$.

$$\phi(\boldsymbol{Y}) = \left(\frac{1}{\sqrt{2\pi}}\right)^{\boldsymbol{n}} \exp\left[-\frac{1}{2}\|\boldsymbol{Y}\|^2\right] \tag{2-8}$$

Here $\boldsymbol{n}$ is the number of standard normal variables.

Since equation (2-8) is rotationally symmetric and decays exponentially with the square of the norm $\|\boldsymbol{Y}\|$, the significant contributions to the Equation (2-7) are those points that are nearest to the origin of the standard normal space. This leads to the following constrained optimization problem

$$Y^* = \min\left\{ \|Y\| \;\middle|\; \mathrm{g}(Y) = 0 \right\} \tag{2-9}$$

Where $\boldsymbol{Y}^*$ is called the design point. To find $\boldsymbol{Y}^*$ subject to the constraints, the Lagrange multiplier λ is introduced,

$$\boldsymbol{L}(\boldsymbol{Y}, \lambda) = \|\boldsymbol{Y}\|^2 + \lambda \boldsymbol{g}(\boldsymbol{Y}) \tag{2-10}$$

Consequently, we have

$$\boldsymbol{Y}^* + \lambda^* \nabla \mathrm{g}\left(\boldsymbol{Y}^*\right) = 0 \tag{2-11}$$

$$\mathrm{g}\left(\boldsymbol{Y}^*\right) = 0 \tag{2-12}$$

Solving Equation (2-11) and (2-12) yields

$$\lambda^* = \frac{\left\|\boldsymbol{Y}^*\right\|}{\left\|\nabla \mathrm{g}\left(\boldsymbol{Y}^*\right)\right\|} \tag{2-13}$$

and substituting Equation (2-13) into Equation (2-11) yields

$$\left\|\nabla \mathrm{g}\left(\boldsymbol{Y}^*\right)\right\| \cdot \boldsymbol{Y}^* + \left\|\boldsymbol{Y}^*\right\| \nabla \mathrm{g}\left(\boldsymbol{Y}^*\right) = 0 \tag{2-14}$$

This means the unit normal to the limit state surface at the design point should point toward the origin.

According to equation (2-14), an iterative algorithm is suggested to get design point $\boldsymbol{Y}^*$ as follows

$$\boldsymbol{Y}_{\boldsymbol{i}+1}^* = \frac{\nabla \mathrm{g}\left(\boldsymbol{Y}_{\boldsymbol{i}}^*\right)^{\boldsymbol{T}} \boldsymbol{Y}_{\boldsymbol{i}}^* - \mathrm{g}\left(\boldsymbol{Y}_{\boldsymbol{i}}^*\right)}{\left\|\nabla \mathrm{g}\left(\boldsymbol{Y}_{\boldsymbol{i}}^*\right)\right\|^2} \nabla \mathrm{g}\left(\boldsymbol{Y}_{\boldsymbol{i}}^*\right) \tag{2-15}$$

where $\nabla g\left(\boldsymbol{Y}_{\boldsymbol{i}}^{*}\right)$ is the partial derivative of limit state function with respect to standard normal vector $\boldsymbol{Y}$. It can be obtained from the partial derivative of limit state function with respect to normal vector $\boldsymbol{X}$ as follows,

$$\nabla g\left(\boldsymbol{Y}^{*}\right)=\frac{\partial \boldsymbol{g}(\ )}{\partial \boldsymbol{X}}\frac{\partial \boldsymbol{X}}{\partial \boldsymbol{Y}}=\frac{\partial \boldsymbol{g}(\ )}{\partial \boldsymbol{X}}\sigma_{\boldsymbol{X}} \tag{2-16}$$

Then, the reliability index β defines as the shortest distance from the origin point to the limit surface in the standard normal space. It is expressed as

$$\beta=\left\|\boldsymbol{Y}_{\boldsymbol{n}}^{*}\right\| \tag{2-17}$$

where $\boldsymbol{Y}_{\boldsymbol{n}}^{*}$ is the latest design point in the iteration which satisfies the convergent criteria as follows

$$g\left(\boldsymbol{Y}_{\boldsymbol{i}+1}^{*}\right)-g\left(\boldsymbol{Y}_{\boldsymbol{i}}^{*}\right)<\varepsilon \tag{2-18}$$

$$\beta_{\boldsymbol{i}+1}-\beta_{\boldsymbol{i}}<\varepsilon \tag{2-19}$$

where ε is the allowed tolerance between ith and (i+1)th iterations.

When the limit state function $g(\boldsymbol{Y})$ is linear, the failure probability is

$$\boldsymbol{p}_{\boldsymbol{f}}=\Phi(-\beta)=1-\Phi(\beta) \tag{2-20}$$

When the limit state function $g(\boldsymbol{Y})$ is non-linear, the failure probability is

$$\boldsymbol{p}_{\boldsymbol{f}}\approx\Phi(-\beta)=1-\Phi(\beta) \tag{2-21}$$

The approximation of probability of failure in Equation (2-21) is because FORM replaces the non-linear limit state surface by the hyperplane tangent to the limit state surface at the design point $\boldsymbol{Y}^{*}$.

The flowchart of FORM algorithm proposed by Rackwitz et al. [12] is shown in Figure 2.2.

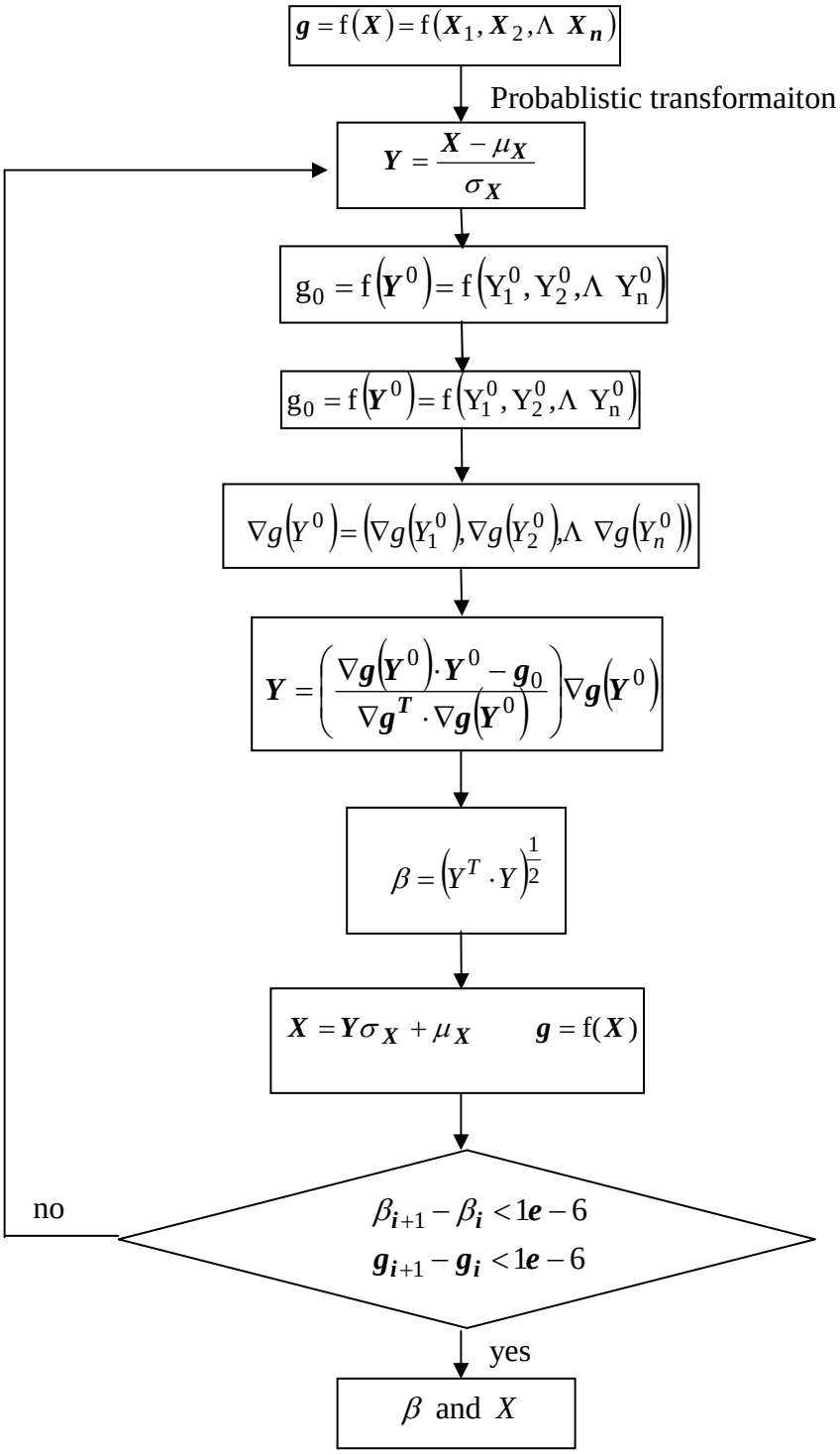

Figure 2.2 Flowchart of FORM algorithm

2.2.2.3 Higher Order Reliability Method

To improve the precision of failure probability when the limit state function is non-linear, Breitung [18] and Der Kiureghian et al. [19, 20] proposed the second order approximation method (SORM). SORM replaces the limit state surface with a quadratic surface whose probabilistic content is known analytically. SORM requires the second derivative of $g(\boldsymbol{Y})$ at design point and the semi-parabolic point fitting of the limit state surface at given points around the design point, and makes computation complicated.

Grandhi et al. [21] introduces higher order approximation method (HORM). HORM approximates the limit state surface by higher order polynomials. Although the accuracy is improved, the computational requirements are large.

2.2.3 Sensitivity of finite element response

When determining the design point, the sensitivities of the limit state function, which depend on the sensitivities of the finite element response through the chain rule of differentiation, enter the iterative convergent procedure. Consistency, efficiency and accuracy of the response sensitivities play an important role in the whole reliability analysis algorithm. When the limit state function is not explicit the exact response sensitivities are not available.

There are several methods used to compute the response sensitivity.

2.2.3.1 Finite Difference Method (FDM)

The FDM is the most common method for computing the sensitivity. It can be used to determine sensitivities for both explicit and implicit limit state functions. It is based on a truncated Taylor series expansion and uses perturbations for each variable. However, the FDM faces the perturbation-size dilemma of choosing perturbation small enough to minimize the truncation error while large enough to avoid subtractive cancellation error [22]. Therefore, for each variable there is an optimal value of perturbation that will minimize the total error. This optimal value is not known a priori and must be guessed.

In the FORM algorithm, the accuracy of the computed response sensitivity by the FDM depends on the size of the finite perturbation of the each random variable and is difficult to fix in advance. Also, the FDM is computationally expensive, because a full deterministic FEM analysis must be done for each random variable.

2.2.3.2 Analytical Method (AM)

The AM is also called direct differentiation method. It derives the response sensitivity directly from the finite element formulation. Therefore, the analytical response sensitivity depends on the specific problem and type of finite element. Its application to complicated problems can be very cumbersome. So far, as well as elastic linear problem, Liu et al. [23] published sensitivity of the geometrically non-linear structures. Zhang et al. [24] introduced response sensitivity of dynamics of J2-elastoplastic structures. In addition, Zhang et al. [25] also obtained response sensitivity of plane stress elastoplastic damaged structures.

2.2.3.3 Semi-analytical Method (SAM)

The SAM combines the efficiency of the analytical method with the easy of use and general nature of the finite difference method. To distinguish with the SACVM, here we call the SAM the semi-analytical finite difference method (SAFDM).

From the finite element global equilibrium equation

$$\boldsymbol{K}\boldsymbol{u} = \boldsymbol{f} \tag{2-22}$$

where the stiffness matrix $\boldsymbol{K}$, displacement $\boldsymbol{u}$ and load vector $\boldsymbol{f}$ are functions of input random variables $\boldsymbol{X} = \left(\mathrm{X}_1, \mathrm{X}_2, \Lambda\ \mathrm{X}_{\boldsymbol{n}}\right)$. Then the derivative of displacement with respect to random variables $\boldsymbol{X}$ can be written as

$$\frac{\partial u}{\partial X} \approx \frac{\Delta u}{\Delta X} = K^{-1}\frac{\Delta f}{\Delta X} - K^{-1}\frac{\Delta K}{\Delta X}u \tag{2-23}$$

In Equation (2-23), the same mean value stiffness matrix $\boldsymbol{K}$ is used for computing displacement $\boldsymbol{u}$ and displacement sensitivity with respect to all the random variables $\partial \boldsymbol{u} / \partial \boldsymbol{X}$.

Furthermore, $\boldsymbol{K}^{-1}$, which is most time consuming part in the computation, only be needed to be calculated once according to Equation (2-22), then can be substituted into Equation (2-23) directly. This makes SAM programming convenient and the efficient. However, since $\partial \boldsymbol{K} / \partial \boldsymbol{X}$ and $\partial \boldsymbol{f} / \partial \boldsymbol{X}$ are still required to compute by FDM, SAM doesn't avoid the drawback of FDM, that is, being sensitive to the choice of step size.

A number of papers (Barthelemy et al. [26], Olhoff et al. [27]) have been reported that the SAFDM exhibits serious inaccuracies in certain cases, particularly in structures modeled by beam, frame, plate or shell elements. Olhoff et al. [27] introduced correction factors to eliminate the error. Cheng et al. [28] employed second order information as a remedy. Cheng et al. [29] used rigid body displacement to correct the error. Mlejned [30] employed the natural FEM approach that yields a nondefective incremental stiffness to correct the error. Oral [31] employed Neumann series to correct the error. Parente [32] used equilibrium relations to improve the sensitivity accuracy for non-linear structures.

2.2.3.4 Complex Variable Method (CVM)

The CVM for sensitivity calculations was first introduced by Lyness et al. [33] and Lyness [34], who use the CVM to obtain the derivatives of complicated functions. Squire et al. [35] employed the CVM to determine the derivatives of real functions. In the aerospace field, Martins et al. [36] used the CVM in three-dimensional aero-structural solver to obtain sensitivities for multidisciplinary design optimization. Martins et al. [37] applied the CVM to find the sensitivities in a two-dimensional computational fluid dynamics program. Anderson et al. [38] used the CVM to determine sensitivity derivatives for turbulent flows. Rodriguez [39] used complex variable method to obtain gradients for the optimizer when this non-liner optimizer is coupled with a Navier-Stokes Equation flow solver to design the inlets of the aircraft. In the structural analysis field, Wang et al. [40] first presented the application of complex variable method for eigenvalue and eigenvector sensitivity analysis. To date, the CVM has not been widely exploited structural nor thermal finite element analysis.

The CVM is based on a Taylor series expansion, taking a complex perturbation in the imaginary dimension.

$$f(x+ih) = f(x) + ihf'(x) - \frac{h^2 f''(x)}{2!} - \frac{ih^3 f'''(x)}{3!} + \Lambda \tag{2-24}$$

Rearranging the terms of equation (2-24) to group the real and imaginary parts, the first order derivatives can be obtained as

$$f'(x) = \frac{\mathrm{Im}[f(x+ih)]}{h} + O(h^2) \tag{2-25}$$

The first derivative obtained from Equation (2-25) doesn't involve any subtraction of two functions. Therefore, the CVM avoids the subtractive cancellation errors that plague the FDM. CVM can obtain accurate derivatives without need to adjust the step size. Therefore, the step size can be as small as possible with no loss of accuracy.

To incorporate the complex variable approach into an existing code, it only requires declaring float point variables as complex variables and adding a complex perturbation to the variable of interest. First-order derivatives of any explicit or implicit function with respect to any input parameter can be readily acquired by obtaining imaginary part of the function divided by the perturbation step size of the input parameter.

On the other hand, the CVM does have drawbacks. The more accurate first derivatives come at a price, namely more computation time and memory. As mentioned by Anderson et al. [38], the computer memory doubles over the original flow solver and the computer time increases by as much as a factor of three when using the CVM to determine the sensitivity derivatives for turbulent flow.

2.3 Semi-analytical Complex Variable Based Stochastic Finite Element Method (SACV-SFEM)

The previous sections have described the basic ideas behind the FORM method and as well as different approaches for calculating the required sensitivities. The FDM approach, typically used with FORM applications, can exhibit inaccuracies due to step size choice as well

as inefficiencies when large numbers of random variables are present. To address these shortcomings, this research aims to combine the positive aspects of the algorithm of SAFD, CVM, and FORM approaches into an accurate and efficient method for computing reliability.

2.3.1 Semi-analytical Complex Variable Method (SACVM)

The SACVM takes advantage of efficiency of SAM and accuracy of the CVM to get response sensitivity of a finite element response. Recall Equation (2-23) in different form,

$$K\frac{\Delta u}{\Delta X}=\frac{\Delta f}{\Delta X}-\frac{\Delta K}{\Delta X}u \tag{2-26}$$

where the inverse global stiffness matrix is computed from the deterministic finite element formulation where float point variables are declared as real variables. The vectors $\Delta f_e / \Delta X$ and $\Delta K_e / \Delta X$ will be readily computed by taking a complex perturbation in imaginary part of the element stiffness matrix and load vector where floating point variables are declared as complex variables. The right side of equation (2-26) will be computed at the element level, and then assembled as a global vector. The most time consuming portion of the computation involves obtaining the inverse global stiffness matrix. In this approach, it is computed only once and only uses real variables so time and memory requirements time or memory are similar to the traditional SAM but can achieve more accurate results. The SACVM is applicable to any structures including beam, frame, plate or shell elements, which has been reported exist serious inaccuracies with SAM. Furthermore, only minor changes are required to source codes. The modifications include adding a complex perturbation in the global stiffness matrix and load vector you have already obtained in deterministic finite element method.

To date, there is no paper in the open literature that can get more efficient and accurate response sensitivity by the SACVM. This proposal introduces this concept into sensitivity analysis, and further applies it into stochastic finite element method.

2.3.2 Semi-analytical Complex Variable based Stochastic Finite Element Method (SACV-SFEM)

As we know, the accuracy and efficiency of the reliability index significantly depends mostly on the consistency, accuracy and efficiency of the method used to find the response sensitivity with respect to each random variable. The proposed SACV-SFEM introduced here aim to achieve these characteristics through the use of the SACVM.

When we apply the FORM algorithm, the partial derivative of limit state function with respect to standard normal variables $\boldsymbol{Y}$ can be calculated as

$$\nabla \mathrm{g}\left(\boldsymbol{Y}_{\boldsymbol{i}}^{*}\right)=\frac{\partial \boldsymbol{g}(\ )}{\partial \boldsymbol{X}} \frac{\partial \boldsymbol{X}}{\partial \boldsymbol{Y}}=\frac{\partial \boldsymbol{g}(\ )}{\partial \boldsymbol{X}} \sigma_{\boldsymbol{X}} \tag{2-27}$$

where $\partial \boldsymbol{g}(\ ) / \partial \boldsymbol{X}$ is the partial derivative of limit state function with respect to input random variables $\boldsymbol{X}$. It will be computed by the SACVM to improve the FORM algorithm.

In each iteration in the design point search, the LU decomposition of global stiffness matrix is only computed once, and can be used for obtaining response sensitivity with respect to each input random variable. Therefore, the number of random variables has little affect on computational cost as their sensitivities are quickly computed once the factored matrix is known. Therefore, the SACV-SFEM exhibits higher computational efficiency than the finite difference based stochastic finite element method (FD-SFEM) and the complex variable based stochastic finite element method (CV-SFEM)

CHAPTER 3

APPLICATION OF THE SACV-SFEM TO BEAM AND PLATE ELEMENTS

3.1 Introduction

The accuracy problem of beam and plate elements for response sensitivity analysis using SAM has been reported in the literature. The source of error is the numerical differentiation of the stiffness matrix and the load vector. Many researchers (Olhoff et al. [27], Cheng et al. [28, 29], Mlejnek[30], Oral [31], and Parente [32]) developed different methods to improve the accuracy of the SAM.

The semi-analytical complex variable method (SACVM) is a new approach to finite element sensitivity analysis. It is employed for beam and plate structures to test the improvement of response sensitivity as well as computational efficiency with the FDM, the SAFDM and the CVM. The SACV-SFEM is used to evaluate the reliability of the limit state in beam and plate structures with input uncertainties. The reliability index obtained from the SACV-SFEM is compared with the SAFD-SFEM and traditional Monte-Carlo method (MC).

3.2 Application of the SACV-SFEM to Thin Plates

A simple square plate has width $\boldsymbol{a} = 1.0$ m, thickness $\boldsymbol{h} = 0.02$ m, elastic modulus $\boldsymbol{E} = 10920$ MPa, and Poisson's ratio $\nu = 0.3$, is shown in Figure 3.1. The whole plate is meshed by 64 four-node isoparametric elements of the shear deformable displacement formulation (Mindlin plate elements). The plate is simply supported along all edges and is subjected to a uniform pressure $\boldsymbol{p} = 1$MPa. Because of symmetry, only ¼ model is used for the computation.

The thin plate bending theory gives the analytical deflection as [33]

$$w(x,y)=\frac{16p}{\pi^6 D}\sum_{m=1,3,5,\Lambda}^{\infty}\sum_{n=1,3,5,\Lambda}^{\infty}\frac{\sin\left(\frac{m\pi x}{a}\right)\sin\left(\frac{m\pi y}{a}\right)}{mn\left[\left(\frac{m}{a}\right)^2+\left(\frac{n}{a}\right)^2\right]^2} \tag{3-1}$$

where $D=\frac{Et^3}{12(1-\nu^2)}$ is the flexural rigidity of the plate.

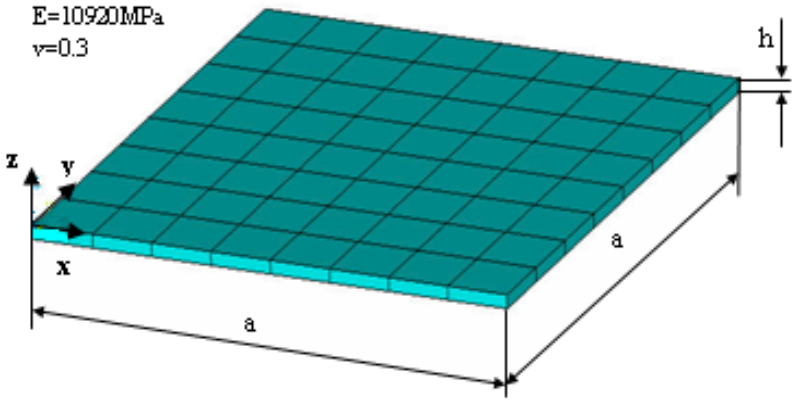

Figure 3.1 Simply supported ¼ square plate subjected uniform pressure

Three terms of Equation (1) gives the central deflection as

$$w_c=0.04436p\frac{a^4}{Eh^3} \tag{3-2}$$

The sensitivity of the central deflection with respect to width a is

$$\frac{\partial w_c}{\partial a}=\frac{4w_c}{a} \tag{3-3}$$

3.2.1 Computation of $\partial w_c/\partial a$ by the SACVM

Using the same perturbation of $\varepsilon=10^{-3}$ of the edge, the sensitivities of the deflection $\partial w_c/\partial a$ along the centerline $y/a=1/2$ obtained from SACVM comparing with the FDM, the CVM and the SAFDM are shown in Table 3.1.

Table 3.1 shows for the same perturbation size, the SAFD has inaccurate sensitivity, while the FDM, the CV and the SACVM obtain an accurate solution. The small error occurs for the FDM, the CVM and the SACVM might because the mesh is not fine enough and round-off errors.

Table 3.1 Sensitivity of central deflection with respect to width in thin plate

x/a		0.125	0.25	0.375	0.5
Analytical solution		0.8116	1.469	1.888	2.031
FDM	$\partial w_c / \partial a$	0.800921	1.457688	1.878644	2.022732
	error	-1.32%	-0.77%	-0.50%	-0.41%
CVM	$\partial w_c / \partial a$	0.8001	1.4562	1.8768	2.0207
	error	-1.41%	-0.87%	-0.59%	-0.51%
SAFDM	$\partial w_c / \partial a$	0.461588	0.832204	1.063348	1.141116
	error	-43.13%	-43.35%	-43.68%	-43.82%
SACVM	$\partial w_c / \partial a$	0.80012	1.456232	1.876767	2.020711
	error	-1.41%	-0.87%	-0.59%	-0.51%

3.2.2 Reliability analysis by the SACV-SFEM

Assume the width of the plate $\boldsymbol{a}$ is a normal distributed random variable $\boldsymbol{a} = \boldsymbol{N}(1.0, 0.2)$ m. The perturbation size used to obtain the response sensitivity is $\varepsilon = 10^{-3}$. The rest of the parameters are same with those in 3.2.1. From the deterministic finite element analysis, the maximum displacement at the center is $\boldsymbol{w_c} = 0.5063\boldsymbol{m}$. The limit state function is specified as $\boldsymbol{g} = \boldsymbol{w_c} - 0.5$ to see the failure probability of that the maximum central displacement is less than 0.5m, $\boldsymbol{g} = \boldsymbol{w_c} - 0.5 < 0$.

The reliability index, failure probability and corresponding computational information obtained from the SACV-SFEM and the SAFD-SFEM are shown in Table 3.2. The failure probability and corresponding computational information obtained from traditional MC is also shown in Table 3.2, too.

Table 3.2 Results obtained from SACV-SFEM in thin plate bending

	SACV-SFEM	SAFD-SFEM	MC method		
Iterations needed	13	6	100	1000	10000
Reliability Index	0.031063	0.031067	-	-	-
Failure Probability	48.76%	48.76%	43%	49.9%	48.59%
Compu. Time (s)	1.031	0.469	2.86	33.469	319.873

The results show the SAFD-SFEM and the SACV-SFEM both can converge to correct reliability index. The SACV-SFEM requires 13 iterations, 1.031 seconds to acquire the result. The SAFD-SFEM requires 6 iterations, 0.469 seconds to get same result. However, MC method has to compute 10000 iterations, and spends 319.873 seconds to obtain comparable accuracy.

If we only saw the solution of failure probability and hadn't check response sensitivity, we would think that there is no trouble to use the SAFD to obtain reliability index. Or we would think we can obtain accurate reliability index even if the response sensitivity is not accurate. However, it is not guaranteed in all cases. The beam problem in next section will show why the accurate response sensitivity is important.

3.3 Application of the SACV-SFEM to Beams

A pure bending beam problem is investigated. Figure 3.2 shows the geometry of the beam. Each beam element has the equal length 1.0 meter, therefore, the whole length of beam is $\boldsymbol{L} = \boldsymbol{m}$ m, where $\boldsymbol{m}$ is the number of elements. The beam is fixed at one end $\boldsymbol{x} = 0$ and loaded by a moment $1/\boldsymbol{m}\ \mathrm{N}\cdot\mathrm{m}$ at free end $\boldsymbol{x} = \boldsymbol{m}$ m. To simplify the problem, assume rigidity $\boldsymbol{EI} = 1\ \mathrm{N}\cdot\mathrm{m}^2$ throughout. The sensitivity of the maximum transverse displacement at $\boldsymbol{x} = \boldsymbol{m} = \boldsymbol{L}$ with respect to the total length $\boldsymbol{L}$, $\partial \boldsymbol{v_p} / \partial \boldsymbol{L}$, can be determined analytically as

$$\frac{\partial \boldsymbol{v_p}}{\partial \boldsymbol{L}} = \frac{\partial}{\partial \boldsymbol{L}}\left(\frac{\boldsymbol{M}\boldsymbol{L}^2}{2\boldsymbol{EI}}\right) = 1 \tag{3-4}$$

Equation shows $\partial \boldsymbol{v}_{\boldsymbol{p}} / \partial \boldsymbol{L}$ is independent of the number of elements $\boldsymbol{m}$. However, If the sensitivity is computed by the SAFDM with the perturbation size $\varepsilon = 10^{-4}$, the error of response sensitivity will increase rapidly with $\boldsymbol{m}$. When $\boldsymbol{m} = 100$, the error becomes 250% (Olhoff et al. [28], Cheng et al. [29, 30], Mlejnek[31]).

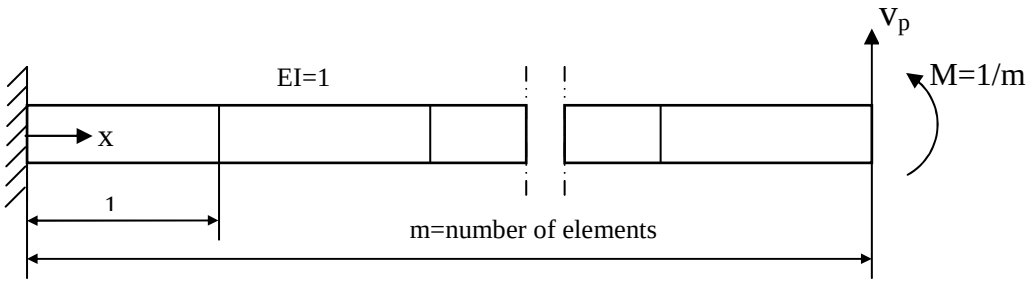

Figure 3.2 Cantilever beam under end moment

3.3.1 Computation of $\partial \boldsymbol{v}_{\boldsymbol{p}} / \partial \boldsymbol{L}$ by the SACVM

At same perturbation of the whole length, the sensitivities $\partial \boldsymbol{v}_{\boldsymbol{p}} / \partial \boldsymbol{L}$ obtained from the SACVM comparing with the FDM, CVM and SAFDM are shown in Table 3.3.

Table 3.3 shows at the same perturbation size, the CVM and the SACVM can always obtain very accurate response sensitivity. While, the FDM and the SAFD are sensitive to the step size, and can not get as accurate results as the CVM and the SACVM. When element size is 1000, the FDM, SAFDM and the SACVM method almost spend same computational time, while the CVM spends extra 15% time. Obviously, the SACVM appears consistent, accurate and efficient.

3.3.2 Reliability analysis by the SACV-SFEM

Assume the total length $\boldsymbol{L}$ is a normal distributed random variable. The mean value of $\boldsymbol{L}$ is $\mu_{\boldsymbol{L}} = 100\,\text{m}$ and the standard deviation is $\sigma_{\boldsymbol{L}} = 10\,\text{m}$. The number of elements is 100 and the perturbation size is $\varepsilon = 10^{-4}$. The rest of the parameters are same with those in 3.3.1.

From deterministic finite element analysis, the maximum displacement at the free end is 50. The limit state function is given as $\boldsymbol{g} = \boldsymbol{v_p} - 45$ to see the failure probability of that the maximum displacement is less than 45 m, $\boldsymbol{g} = \boldsymbol{v_p} - 45 < 0$.

Table 3.3 Sensitivity of maximum displacement with respect to total length in beam

Number of elements		m=100	m=1000
Analytical Solution		1.0	1.0
Step size		$\varepsilon = 10^{-4}$	$\varepsilon = 10^{-6}$
FDM	$\partial v_p / \partial L$	1.000158	4.498377
	error	0.0158%	349.8377%
	Computation Time (s)	-	176
CVM	$\partial v_p / \partial L$	1.000000	1.000027
	error	0.0000%	0.0027%
	Computation Time (s)	-	201
SAFDM	$\partial v_p / \partial L$	-1.4993500	-1.500105
	error	-249.9350%	-250.0105%
	Computation Time (s)	-	174
SACVM	$\partial v_p / \partial L$	0.9992500	0.999977
	error	0.0750%	0.0023%
	Computation Time (s)	-	174

The reliability index, failure probability, and corresponding computational information obtained from the SACV-SFEM and SAFD-SFEM are shown in Table 3.4. The failure probability and corresponding computational information obtained from the traditional Monte Carlo method (MC) is shown in Table 3.4, too.

The results show the SAFD-SFEM converges to the wrong reliability index after 51 iterations. The SACV-SFEM only requires 3 iterations, 0.4 seconds to obtain an accurate result, while the MC method has to compute 10000 iterations, and spends 392 seconds to obtain the same level accuracy. Comparing the SAFD-SFEM and the Monte-Carlo method, the SACV-SFEM presents its accuracy and efficiency.

Table 3.4 Results obtained from the SACV-SFEM in beam bending

	SACV-SFEM	SAFD-SFEM	MC method		
Iterations needed	4	51	100	1000	10000
Reliability Index	0.503167	19.487	-	-	-
Failure Probability	30.39%	0	26%	31.8%	30.41%
Computation Time (s)	0.4	51	4	41	392

3.4 Conclusions

The application of the SACV-SFEM to beam bending and thin plate bending problems are explored in this chapter. The results obtained from SACV-SFEM are compared with the SAFD-SFEM and traditional Monte Carlo method. The response sensitivities obtained by the FDM, CVM, SAFDM and SACVM are evaluated too.

The SAFD-SFEM obtained the correct reliability index for the thin plate problem even if the response sensitivities are inaccurate, which readily mislead people to believe that the SAFD-SFEM can always obtain reliable solution, or that the response sensitivity inaccuracy will not affect the final reliability index. However, this is not true. The application of the SAFD-SFEM in beam bending problem proves that sensitivity accuracy is important. Because of the inaccurate response sensitivity, I obtained a totally wrong reliability index. Therefore it is not safe to use the SAFDM to obtain the response sensitivity in a general purpose SFEM code.

As a basic and powerful tool, traditional Monte Carlo method is used to verify the solutions obtained from other methods. Comparing to the SAFD-SFEM and SACV-SFEM, it is more time consuming.

The sensitivity analysis by the SA-CVM eliminates the drawback of extra computational cost of the CVM and the sensitivity to the perturbation size choice in the SAFDM. Combining the efficiency of the SAM with the accuracy of the CVM gives the SACVM application versatility. It also explains why the SACV-SFEM can always get as accurate results as Monte Carlo method, with the same computational efficiency as the SAFD-SFEM.

CHAPTER 4

APPLICATION OF THE SACV-SFEM TO HEAT CONDUCTION

4.1 Introduction

The numerical analysis of heat conduction by finite element method (FEM) is well established. It is usually assumed that the parameters relevant to the heat transfer process are accurately known. In reality many of these parameters may vary in a random way. As a consequence, the temperature, which depends on these random parameters, will have a response. In the thermal field, Nicolai et al. [42, 43, 44] employed finite element perturbation analysis of non-linear heat conduction problems with random field parameters. Hien and Kleiber [45, 46] combined the second order perturbation and mean-based second moment analysis to compute the first two probabilistic moments of the random temperature field in linear and nonlinear transient heat transfer problems with random parameters. Xiu et al [47] employed polynomial chaos for the solution of transient heat conduction subject to uncertain inputs. Until now, few papers are found that apply first order reliability method (FORM) on the basis of FEM to evaluate the reliability of a performance for thermal applications. This chapter will illustrate FORM algorithm based stochastic finite element method (SFEM) to evaluate the reliability of applications governed by linear steady heat conduction.

In the FORM algorithm based SFEM, a common characteristic is the need for the gradient vector of the FEM responses (sensitivities) with respect to the input random parameters. Many researchers used different methods to compute the sensitivities in the thermal field. Blackwell et al. [48] compared various methods used for computing sensitivities. Dems K. et al. [49] presented sensitivity analysis for transient heat conduction in a solid body using the direct differentiation and adjoint method. Fadale et al. [50] employed finite element

perturbation method to consider the transient effects of uncertainties on the sensitivities of temperatures and heat flux. Dowding et al. [51] derived sensitivity equations for heat conductions with temperature-dependent parameters.

In this chapter, the semi-analytical complex variable method (SACVM) is used to compute the sensitivities of the finite element response with respect to the input random variables in heat conduction problems. Then the SACVM based stochastic finite element method (SACV-SFEM) is applied to evaluate the reliability of the limit state in linear steady state heat conduction with input uncertainties.

An infinitely long hollow cylinder with an analytical solution is employed to test the reliability of the finite element codes for steady state heat conduction. A benchmark problem in steady state linear heat conduction is considered to gage the performance and accuracy of the SACV-SFEM. As being mentioned in structural sensitivity analysis, an accuracy problem will happen when using the semi-analytical finite difference method (SAFDM). Some benchmark cases are used to explore if the finite element response sensitivities with respect to shape parameters in heat conduction problems have accuracy problems, The benchnark considers the shape parameters as random variables and without shape parameters as random variables. I also consider a uniform thermal conductivity of the plate or two thermal conductivities of the plate.

The applications of the SACV-SFEM to steady state linear heat conduction of an electronic BGA packaging is then studied. Six different thermal conductivities, and the heat source are considered as random variables. Two cases are computed. One case considers a fixed geometry. The other case includes the height of the DIE as a random variable.

The results obtained from the SACV-SFEM in benchmark and electronic packaging problems are compared with the FD-SFEM, the SAFD-SFEM and the CV-SFEM.

4.2 Verification of FEM Codes Used in the SACV and FD for Steady State Heat Conduction

Consider heat conduction across an infinitely long hollow cylinder having outer and inner radii of $r_o = 10$ m and $r_i = 5$ m, as shown in Figure 4.1. The temperatures at the two radius are maintained at $T_o = 10^{\circ}\mathrm{C}$ and $T_i = 100^{\circ}\mathrm{C}$, respectively.

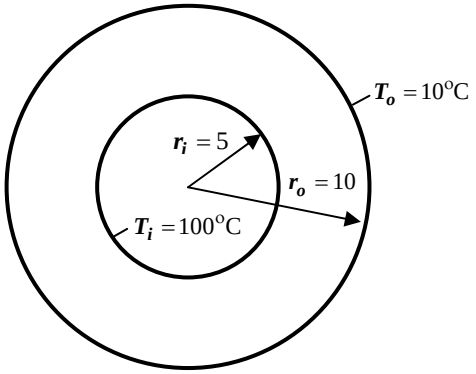

Figure 4.1 Steady state heat conduction across a long hollow cylinder

Since the cylinder is infinite in length and there is axial symmetry, the heat flows only in radial direction and $T = f(r)$. From Fourier's law, we can readily get the analytical expression of radial heat flow rate per unit length q / L [52].

$$\frac{q}{L} = \frac{2\pi k(T_o - T_i)}{\ln(r_o / r_i)} = 8158.2483 \text{ W/m} \tag{4-1}$$

where k is the thermal conductivity and L is the length of cylinder.

From Equation (4-1), the sensitivity of the radial heat flow rate per length with respect to the radius is

$$\frac{d(q / L)}{dr_i} = \frac{2\pi k(T_o - T_i) r_o}{r_i \cdot [\ln(r_o / r_i)]^2} = 2353.9729 \text{ W/m}^2 \tag{4-2}$$

Two FE models are used to compute the heat flow rate per length and sensitivities of the heat flow rate per length with respect to thermal conductivity and radius. The coarse mesh

model has 348 nodes and 592 elements, as shown in Figure 4.2 (a). The fine mesh model has 2828 nodes and 5340 elements, as shown in Figure 4.2 (b).

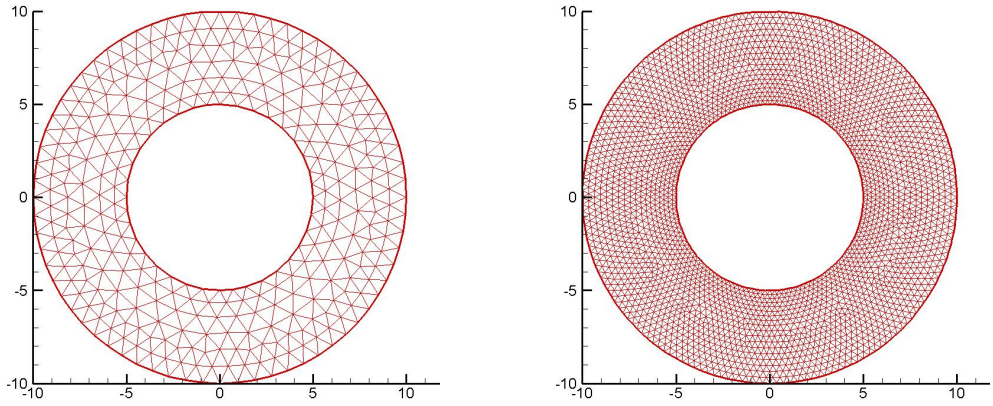

Figure 4.2 Two FE models (a) coarse mesh, (b) fine mesh, of steady state heat conduction across a long hollow cylinder

The SACVM and FDM are employed to compare the results with the analytical solution. The heat flow rate per length obtained from the finite element analysis of the coarse mesh model is 8166.092. The relative error comparing to the analytical solution is 0.096%. The heat flow rate per length obtained from the finite element analysis of the fine mesh model is 8159.9358. The relative error comparing to the analytical solution is 0.021%. The relative errors of $\boldsymbol{d(q/L)/dr_i}$ comparing to the analytical solution at different perturbation sizes for two models are shown in Figure 4.3.

The relative errors of the heat flow rate per length and sensitivities of the heat flow rate per length show that FE codes used to calculate the heat conduction problem match the analytical solution well. Therefore, this FE codes can be used for similar heat conduction problems without analytical solution. Figure 4.3 also shows that finer mesh can improve the accuracy of FE analysis, however, it decrease the perturbation range for obtaining stable sensitivities.

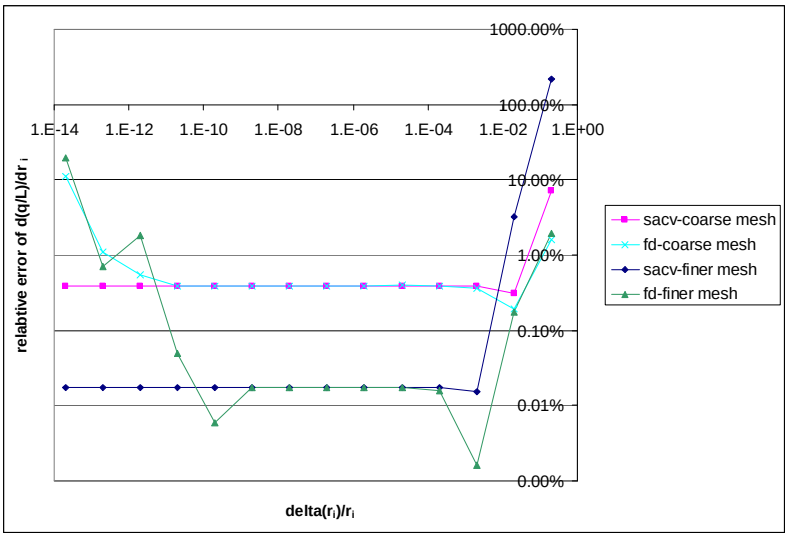

Figure 4.3 Relative errors of $d(q/L)/dr_i$ via $\Delta r_i / r_i$ in long hollow cylinder

4.3 Application of the SACV-SFEM to Benchmark Plate

4.3.1 Response sensitivities

In the benchmark problem, we are interested in the normal heat flux across the boundary, $Gflux$. The SACVM is used to compute the sensitivity of the heat flux with respect to input variables, $dGflux/dx$. The flowchart of computing $dGflux/dx$ is shown in Figure 4.4.

The computation of $dGflux/dx$ by SACVM only does the most time consuming part, the LU decomposition, once. It employs the same intermediate upper triangular matrix and work vector to solve two equations, $KU = F$ and $K \cdot dU/dx = F\_dudx$. Comparing with the FDM or the CVM which needs $n+1$ times LU decompositions for computing sensitivities of n parameters, the SACVM computes more efficiently. Furthermore the SACVM does the LU decomposition in real variable space, so it doesn't need much additional computation time in complex variable space. By employing the CVM, the perturbation of the global stiffness matrix ΔK and load vector ΔF caused by the perturbation of the input variable Δx can be obtained accurately without any truncation errors or being sensitive to the perturbation size. This

significantly improves the consistency and accuracy of $\Delta \boldsymbol{K}$ and $\Delta \boldsymbol{F}$ and finally obtains the consistent and accurate $\boldsymbol{dU}/\boldsymbol{dx}$.

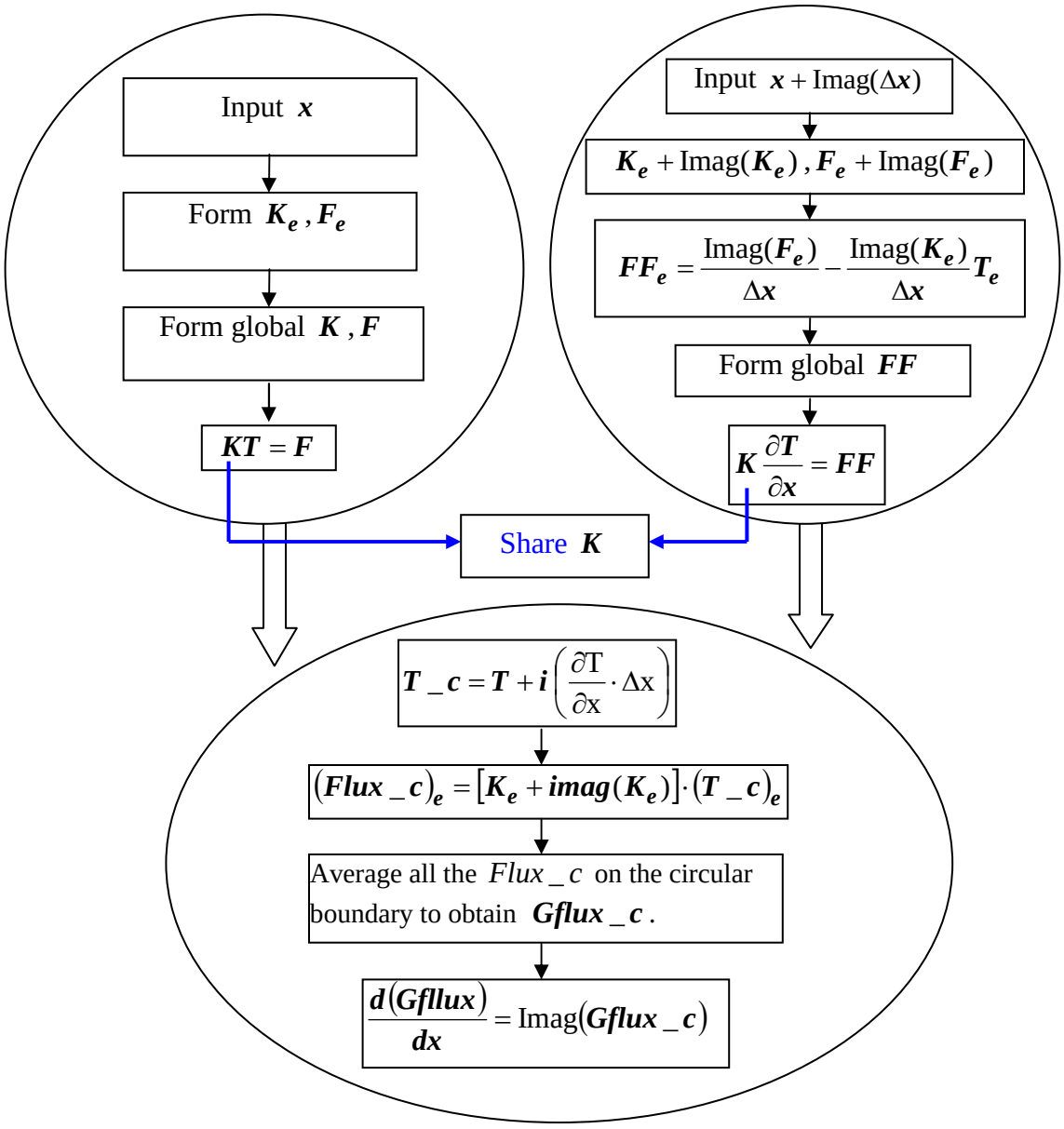

Figure 4.4 Flowchart of computing $\boldsymbol{dGflux}/\boldsymbol{dx_i}$

4.3.2 Reliability analysis procedure

The main flowchart of reliability analysis by SACV-SFEM in the benchmark problems is shown in Figure 4.5. By using SACV-SFEM, the entire analysis will save significant computation time compared with the FDM-SFEM and CVM-SFEM. In each iteration of the FORM algorithm for finding new design points of random variables, the LU decomposition will only be needed to be computed once. Therefore, the more input random variables are computed, more time are saved. For different random variable, we only need to calculate $\Delta \boldsymbol{K}$ and $\Delta \boldsymbol{F}$ of each random variable in element level to obtain the sensitivities of heat flux with respect to each random variable.

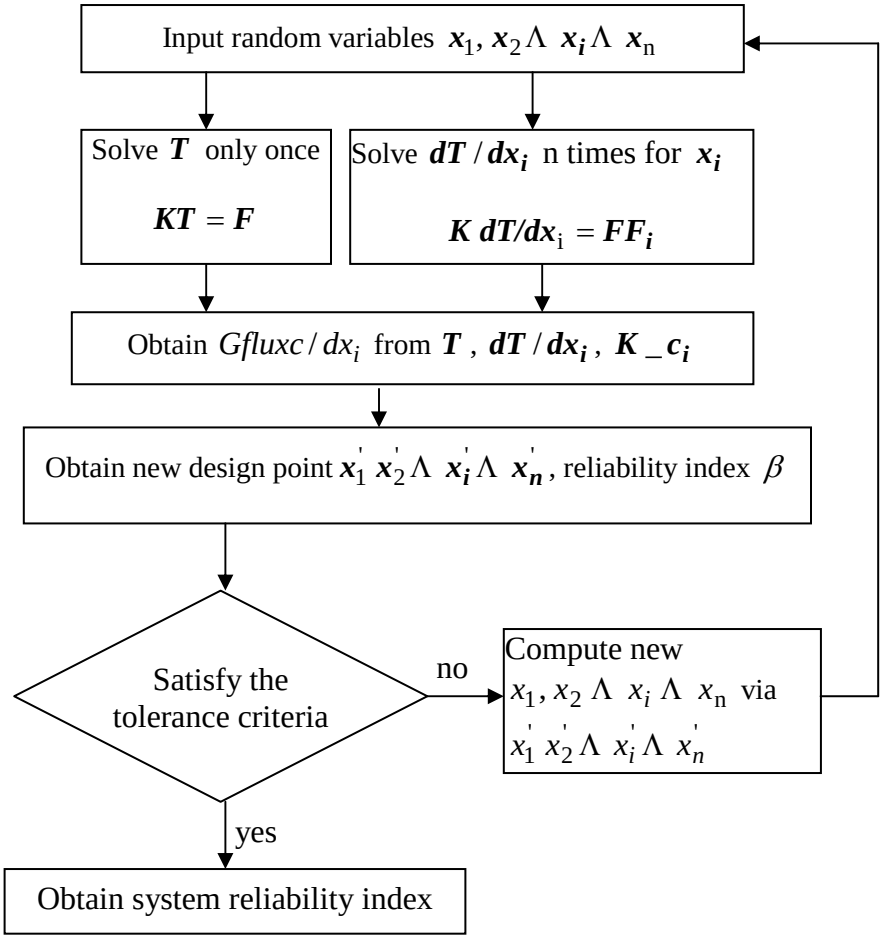

Figure 4.5 Main flowchart of reliability analysis by SACV-SFEM

4.3.3 Four cases of benchmark plate

A two-dimensional, steady-state heat conduction with uniform source is considered on a $10\text{m}\times 10\text{m}$ square plate with a hole $\boldsymbol{r}=1\text{m}$ in the middle of it. The temperature on the square edge is $\boldsymbol{T}_1=10°\boldsymbol{C}$ and the temperature on the circle edge is $\boldsymbol{T}_2=100°\boldsymbol{C}$. The mesh of the plate is shown in Figure 4.6. There are 794 nodes and 1478 elements in all.

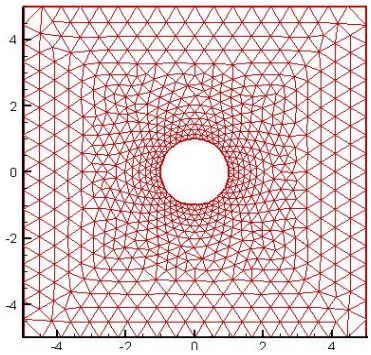

Figure 4.6 Mesh of the benchmark plate

The criteria of the limit state function is defined as the integrated normal heat flux across the circular boundary is less than a certain value with considering some uncertain input random parameters.

$$\boldsymbol{f}=\boldsymbol{Gflux}-\boldsymbol{a} \tag{4-3}$$

where $\boldsymbol{Gflux}$ is the normal heat flux across the circular boundary, and $\boldsymbol{a}$ is a certain value that represents the limited value of the normal heat flux across the circular boundary. In the following four cases, $\boldsymbol{a}=35000$ W.

The gradient of the limit state function with respect to the random variable $\boldsymbol{x}$ can be calculated by the chain rule of the differentiation as

$$\frac{\partial \boldsymbol{f}}{\partial \boldsymbol{x}}=\frac{\partial \boldsymbol{f}}{\partial \boldsymbol{Gflux}}\cdot\frac{\partial \boldsymbol{Gflux}}{\partial \boldsymbol{x}}=\frac{\partial \boldsymbol{Gflux}}{\partial \boldsymbol{x}} \tag{4-4}$$

Four cases are studied to obtain the reliability index of the limit state function. Case 1 considers the uniform thermal conductivity and heat source are normal-distributed random variables. Case 2 considers the uniform thermal conductivity, heat source and the length of the

square plate are normal-distributed random variables. Case 3 considers the plate has two different heat conductivities, which are both normal-distributed random variables. And the heat source is normal-distributed random variables, too. Case 4 considers two different heat conductivities, heat source and the length of the plate are all normal-distributed random variables.

4.3.1.1 Case 1: Two Input Random Variables without Random Length Parameter

Assume the thermal conductivity of the plate $\boldsymbol{k}$ is homogeneous everywhere, and is a normally-distributed random variable, $\boldsymbol{k} = \boldsymbol{N}\left(10\ \mathrm{W/m\cdot^{o}C}, 1\ \mathrm{W/m\cdot^{o}C}\right)$. The uniform heat source $\boldsymbol{Q}$ is also a normally-distributed random variable, $\boldsymbol{Q} = \boldsymbol{N}\left(1000\mathrm{W/m^2}, 100\mathrm{W/m^2}\right)$, as shown in Figure 4.7. The temperature distribution for the thermal conductivity $\boldsymbol{k} = 10\ \mathrm{W/m\cdot^{o}C}$ and heat source $\boldsymbol{Q} = 1000\ \mathrm{W/m^2}$ is shown in Figure 4.8.

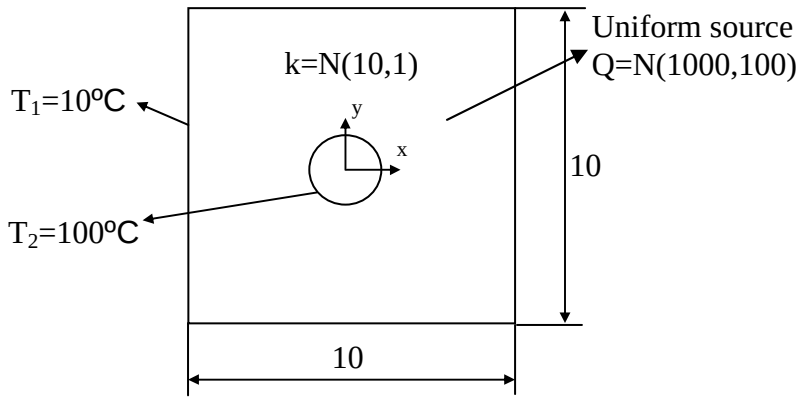

Figure 4.7 Case 1 of the benchmark plate

The computation time and needed iterations for solving Case 1 of benchmark problem by the SACV-SFEM, CV-FEM, FD-SFEM and SAFD-SFEM are listed in Table 4.1 and Figure 4.9. The obtained reliability index of the limit state function is $\beta = 3.4685$. The CV-SFEM and the SACV-SFEM can always obtain correct reliability index in two iterations. However, the CV-SFEM needs about 8 times computation time than the SACV-SFEM. The FD-SFEM can obtain

$\beta = 3.4685$ in 2 iterations when the perturbation size is in the range from 10^{-1} to 10^{-8}. But when the perturbation size is 10^{-10}, it takes 8 iterations to obtain $\beta = 3.469$. The SAFD-SFEM takes different iterations to obtain $\beta = 3.4685$ when using different perturbation size. Both the FD-SFEM and the SAFD-SFEM can not calculate when the perturbation size is 10^{-20}, while the CV-SFEM and SACV-SFEM can readily obtain the accurate reliability index.

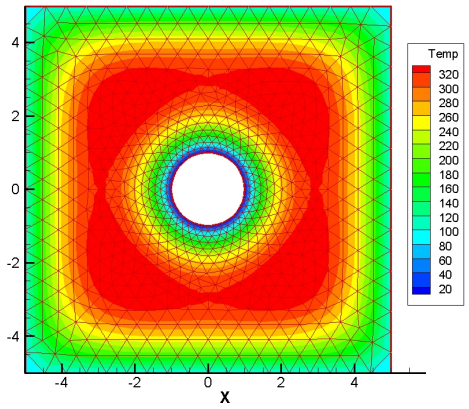

Figure 4.8 Temperature distribution of case 1 for random variables at mean values

Table 4.1 Computation time and needed iterations of four methods in case1 of the benchmark plate

Perturba-tion	FD-SFEM		SAFD-SFEM		CV-SFEM		SACV-SFEM	
	Compu. Time (s)	Iter.	Compu. Time (s)	Iter.	Compu. Time (s)	Iter.	Compu. Time (s)	Iter.
10^{-1}	18	2	17	5	77	2	9	2
10^{-2}	18	2	14	4	77	2	9	2
10^{-3}	18	2	11	3	77	2	9	2
10^{-6}	18	2	8	2	77	2	9	2
10^{-8}	18	2	11	3	77	2	9	2
10^{-10}	67	8	11	3	77	2	9	2
10^{-20}	X		X		77	2	9	2

"X" represents not converge.

To explore why the FD-SFEM and SAFD-SFEM take more iterations to compute the reliability index, the sensitivities of normal heat flux across the circular boundary with respect to the input random variables $\boldsymbol{dGflux/dk}$ and $\boldsymbol{dGflux/dQ}$ for 4 methods in different

perturbation sizes are studied. When the random variables equal to mean value, $dGflux/dk$ via perturbation size computed by 4 methods is shown in Figure 4.10, and $dGflux/dQ$ via perturbation size computed by 4 methods is shown in Figure 4.11.

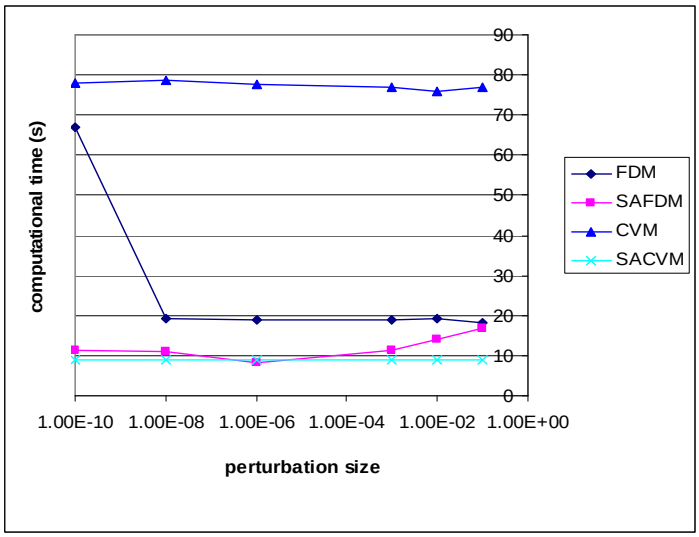

Figure 4.9 Computation time in case 1

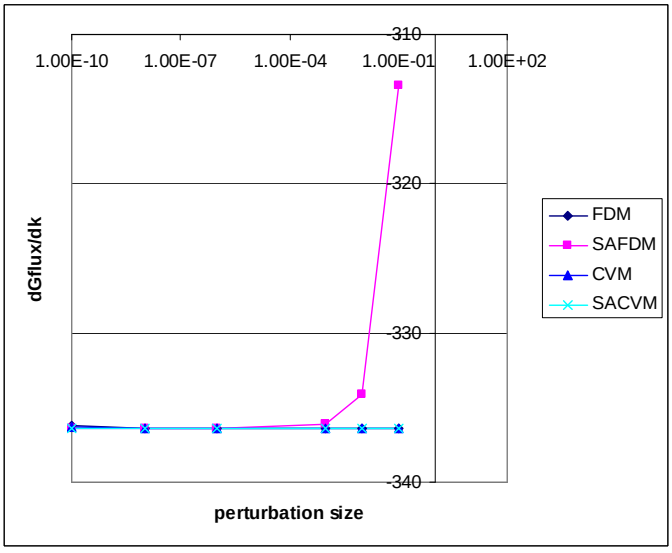

Figure 4.10 $dGflux/dk$ via perturbation size in case 1

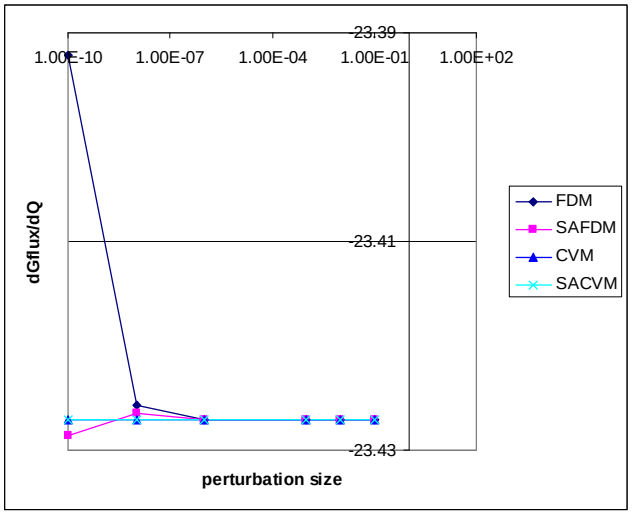

Figure 4.11 $dGflux/dQ$ via perturbation size in case 1

From Figure 4.10 and Figure 4.11, $Gflux/dk$ and $Gflux/dQ$ computed by the FDM and the SAFDM is sensitive to the perturbation size when the perturbation sizes are too small or too big. However those computed by the CV-SFEM and SACV-SFEM are not sensitive to the perturbation size at all.

4.3.1.2 Case 2 : Three Input Random Variables Including Random Length Parameter

The homogeneous thermal conductivity of the plate k, the uniform heat source Q and the edge of the square a are normally-distributed random variables, $k = N\left(10\ \mathrm{W/m}\cdot^{\mathrm{o}}C, 1\ \mathrm{W/m}\cdot^{\mathrm{o}}C\right)$, $Q = N\left(1000\mathrm{W/m}^2, 100\mathrm{W/m}^2\right)$ and $a = N\left(10\mathrm{m}, 1\mathrm{m}\right)$, as shown in Figure 4.12.

The computation time and needed iterations for solving the benchmark problem by SACV-SFEM, CV-FEM, FD-SFEM and SAFD-SFEM are listed in Table 4.2 and Figure 4.13.

The reliability index of the limit state function is $\beta = 1.4162$. The CV-SFEM and the SACV-SFEM can always obtain $\beta = 1.4162$ in 5 iterations. They are not sensitive to the perturbation size. However, the computation time of the SACV-SFEM is almost 12 times less than that of the CV-SFEM. The FD-SFEM and SAFD-SFEM can obtain $\beta = 1.4162$ in 5

iterations when the perturbation size is between 10^{-2} and 10^{-8}. When the perturbation size is 10^{-1} or 10^{-10}, they need more iterations to obtain final reliability index. Both the FD-SFEM and the SAFD-SFEM can not calculate when the perturbation size is 10^{-20}, while the CV-SFEM and the SACV-SFEM can readily obtain the accurate reliability index.

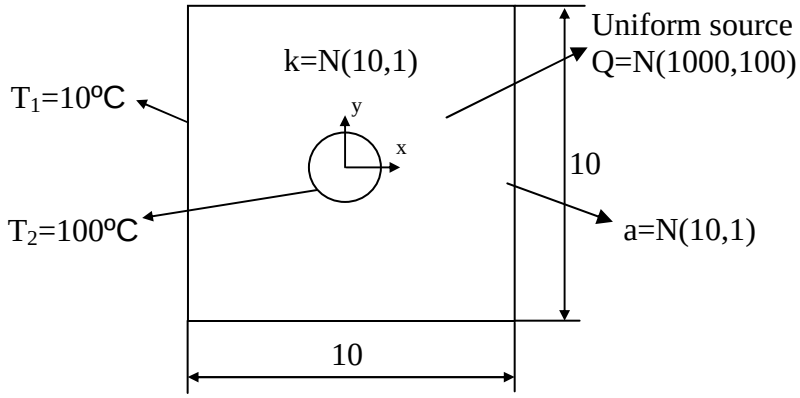

Figure 4.12 Case 2 of the benchmark plate

Table 4.2 Computation time and needed iterations of four methods in case 2 of the benchmark plate

Perturba-tion	FD-SFEM		SAFD-SFEM		CV-SFEM		SACV-SFEM	
	Compu. Time (s)	Iter.	Compu. Time (s)	Iter.	Compu. Time (s)	Iter.	Compu. Time (s)	Iter.
10^{-1}	68	6	20	6	217	5	18	5
10^{-2}	56	5	17	5	217	5	18	5
10^{-3}	56	5	17	5	217	5	18	5
10^{-6}	56	5	17	5	217	5	18	5
10^{-8}	56	5	17	5	217	5	18	5
10^{-10}	264	23	83	25	217	5	18	5
10^{-20}	X		X		217	5	18	5

"X" represents not converge.

When the thermal conductivities $\boldsymbol{k}_1$, $\boldsymbol{k}_2$, and heat source $\boldsymbol{Q}$ are at mean values, the sensitivities of the normal heat flux across the circular boundary with respect to the input random variables, $\boldsymbol{dGflux/dk}$, $\boldsymbol{dGflux/dQ}$ and $\boldsymbol{dGflux/da}$ computed by 4 methods at different perturbation size are shown in Figure 4.10, Figure 4.11 and Figure 4.14.

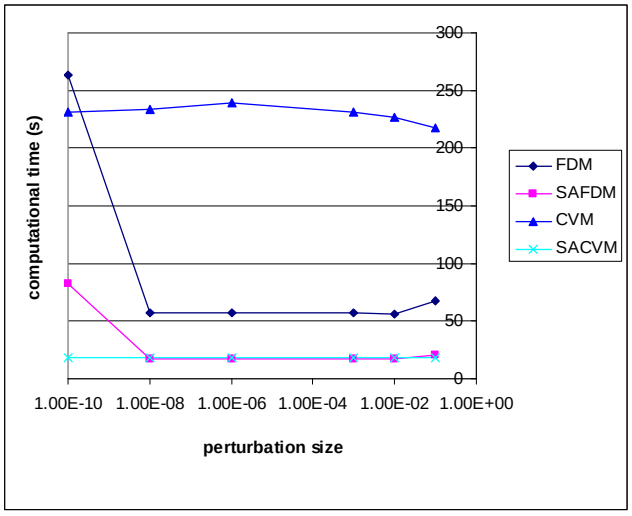

Figure 4.13 Computation time in case 2

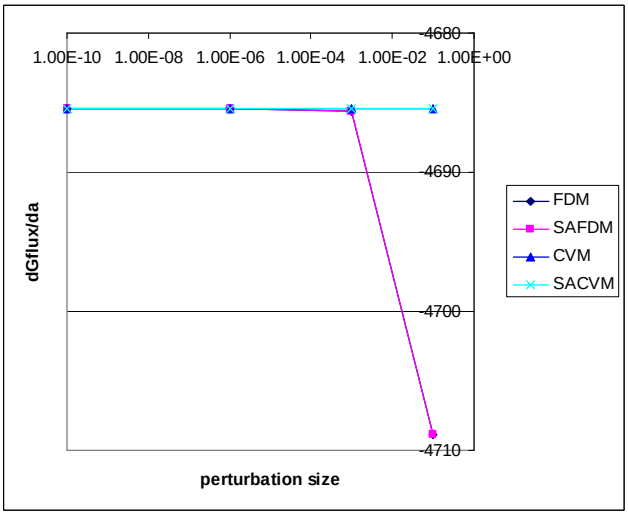

Figure 4.14 $dGflux/da$ via perturbation size in case 2

From Figure 4.10, 4.11 and 4.14, when the perturbation size is 10^{-1}, the SAFDM is not able to accurate sensitivities $dGflux/dk$ and $dGflux/da$. When the perturbation size is 10^{-10}, the FDM can not obtain accurate sensitivity $dGflux/dQ$. The CVM and SACVM are not sensitive to the perturbation sizes at all. This explains why the CVM-SFEM and the SACVM-SFEM can always obtain same reliability index in same iterations at different perturbation sizes, however the FD-SFEM and the SAFD-SFEM need more iterations and computation time.

4.3.1.3 Case 3 : Three Input Random Variables without Random Shape Parameter

In this case assumes the plate is composed of two different materials. The thermal conductivity of the area $y \geq 0$ is a normally-distributed random variable, $k_1 = N\left(10\ \mathrm{W/m\cdot^{o}C}, 1\ \mathrm{W/m\cdot^{o}C}\right)$, and the thermal conductivity of the area $y < 0$ is a normally-distributed random variable, $k_2 = N\left(20\ \mathrm{W/m\cdot^{o}C}, 2\ \mathrm{W/m\cdot^{o}C}\right)$. Also, the uniform heat source is a normally-distributed random variable, $Q = N\left(1000\mathrm{W/m^2}, 100\mathrm{W/m^2}\right)$, as shown in Figure 4.15. The temperature distribution for the thermal conductivities $k_1 = 10\ \mathrm{W/m\cdot^{o}C}$, $k_2 = 20\ \mathrm{W/m\cdot^{o}C}$ and heat source $Q = 1000\ \mathrm{W/m^2}$ is shown in Figure 4.16.

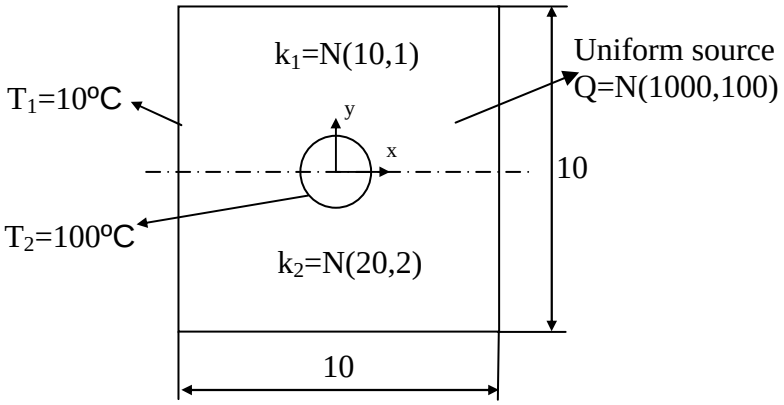

Figure 4.15 Case 3 of the benchmark plate

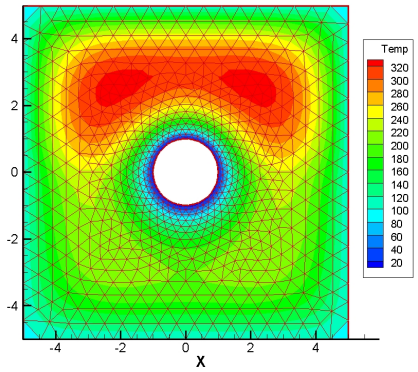

Figure 4.16 Temperature distribution of case 3 for random variables at mean values

The reliability index of the limit state function is $\beta = 2.7741$. The computation time and needed iterations for solving the benchmark problem by SACV-SFEM, CV-FEM, FD-SFEM and SAFD-SFEM are listed in Table 4.3 and Figure 4.17.

Table 4.3 Computation time and needed iterations of four methods in case3 of the benchmark plate

Perturba-tion	FD-SFEM		SAFD-SFEM		CV-SFEM		SACV-SFEM	
	Compu. Time (s)	Iter.	Compu. Time (s)	Iter.	Compu. Time (s)	Iter.	Compu. Time (s)	Iter.
10^{-1}	35	3	14	4	144	3	13	3
10^{-2}	35	3	11	3	144	3	13	3
10^{-3}	35	3	11	3	144	3	13	3
10^{-6}	35	3	11	3	144	3	13	3
10^{-8}	35	3	11	3	144	3	13	3
10^{-10}	46	4	17	5	144	3	13	3
10^{-20}	X		X		144	3	13	3

"X" represents not converge.

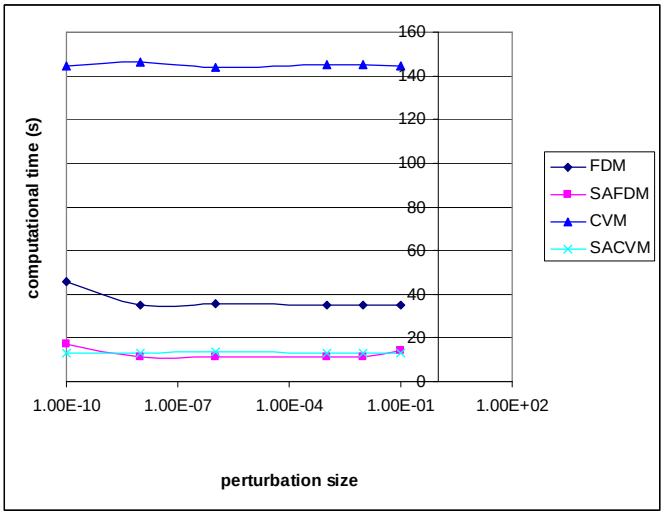

Figure 4.17 Computation time in case 3

From Figure 4.17, except the perturbation size 10^{-1} and 10^{-10}, the SAFD-SEFM and the SACV-SFEM have comparable computation time and same iterations to obtain the final reliability index. However, when the perturbation size is 10^{-1} or 10^{-10}, the SAFD-SEFM needs

more iterations and computation time. The computation time of FD-SFEM is almost three times than the SAFD-SFEM and the SACV-SFEM when the perturbation size is between 10^{-1} and 10^{-8}. When the perturbation size is 10^{-10}, the FD-SFEM and the SAFD-SFEM needs more iterations and computation time than the other perturbation sizes. The CV-SFEM can always obtain accurate reliability index, however, it has to pay about 10 times more computation time than the SAFD-SFEM and the SACV-SFEM.

When the thermal conductivities $\boldsymbol{k}_1$ and $\boldsymbol{k}_2$, and heat source $\boldsymbol{Q}$ are at mean value, for different perturbation size, the first derivatives of the normal heat flux across the circular boundary with respect to the input random variables, $\boldsymbol{dGflux/dk}_1$, $\boldsymbol{dGflux/dk}_2$, and $\boldsymbol{dGflux/dQ}$, are shown in Figure 4.18, 4.19 and 4.20.

From Figure 4.18, 4.19 and 4.20, when the perturbation size is 10^{-1} or 10^{-10}, the sensitivities computed by the FDM and the SAFDM are not accurate. The CVM and the SACVM can obtain accurate sensitivities whenever the perturbation size is big as 10^{-1}, or small as 10^{-10}, even smaller than 10^{-20}. This explains why the CVM-SFEM and the SACV-SFEM can always obtain same reliability index at different perturbation sizes, however, the FD-SFEM and the SAFD-SFEM need more computation time and more iterations to obtain the final reliability index when the perturbation size is 10^{-1} or 10^{-10}.

4.3.1.4 Case 4 : Three Input Random Variables with Random length Parameter

Except that the edge of the plate is a normally-distributed random variable too, $\boldsymbol{a} = \boldsymbol{N}(10\text{m}, 1\text{m})$, the other conditions are same with case 3, as shown in Figure 4.21.

The reliability index of the limit state function is $\beta = 1.1555$. The computation time and needed iterations for solving the benchmark problem by SACV-SFEM, CV-FEM, FD-SFEM and SAFD-SFEM are listed in Table 4.4 and Figure 4.22.

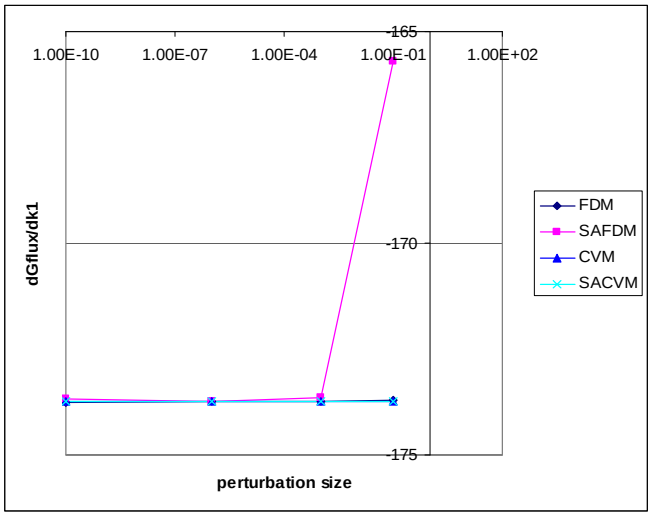

Figure 4.18 $\boldsymbol{dGflux/dk_1}$ via perturbation size in case 3

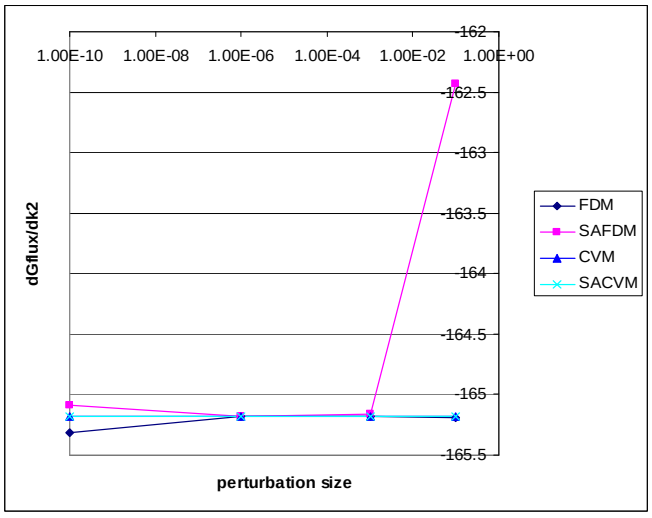

Figure 4.19 $\boldsymbol{dGflux/dk_2}$ via perturbation size in case 3

From Figure 4.22, when the perturbation size is between 10^{-2} and 10^{-8}, the SAFD-SEFM and the SACV-SFEM have comparable computation time and same iterations to obtain the final reliability. When the perturbation size is 10^{-1} or 10^{-10}, the FD-SFEM and the SAFD-SFEM need more computation time and iterations to obtain the final reliability index than the SACV-SFEM and the CVM. The CV-SFEM and the SACV-SFEM can always obtain the accurate reliability index in 5 iterations and is not sensitive to the perturbation size at all.

However, the CV-SFEM needs about 14 times computation time than the SACV-SFEM. The FDM needs more than three times computation time than the SACV-SFEM.

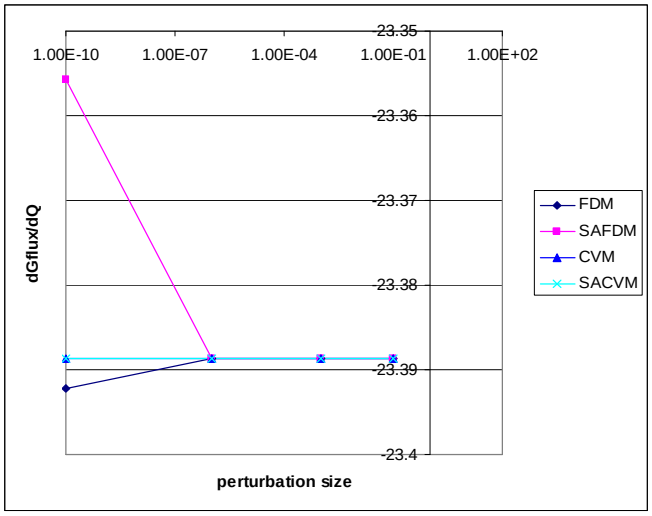

Figure 4.20 $dGflux/dQ$ via perturbation size in case 3

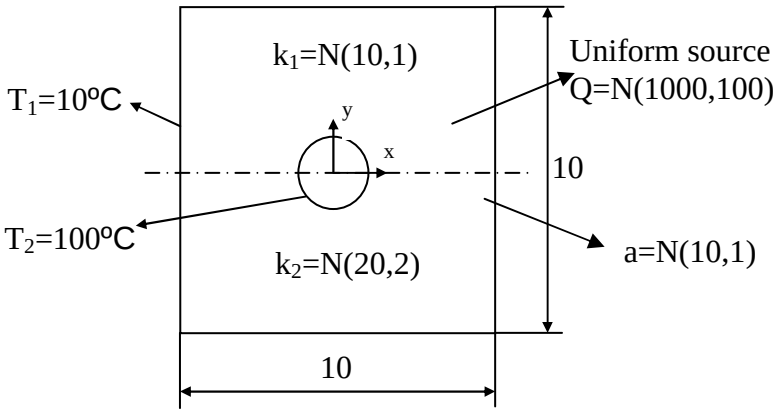

Figure 4.21 Case 4 of the benchmark plate

When the thermal conductivities k_1 and k_2, heat source Q and the edge of the plate a are at the mean values, the sensitivities of the normal heat flux across the circular boundary with respect to the input random variables, $dGflux/dk_1$, $dGflux/dk_2$, $dGflux/dQ$ and $dGflux/da$ computed at different perturbation size, are shown in Figure 4.18-4.20 and Figure 4.23.

Table 4.4 Computation time and needed iterations of four methods in case 4 of the benchmark plate

Perturba-tion	FD-SFEM		SAFD-SFEM		CV-SFEM		SACV-SFEM	
	Compu. Time (s)	Iter.	Compu. Time (s)	Iter.	Compu. Time (s)	Iter.	Compu. Time (s)	Iter.
10^{-1}	83	6	20	6	292	5	20	5
10^{-2}	70	5	18	5	292	5	20	5
10^{-3}	70	5	18	5	292	5	20	5
10^{-6}	70	5	18	5	292	5	20	5
10^{-8}	70	5	18	5	292	5	20	5
10^{-10}	247	18	18	5	292	5	20	5
10^{-20}	X		X		292	5	20	5

"X" represents not converge.

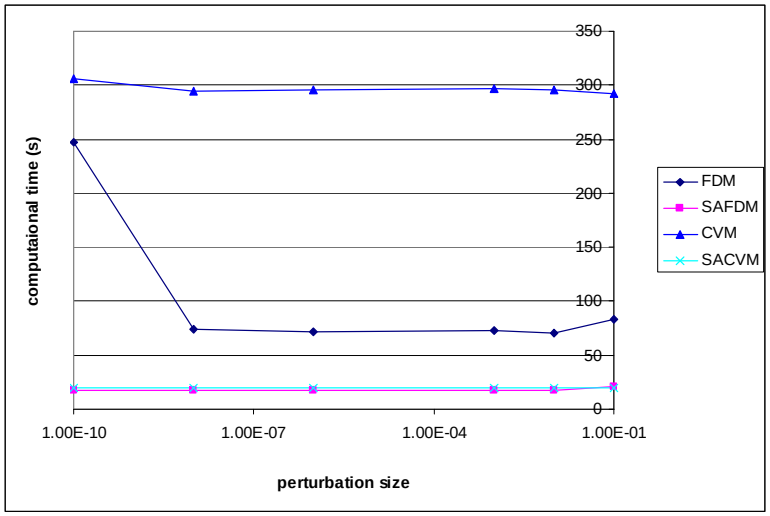

Figure 4.22 Computation time in case 4

From Figure 4.18-4.20 and Figure 4.23, $dGflux/dk_1$, $dGflux/dk_2$, $dGflux/dQ$ and $dGflux/da$ computed by the FDM and SAFDM are not accurate when the perturbation size is 10^{-1} or 10^{-10}. However, $dGflux/dk_1$, $dGflux/dk_2$, $dGflux/dQ$ and $dGflux/da$ computed by the CVM and the SACVM is not sensitive to the perturbation size at all. This explains why the CVM-SFEM and the SACV-SFEM can always obtain same reliability index at different

perturbation sizes, however, the FD-SFEM and the SAFD-SFEM need more computation time and iterations to obtain the final reliability index when the perturbation size it too large or small.

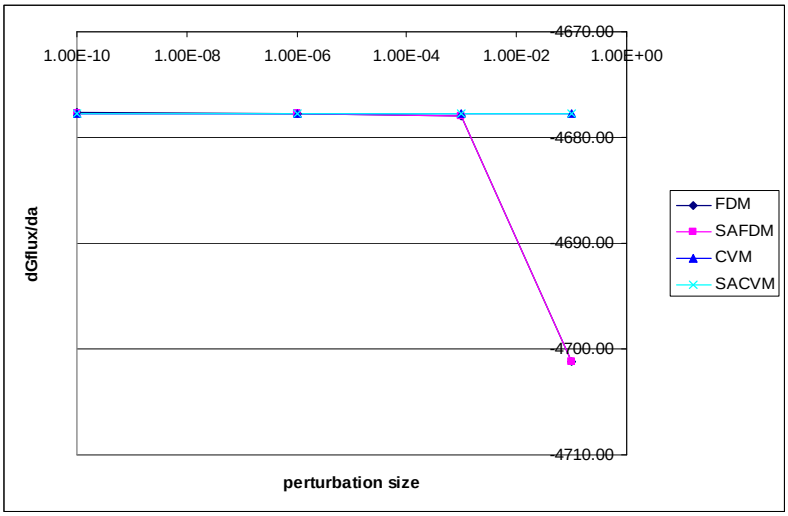

Figure 4.23 $dGflux/da$ via the perturbation size in case 4

4.4 Application of the SACV-SFEM to Electronic BGA Packaging

With continuing shrinking of feature size and increasing clock speed of the silicon integrated circuits, there is a trend toward increasing power and heat flux on the silicon. For flip chip package[53,54,55,56,57], with the chip connected with solder ball interconnection to the substrate on the circuit side, the other side of the chip is flipped and can be used as a thermal conduction path for cooling.

The problem of interest concerns a flip chip BGA package as shown in Figure 4.24. The heat source of die, Q, is the normal-distributed random variable, its mean value and deviation are $1.93\times10^{10}\,\mathrm{W/m^2}$ and $1\times10^{9}\,\mathrm{W/m^2}$, respectively. The thermal conductivities of the die, substrate, underfill, heat spreader and other components are also normal-distributed random variables. The thickness, mean value and deviation of thermal conductivity of each component are shown in Table 4.5. We are interested in the average temperature along the interface between the die and heat spreader. The FD-SFEM, the SAFD-SFEM, the CV-SFEM and the

SACV-SFEM are used to compute the reliability index about the average temperature is less than a certain temperature when considering these random variables.

The difference of mean values of the input random variables is very large. The largest variable is the mean value of heat source $\boldsymbol{Q} = 1.93 \times 10^{10}\,\mathrm{W/m^2}$. And the smallest variable is the mean value of the thermal conductivity of adhesive, $\boldsymbol{k} = 0.5\,\mathrm{W/m \cdot K}$. It is difficult and complicated for the FDM or the SAFDM to find a single perturbation size for all the random variables because of the subtraction error. By CV-SFEM and the SACV-SFEM, we can avoid this shortcoming and use the same perturbation size for all the random variables.

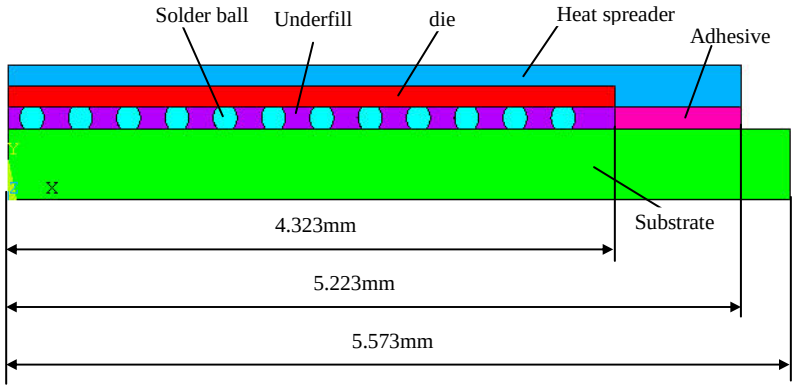

Figure 4.24 Flip chip BGA package

A half-symmetry finite element model is built. The mesh is composed of 745 nodes and 1393 linear triangle elements. The mesh of the half flip chip BGA package is shown in Figure 4.25. Except the symmetry boundary, all the other boundaries have the convective boundary condition imposed. The ambient temperature is the room temperature, $298\mathrm{K}$. The temperature distribution of the package for all uncertainties being the mean values is shown in Figure 4.26.

The limit state function is

$$\boldsymbol{f} = \boldsymbol{T_{avg}} - 370 \tag{4-5}$$

where $\boldsymbol{T_{avg}}$ is the average interface temperature between the DIE and the heat spreader. And 370 is the allowable average temperature along the interface between the die and heat spreader.

Table 4.5. Parameters of components of BGA packaging

	Thickness(mm)	Mean value of conductivity $(\mathrm{W/m \cdot K})$	Deviation of conductivity $(\mathrm{W/m \cdot K})$
Solder ball	0.15	10.05	1.0
Underfill	0.15	4.3	0.43
DIE	0.15	110	11.0
Heat spreader	0.15	389	38.9
Adhesive	0.15	0.5	0.05
Substrate	0.5	17.5	1.75

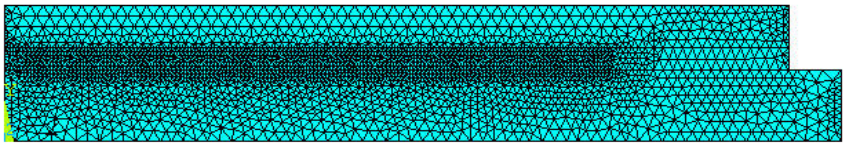

Figure 4.25 Mesh of the flip chip BGA package

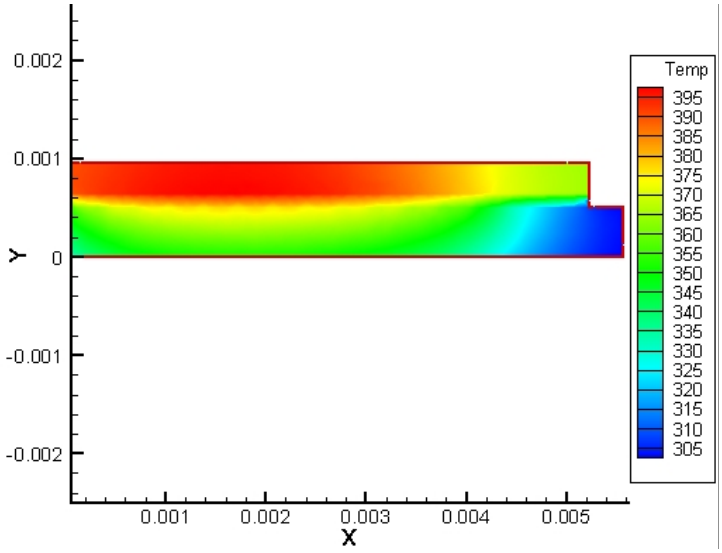

Figure 4.26 Temperature distribution of the flip chip BGA package

Two cases are considered to compute the reliability index of this electronic packaging problem. Case 1 considers the heat source and all six material's thermal conductivity are

random variables. Case 2 treats the height of the die as a random variable as well as the heat source and six thermal conductivities.

4.4.1 Case 1: heat source and 6 thermal conductivities are random variables

The computation time and needed iterations for solving the electronic packaging problem by the SACV-SFEM, the CV-SFEM, the FD-SFEM and the SAFD-SFEM are shown in Table 4.6 and Figure 4.27.

Table 4.6 Computation time and needed iterations of four methods in case 1 of flip chip BAG package

Perturba-tion	FD-SFEM		SAFD-SFEM		CV-SFEM		SACV-SFEM	
	Compu. Time (s)	Iter.	Compu. Time (s)	Iter.	Compu. Time (s)	Iter.	Compu. Time (s)	Iter.
10^{-1}	56	3	X		230	3	10	3
10^{-2}	56	3	16	5	230	3	10	3
10^{-3}	56	3	10	3	230	3	10	3
10^{-4}	315	18	101	38	230	3	10	3
10^{-6}	*		*		230	3	10	3
10^{-8}	*		*		230	3	10	3
10^{-10}	X		X		230	3	10	3
10^{-20}	X		X		230	3	10	3

"X" represents not converge. "*" represents obtaining wrong reliability index.

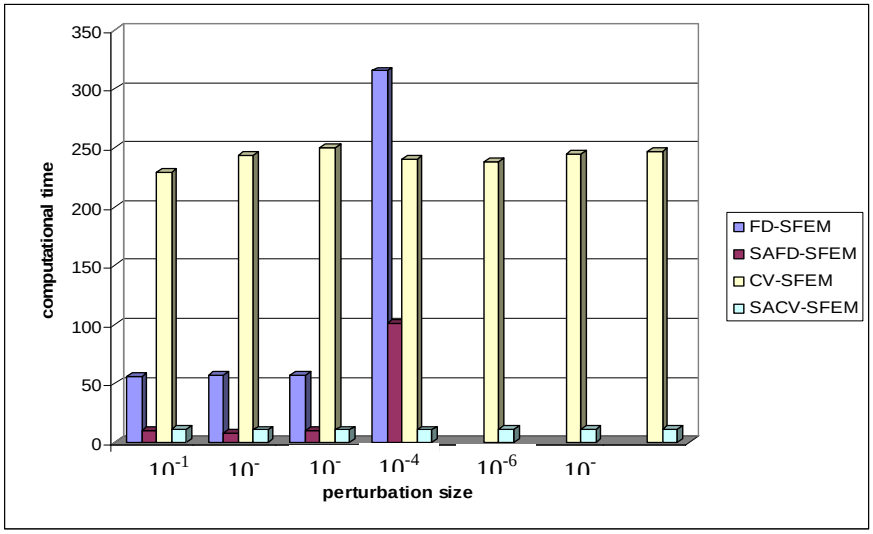

Figure 4.27 Computation time via perturbation size in case1

The final reliability index is $\beta = 0.4824$. When the perturbation sizes are 10^{-1}, 10^{-2} and 10^{-3}, all four methods can obtain the final reliability index. The SAFD-SFEM and the SACV-SFEM has the comparable computation time. The computation time of the FD-SFEM is about 5 times than that of the SAFD-SFEM and the SACV-SFEM. And the computation time of the CV-SFEM is over 20 times than that of the SAFD-SFEM and the SACV-SFEM. When the perturbation size is 10^{-4}, the FD-SFEM and the SAFD-SFEM need 18 iterations, 38 iterations, respectively, to obtain the final reliability index. When the perturbation sizes is less than 10^{-4}, the FD-SFEM and SAFD-SFEM obtain the wrong reliability index. While the CV-SFEM and the SACV-SFEM can always obtain accurate final reliability index in three iterations as long as the perturbation size is less than 10^{-1}. The SACV-SFEM always saves 20 times computation time compared to the CV-SFEM.

4.4.2 Case 2: heat source, 6 thermal conductivities and the height of DIE are random variables

Assume the height of the DIE is a normally-distributed random variable, $\boldsymbol{a} = \boldsymbol{N}\left(1.5\times10^{-4}\,\mathrm{m}, 1.5\times10^{-5}\,\mathrm{m}\right)$. All the other parameters are same as Case 1. Among total 8 random variables, the differences of the values are large. The largest value is the heat source $\boldsymbol{Q} = 1.93\times10^{10}\,\mathrm{W/m^2}$. The smallest value is the height of the DIE $\boldsymbol{h} = 1.5\times10^{-4}\,\mathrm{m}$. Because of the limitation of the computer, it is impossible for the FD-SFEM and the SAFD-SFEM to employ the same perturbation size to all the variables. However, the CV-SFEM and the SACV-SEFM can use the same perturbation size for all the random variables to get accurate reliability index.

The computation time and needed iterations for solving the electronic packaging problem by the SACV-SFEM, the CV-SFEM, the FD-SFEM and the SAFD-SFEM are listed in Table 4.7.

The final reliability index is $\beta = 0.8755$. The CV-SFEM and the SACV-SFEM can always obtain the accurate reliability index in 20 iterations when all the variables use the same

or different less than 10^{-6} perturbation size. The computation time of CV-SFEM is about 28 times more than the SACV-SFEM. The FD-SFEM and the SAFD-SFEM can not use the same perturbation size for all the parameters because the large difference of their values. To use the FD-SFEM and the SAFD-SFEM, one must choose suitable perturbation size to obtain the correct reliability index. However, the suitable perturbation size is not known a priori the accuracy of the reliability index obtained has to depend on other verification. The SAFD-SFEM that obtained correct reliability index has a comparable computation time with the SACV-SFEM, while the FD-SFEM has more than 6 times computation time than SAFD-SFEM or SACV-SFEM.

Table 4.7 Computation time and needed iterations of four methods in case 2 of flip chip BAG package

Perturbation	FD-SFEM		SAFD-SFEM		CV-SFEM		SACV-SFEM	
	Compu. Time	Iter.	Compu. Time	Iter.	Compu. Time	Iter.	Compu. Time	Iter.
$\varepsilon_{\boldsymbol{Q}} = \varepsilon_{\boldsymbol{h}} = \varepsilon = 10^{-6}$	X		X		1658	20	59	20
$\varepsilon_{\boldsymbol{Q}} = \varepsilon_{\boldsymbol{h}} = \varepsilon = 10^{-10}$	X		X		1658	20	59	20
$\varepsilon_{\boldsymbol{Q}} = 1.0 \quad \varepsilon_{\boldsymbol{h}} = 10^{-8}$ $\varepsilon = 10^{-3}$	403	20	53	20	1658	20	59	20
$\varepsilon_{\boldsymbol{Q}} = 10^{-1}$ $\varepsilon_{\boldsymbol{h}} = 10^{-10} \quad \varepsilon = 10^{-6}$	403	20	52	20	1658	20	59	20
$\varepsilon_{\boldsymbol{Q}} = 10 \quad \varepsilon_{\boldsymbol{h}} = 10^{-10}$ $\varepsilon = 10^{-8}$	403	20	53	20	1658	20	59	20

"$\varepsilon_{\boldsymbol{Q}}$" is the perturbation size of the hear source. "$\varepsilon_{\boldsymbol{h}}$" is the perturbation size of the height of the DIE. "ε" is the perturbation size of the rest variables. "X" represents not converge.

4.5 Conclusions

The SACV-SFEM combines the semi-analytical algorithm, the CVM with FORM algorithm based SFEM and provides a novel perspective for the application, development, and evaluation of reliability analysis. The SACVM computes consistent, accurate response

sensitivities with incorporating the CVM that doesn't produce any subtraction error. To obtain the response sensitivity with respect to one parameter, the semi-analytical procedure combined in the SACVM only requires doing LU decomposition of global stiffness matrix once, while the FDM has to do LU decomposition twice. Therefore, the SECVM shows more computational efficient than the FDM. This aspect of efficiency shows great advantages in the SACV-SFEM algorithm. In each iteration for searching new design points for $\boldsymbol{n}$ random variables, the LU decomposition of global stiffness matrix can be computed only once for obtaining sensitivities of all $\boldsymbol{n}$ design variables. Comparing to the FDM, the SACV-SFEM saves n times computation time of LU decomposition, which is the most time consuming part in the FORM algorithm.

One test problem, four cases of one benchmark problem and two cases with an electronic BGA packaging application show that the SACV-SFEM can always determine the reliability index very efficiently and is not sensitive to the perturbation size.

An infinitely long hollow cylinder which has the analytical solution is employed to test the reliability of the finite element codes of steady state heat conduction. The relative errors of the heat flow rate per unit length and sensitivities of the heat flow rate per unit length computed by the finite element codes match the analytical solution well. Therefore, the finite element codes for heat conduction can be used for similar heat conduction problems without an analytical solution. The results also show that a finer mesh can improve the accuracy of finite element analysis, however, it decrease the perturbation range for obtaining consistent and accurate sensitivities.

Four cases of the benchmark square plate in linear steady-state heat conduction field were computed by SACV-SFEM to get the reliability index of the implicit limit state function. Comparing to the FD-SFEM, SAFD-SFEM and CV-SFEM, the SACV-SFEM is not sensitive to the relatively big or small perturbation size which however can not be used in the FD-SFEM or the SAFD-SFEM to obtain the right or convergent reliability index. When the perturbation size works for all four methods, the computation time of the SACV-SFEM is comparable to the

SAFD-SFEM and much faster than the FD-SFEM and the CV-SFEM. The reason why the FD-SFEM and the SAFD-SFEM can not use relatively big or small perturbation size is that the sensitivities computed by the FDM or SAFDM are not accurate enough because of the subtraction error.

Further application of the SACV-SFEM to the two cases of electronic BGA packaging problem shows that the SACV-SFEM can always obtain the accurate reliability index without considering the big difference between the values of input random variables. The SACV-SFEM can use only one perturbation size for all the variables. However, the FD-SFEM and the SAFD-SFEM can not obtain convergent correct reliability index by using only one perturbation size for all the variables. The computation time of the SACV-SFEM is much faster than that of the CV-SFEM and the FD-SFEM. The SACV-SFEM shows computation efficiency, accurate and convenient in this electronic packaging problem.

CHAPTER 5

APPLICATION OF THE SACV-SFEM TO LINEAR ELASTIC FRACTURE PROBLEMS

5.1 Introduction

Probabilistic fracture mechanics (PFM) [58] is becoming increasing popular to evaluate the reliability of cracked structures. The theory of fracture mechanics provides a mechanistic relationship between the maximum permissible load acting on a structural component to the size and location of a crack. The theory of probability determines how the uncertainties in crack size, loads and material properties affect the integrity of the cracked structures. The PFM combines the fractures mechanics and probability to describe the actual behavior and reliability of structures than the traditional deterministic models.

A number of papers have been published to estimate statistics of various fracture response and reliability. Grigoriu et al. [59] applied FORM/SORM algorithms to predict the probability of fracture initiation and the confidence interval of the direction of crack extension. Chen and Rahman et al. [60, 61] presented a new method for continuum-based sensitivity and reliability analyses of crack in a homogeneous, isotropic, linear-elastic and nonlinearly elastic body subject to mode-I loading. Rahman [62] studied the adequacy of current J-estimation models commonly used in probabilistic elastic-plastic analysis of ductile cracked structures. Tarcoco [63] presented the shape sensitivity analysis of an elastic solid in equilibrium with a known load system applied over its boundary. Puatatsananon [64] developed a Windows-based framework to undertake probabilistic fracture mechanics. Besterfield [65,66] studied the brittle fracture reliability and fatigue crack growth reliability by PFM. Feijoo et al. [67] presented the shape sensitivities analysis for energy release rate evaluations and its application to the study of three dimensional cracked bodies.

In linear-elastic fracture mechanics (LFEM), the performance function builds on stress intensity factor (SIF). Sensitivities of SIF with respect to load, material parameters and crack size are needed for reliability analysis. In the present chapter, the SACVM is employed to compute sensitivities of SIF in homogeneous, isotropic, and linear-elastic 2D geometries subject to mode-I loading conditions. The sensitivities obtained the SACVM are compared with results from the FDM, SAFDM and CVM. Based on the sensitivities, FORM algorithm based SFEM is applied to predict the reliability of cracked structures with material, load and shape uncertainties. The reliabilities obtained from the SACV-SFEM are compared with the FD-SFEM, SAFD-SFEM and CV-SFEM.

Three cracked specimens such as center cracked tension (CCT), single edge notched tension (SENT) and double edge notched tension (DENT) are used to illustrate consistency, accuracy and efficiency of the proposed SACV-SFEM. The quarter-point parametric elements which can easily represent the specific stress singularities exist at crack tips are used to compute the stress intensity factor of the crack tip.

5.2 Quarter-point Singular Element

The quarter-point singular element was first proposed by Barsoum [68, 69] and independently by Henshell and Shaw [70]. There have been a number of articles written about the quarter-point elements with demonstrations of its efficiency [71, 72, 73]. The quarter-point singular element provides one of the easiest and most powerful techniques for generating singularity at the crack tip. The $\boldsymbol{r}^{-1/2}$ singularity characteristic of linear elastic fracture mechanics is presented by two-dimensional 8-node isoparametric elements when the midside nodes near the crack tip are placed at the quarter points and one side of a quadratic plane element is collapsed, as shown in Figure 5.1

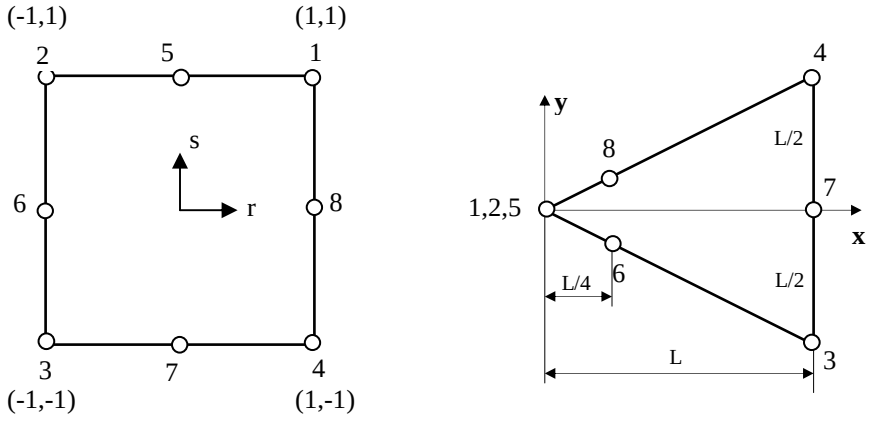

Figure 5.1 Quarter-point singular element, (a) 8-node isoparametric element in natural coordinate, (b) derived element in global coordinate

The shape functions of 8-node isoparametric elements in the natural coordinate system are shown in Equation (5.1).

$$N_1 = \frac{1}{4}(1+r)(1+s)(-1+r+s) \quad N_2 = \frac{1}{4}(1-r)(1+s)(-1-r+s)$$

$$N_3 = \frac{1}{4}(1-r)(1-s)(-1-r-s) \quad N_4 = \frac{1}{4}(1+r)(1-s)(-1+r-s) \tag{5-1}$$

$$N_5 = \frac{1}{2}(1-r^2)(1+s) \qquad N_6 = \frac{1}{2}(1-r)(1-s^2)$$

$$N_7 = \frac{1}{2}(1-r^2)(1-s) \qquad N_8 = \frac{1}{2}(1+r)(1-s^2)$$

The shape functions of 8-node isoparametric elements after one side is collapsed and nodes near the crack tip are placed at the quarter points, as shown in Figure 5.1 (b), are given in Equation (5.2).

$$N_1 = N_1 + N_2 + N_5 = \frac{1}{2}(1+s) - \frac{1}{2}(1-s^2) \quad N_3 = \frac{1}{4}(1-r)(1-s)(-1-r-s)$$

$$N_4 = \frac{1}{4}(1+\boldsymbol{r})(1-\boldsymbol{s})(-1+\boldsymbol{r}-\boldsymbol{s}) \qquad N_6 = \frac{1}{2}(1-\boldsymbol{r})(1-\boldsymbol{s}^2) \tag{5-2}$$

$$N_7 = \frac{1}{2}(1-\boldsymbol{r}^2)(1-\boldsymbol{s}) \qquad N_8 = \frac{1}{2}(1+\boldsymbol{r})(1-\boldsymbol{s}^2)$$

At $\boldsymbol{r} = 0$, $\boldsymbol{x}_1 = 0$, $\boldsymbol{x}_6 = \boldsymbol{x}_8 = \boldsymbol{L}/4$, and $\boldsymbol{x}_3 = \boldsymbol{x}_4 = \boldsymbol{x}_7 = \boldsymbol{L}$, then

$$\boldsymbol{x} = \sum_{\boldsymbol{i}=1}^{8} \boldsymbol{N_i x_i} = \frac{\boldsymbol{L}}{4} - \frac{\boldsymbol{L}}{2}\boldsymbol{s} + \frac{\boldsymbol{L}}{4}\boldsymbol{s}^2 \tag{5-3}$$

Therefore, $\boldsymbol{s} = 1 - 2\sqrt{\frac{\boldsymbol{x}}{\boldsymbol{L}}}$, $\quad 0 \le \boldsymbol{s} \le 1$, and

$$\frac{\boldsymbol{dx}}{\boldsymbol{ds}} = \frac{\boldsymbol{L}(\boldsymbol{s}-1)}{2} = \boldsymbol{L}\left(-\sqrt{\frac{\boldsymbol{x}}{\boldsymbol{L}}}\right) = -\sqrt{\boldsymbol{xL}} \tag{5-4}$$

When $\boldsymbol{x} = 0$, $\frac{\boldsymbol{dx}}{\boldsymbol{ds}} = 0$, which causes the strain is singular at node 1.

The displacement $\boldsymbol{u}$ along x coordinate is given as follows,

$$\boldsymbol{u} = \boldsymbol{N}_1\boldsymbol{u}_1 + \boldsymbol{N}_7\boldsymbol{u}_7 = \left[\frac{1}{2}(1+\boldsymbol{s}) - \frac{1}{2}(1-\boldsymbol{s}^2)\right]\boldsymbol{u}_1 + \left[\frac{1}{2}(1-\boldsymbol{s})\right]\boldsymbol{u}_7 \tag{5-5}$$

The first derivative of $\boldsymbol{x}$ with respect to $\boldsymbol{s}$ is

$$\frac{\boldsymbol{du}}{\boldsymbol{ds}} = \left(\frac{1}{2} + \boldsymbol{s}\right)\boldsymbol{u}_1 - \frac{1}{2}\boldsymbol{u}_7 \tag{5-6}$$

Therefore, the strain in the x direction is

$$\begin{aligned} \varepsilon_{\boldsymbol{xx}} = \frac{\boldsymbol{du}}{\boldsymbol{dx}} &= \frac{\boldsymbol{du}}{\boldsymbol{ds}} \cdot \frac{\boldsymbol{ds}}{\boldsymbol{dx}} = \left[\left(\frac{1}{2} + \boldsymbol{s}\right)\boldsymbol{u}_1 - \frac{1}{2}\boldsymbol{u}_7\right] \cdot \left(\frac{-1}{\sqrt{\boldsymbol{xL}}}\right) \\ &= \frac{-3}{2\sqrt{\boldsymbol{xL}}}\boldsymbol{u}_1 + \frac{2\boldsymbol{u}_1}{\boldsymbol{L}} + \frac{1}{2\sqrt{\boldsymbol{xL}}}\boldsymbol{u}_7 \end{aligned} \tag{5-7}$$

The strain $\varepsilon_{\boldsymbol{xx}}$ shows square root singularity at the crack tip $\boldsymbol{x} = 0$. And the stress field should also show the same square root singularity.

The main advantage of the quarter-point singular element is that it can produce accurate results without requiring a special crack tip element. The standard shape functions are used for the crack tip elements without any change. Only the physical domain of the middle nodes on the element boundaries adjacent to the crack tip is different from the standard shape of the element.

5.3 Computation of Stress Intensity Factor

The methods which are employed to compute the stress intensity factor include displacement correlation technique (DCT), quarter point displacement technique (QPDT), displacement extrapolation technique (DET), reduced displacement extrapolation technique (RDET), limited displacement extrapolation technique (LDET), J-integral technique, Griffith's energy technique, and the stiffness derivative technique. Some researchers compared these techniques. Lim et al. [74] compared DCT, QPDT, DET, RDET and LDET on the basis of extensive numerical analysis, and found that the QPDT generally performs better than the DCT. Both the QPDT and the LDET performed equally well and were superior to the other methods. Banks-sills L. and Sherman D. [75] compared the LDET, J-integral technique, Griffith's energy technique and the stiffness derivative technique for calculating stress intensity factors with quarter-point elements. They found that the stiffness derivative technique yields the most accurate result, whereas LDET is the easiest method to implement and still yields reasonable accuracy.

The FEA software ANSYS [76] employed LDET with quarter-point elements to compute stress intensity factors. In this chapter, LDET with quarter-point elements will be used in the original finite element codes to evaluate the sensitivities of stress intensity factors in cracked structures. The LDET method is introduced below.

The stress intensity factor at a crack for a linear elastic fracture mechanics may be computed using the nodal displacements in the vicinity of the crack. The displacement at and near a crack for linear elastic materials, as shown in Figure 5.2, are [77]:

$$\boldsymbol{u} = \frac{\boldsymbol{K_I}}{2\boldsymbol{G}}\sqrt{\frac{\boldsymbol{r}}{2\pi}}\cos\frac{\theta}{2}\left[\kappa - 1 + 2\sin^2\frac{\theta}{2}\right] + \frac{\boldsymbol{K_{II}}}{2\boldsymbol{G}}\sqrt{\frac{\boldsymbol{r}}{2\pi}}\sin\frac{\theta}{2}\left[\kappa + 1 + 2\cos^2\frac{\theta}{2}\right] + \Omega(\boldsymbol{r})$$

$$\boldsymbol{v} = \frac{\boldsymbol{K_I}}{2\boldsymbol{G}}\sqrt{\frac{\boldsymbol{r}}{2\pi}}\sin\frac{\theta}{2}\left[\kappa + 1 - 2\cos^2\frac{\theta}{2}\right] - \frac{\boldsymbol{K_{II}}}{2\boldsymbol{G}}\sqrt{\frac{\boldsymbol{r}}{2\pi}}\cos\frac{\theta}{2}\left[\kappa - 1 - 2\sin^2\frac{\theta}{2}\right] + \Omega(\boldsymbol{r}) \qquad (5\text{-}8)$$

$$\boldsymbol{w} = \frac{\boldsymbol{K_{III}}}{\boldsymbol{G}}\sqrt{\frac{\boldsymbol{r}}{2\pi}}\sin\frac{\theta}{2} + \Omega(\boldsymbol{r})$$

where, $\boldsymbol{K_I}$, $\boldsymbol{K_{II}}$ and $\boldsymbol{K_{III}}$ are the stress intensity factors relating to opening mode, shearing mode and tearing mode, respectively. $\boldsymbol{u}$, $\boldsymbol{v}$, and $\boldsymbol{w}$ are the displacements in a local Cartesian coordinate system. $\boldsymbol{r}$, θ are the coordinates in a local cylindrical coordinate system, $\boldsymbol{G}$ is the shear modulus. $\Omega(\boldsymbol{r})$ is terms of order r or higher.

$$\kappa = \begin{cases} 3 - 4\nu & \text{if plane strain or axisymmetric} \\ \dfrac{3\nu}{1+\nu} & \text{if plane stress} \end{cases} \qquad (5\text{-}9)$$

and ν is the poisson's ratio.

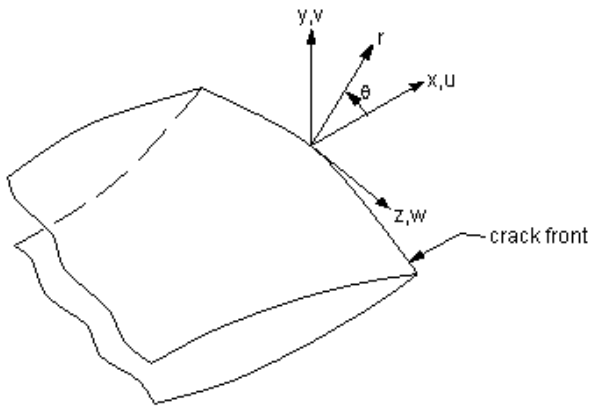

Figure 5.2 Local coordinates of the crack front

Dropping the higher order and evaluating at $\theta = 180^{\circ}$, the displacement expressions yield

$$u = \frac{K_{II}}{2G}\sqrt{\frac{r}{2\pi}}(1+\kappa)$$

$$v = \frac{K_{I}}{2G}\sqrt{\frac{r}{2\pi}}(1+\kappa) \tag{5-10}$$

$$w = \frac{2K_{III}}{G}\sqrt{\frac{r}{2\pi}}$$

For models symmetric about the crack plane, as shown in Figure 5.3, K_I, K_{II} and K_{III} can be obtained as

$$K_I = \sqrt{2\pi}\frac{2G}{1+\kappa}\frac{|v|}{\sqrt{r}}$$

$$K_{II} = \sqrt{2\pi}\frac{2G}{1+\kappa}\frac{|u|}{\sqrt{r}} \tag{5-11}$$

$$K_{III} = \sqrt{2\pi}\frac{2G}{1+\kappa}\frac{|w|}{\sqrt{r}}$$

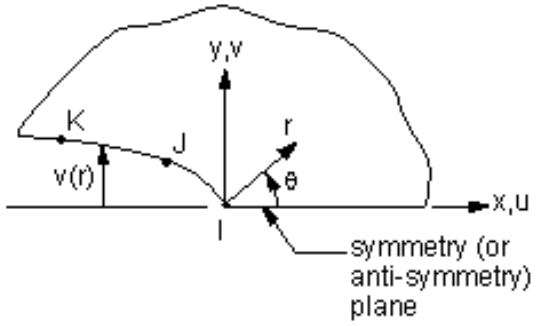

Figure 5.3 Nodes used for computing the stress intensity factor

To compute K_I (same procedure can be used for K_{II} and K_{III}), the factor $\frac{|v|}{\sqrt{r}}$ needs to be evaluated based on the nodal displacement and locations. Three nodes I, J, and K

at and near crack tips are used, as shown in Figure 5.3. The relationship between the $\frac{|v|}{\sqrt{r}}$ and r can be computed at nodes J and K as follows

$$\frac{|v|}{\sqrt{r}} = A + Br \tag{5-12}$$

When r approaches 0

$$\lim_{r \to 0} \frac{|v|}{\sqrt{r}} = A \tag{5-13}$$

Thus, K_I is evaluated as

$$K_I = \sqrt{2\pi}\,\frac{2G}{1+\kappa}\,A \tag{5-14}$$

K_{II} and K_{III} can be obtained in the same manner.

5.4 Reliability Analysis of Center Cracked Tension (CCT) Specimen

Consider a center cracked tension specimen (CCT) with width $2W = 20$ m, length $2L = 20$ m and crack length $2a$, subjected to a far-field tensile stress, $\sigma = 100$ MPa, as shown in Figure 5.4. The crack size $a/W = 0.1$ is considered. The elastic modulus and Poisson's ratio ν are 10^7 MPa and 0.3, respectively. The plane strain condition is studied.

Due to the double symmetry of this specimen, ¼ model is used to do the finite element analysis. 8-node quadratic isoparametic elements are employed. Around the crack tip, the 8-node quadratic elements are collapsed into 6-node triangular elements. The model consists of 1544 nodes and 495 elements. A 2×2 Gaussian integration is used. The mesh of the model is shown in Figure 5.5. The displacement distribution of the quarter model is shown in Figure 5.6.

5.4.1 Sensitivity analysis of CCT specimen

One of the polynomial formulas of SIF for CCT specimen is given by [78, 79]

$$K_I = \sigma\sqrt{\pi a}\left[\sec\left(\frac{\pi a}{2W}\right)\right]^{1/2}\left[1-0.025\left(\frac{a}{W}\right)^2+0.06\left(\frac{a}{W}\right)^4\right] \quad (5\text{-}15)$$

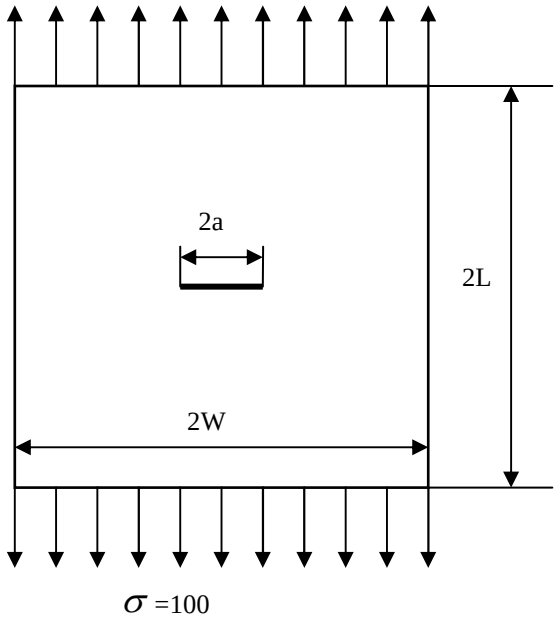

Figure 5.4 Center cracked tension (CCT) specimen

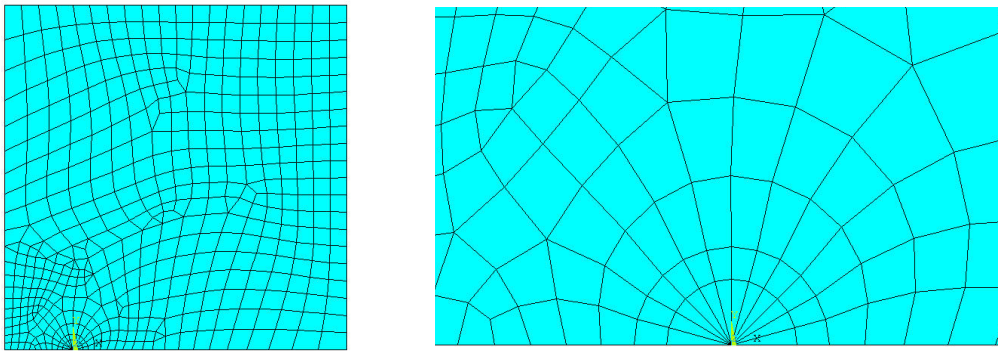

(a) (b)

Figure 5.5 Mesh of the CCT specimen, (a) mesh of ¼ model, (b) mesh around crack tip

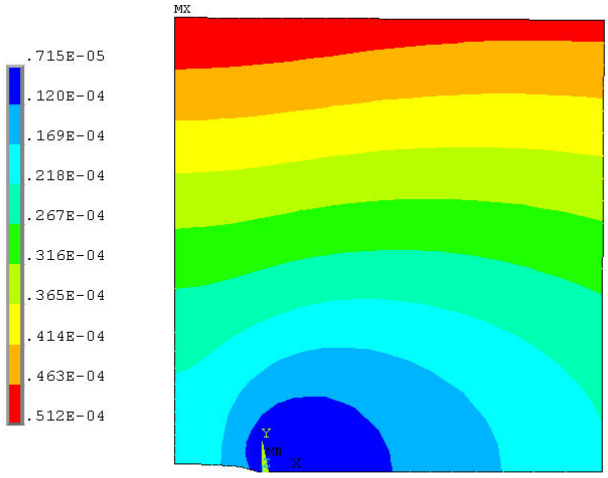

Figure 5.6 Displacement distribution of ¼ CCT specimen

From the equation (5-15), the sensitivity of SIF with respect to the crack length dK_I / da at $W = 10$ m and $\sigma = 100$ MPa is $99.766\ \mathrm{MPa}\sqrt{\mathrm{m}}$. The sensitivity of SIF with respect to the tensile stress $dK_I / d\sigma$ at $W = 10$ m and $a = 1$ m is 1.8158.

The sensitivities of SIF with respect to the crack size, tensile stress and poisson's ratio computed by the FDM, SAFDM, SACVM and CVM are shown in Table 5.1, Table 5.2 and Table 5.3.

Table 5.1 Sensitivity of SIF with respect to the crack size, dK_I / da in CCT specimen

Perturbation size	FD	SAFD	SACV	CV
10^{-3}	93.5368	-101.3587	98.1126	100.2327
10^{-4}	99.7608	79.9219	100.4396	100.4608
10^{-5}	100.5316	98.4053	100.4629	100.4633
10^{-6}	103.4085	100.2573	100.4632	100.4633
10^{-7}	97.4671	100.4426	100.4632	100.4633
10^{-8}	171.1704	100.4611	100.4632	100.4632
10^{-9}	404.7838	100.4732	100.4632	100.4632
10^{-10}	624.9705	100.6222	100.4632	100.4632
10^{-11}	3.4373E5	101.4854	100.4632	100.4632
10^{-12}	2.5916E6	103.0571	100.4632	100.4632

Table 5.2 Sensitivity of SIF with respect to the tensile stress, $dK_I / d\sigma$ in CCT specimen

Perturbation size	FD	SAFD	SACV	CV
10^{-3}	1.8721	1.8721	1.8721	1.8721
10^{-4}	1.8721	1.8721	1.8721	1.8721
10^{-5}	1.8721	1.8721	1.8721	1.8721
10^{-6}	1.8721	1.8721	1.8721	1.8721
10^{-7}	1.8721	1.8721	1.8721	1.8721
10^{-8}	1.8721	1.8721	1.8721	1.8721
10^{-9}	1.8721	1.8721	1.8721	1.8721
10^{-10}	1.8721	1.8716	1.8721	1.8721
10^{-11}	1.8673	1.8474	1.8721	1.8721
10^{-12}	1.8758	1.8758	1.8721	1.8721

Table 5.3 Sensitivity of SIF with respect to the Poisson's ratio, $dK_I / d\nu$ in CCT specimen

Perturbation size	FD	SAFD	SACV	CV
10^{-3}	0.4928	-0.5452	0.5009	0.4953
10^{-4}	0.4874	0.3918	0.4954	0.4953
10^{-5}	0.4965	0.4850	0.4953	0.4953
10^{-6}	2.7374	0.4943	0.4953	0.4953
10^{-7}	22.1521	0.4953	0.4953	0.4953
10^{-8}	546.9623	0.4967	0.4953	0.4953
10^{-9}	-412.524	0.5093	0.4953	0.4954
10^{-10}	5044.718	0.5360	0.4953	0.4953
10^{-11}	2.9156E5	2.6744	0.4953	0.4953
10^{-12}	1.6455E4	13.8414	0.4953	0.4953

The relative error of the sensitivities of SIF with respect to variables, $\boldsymbol{x} = (a, \sigma, \nu)$ is defines as

$$\varepsilon_r = \frac{\left(dK_I / dx\right)_{FEM} - \left(dK_I / dx\right)_{FORMULA}}{\left(dK_I / dx\right)_{FORMULA}} \times 100\% \quad (5\text{-}16)$$

where $\left(dK_I / dx\right)_{FEM}$ are the sensitivities computed by FEM codes, and $\left(dK_I / dx\right)_{FORMULA}$ are the sensitivities obtained from the equation (5-16).

At different perturbation size, the relative errors of the sensitivities of SIF with respect to crack length a, tensile stress σ computed by the FDM, the SAFDM, the SACVM and the CVM are shown in Figure 5.7 and Figure 5.8, respectively. The sensitivities of SIF with respect to poisson's ration ν by four methods are shown in Figure 5.9.

From Figure 5.7 to Figure 5.9, the sensitivities dK_I / da, $dK_I / d\sigma$ and $dK_I / d\upsilon$ computed by the SACVM and the CVM keep stable when the perturbation sizes are less than 10^{-4}. The sensitivities computed by the SAFDM vary very few when the perturbation sizes are in a certain range. However, because of the subtraction error, the sensitivities oscillate when the perturbation sizes is smaller than 10^{-10}. The sensitivities dK_I / da and $dK_I / d\upsilon$ computed by finite difference method (FDM) at different perturbation sizes have large difference. Further research found that the global stiffness matrix K in the linear system $Ku = f$ had a large condition number, 5.68×10^{10}, which means the linear system $Ku = f$ is ill-conditioned.

To computing the sensitivities by FDM accurately, a simple iterative procedure [80] is introduced to solve linear system $Ku = f$. Let $u^{(0)}$ be the approximate solution of the system. Define the residue vector $r^{(0)} = f - Ku^{(0)}$. Then find the solution vector $z^{(1)}$ for the system

$$Kz^{(1)} = f - Ku^{(0)} = r^{(0)} \quad (5\text{-}17)$$

and set $\boldsymbol{u}^{(1)} = \boldsymbol{u}^{(0)} + \boldsymbol{z}^{(1)}$. With $\boldsymbol{u}^{(1)}$ we can form the new residue vector $\boldsymbol{r}^{(1)} = \boldsymbol{f} - \boldsymbol{K}\boldsymbol{u}^{(1)}$, and repeat the process until the successively corrected solution vector do not change any more or until the relative improvement satisfies

$$\frac{\left|\boldsymbol{z}^{(i+1)}\right|}{\left|\boldsymbol{u}^{(i)}\right|} < \varepsilon \text{ for an } \varepsilon > 0 \tag{5-18}$$

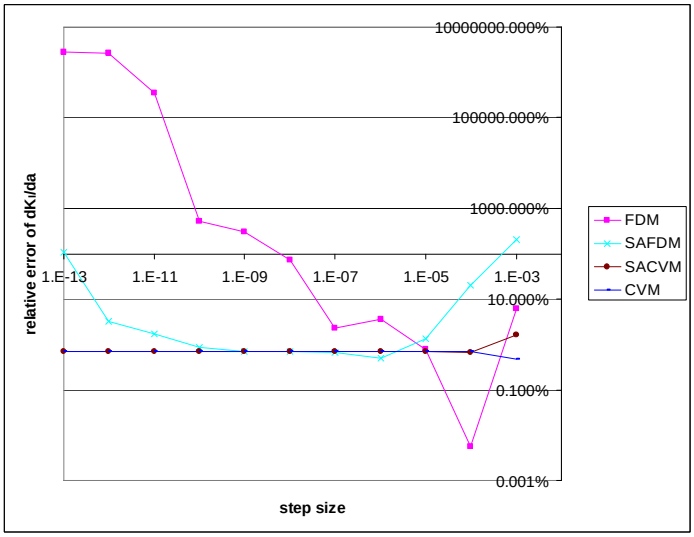

Figure 5.7 Relative error of $\boldsymbol{dK_I / da}$ via perturbation size in CCT specimen

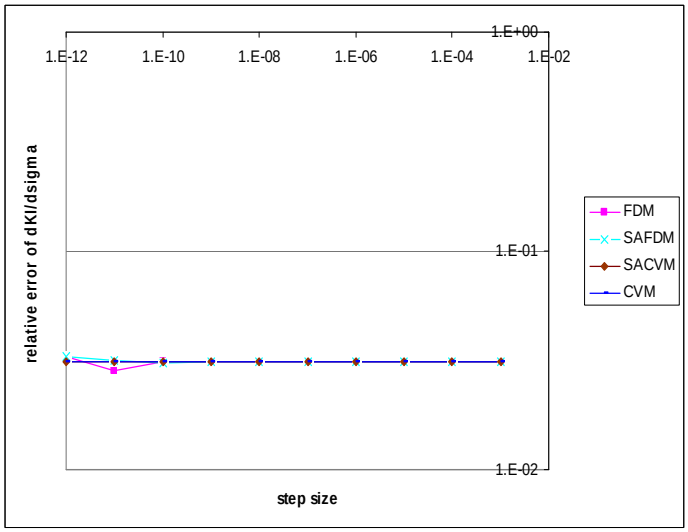

Figure 5.8 Relative error of $\boldsymbol{dK_I / d\sigma}$ via perturbation size in CCT specimen

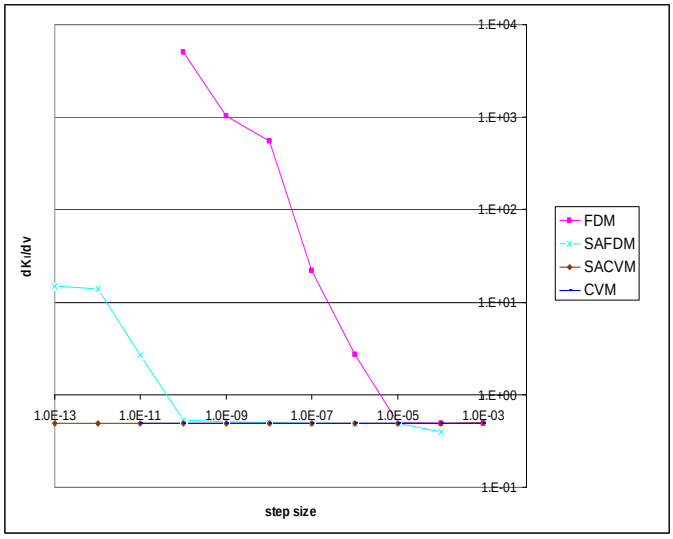

Figure 5.9 $dK_I / d\upsilon$ via perturbation size in CCT specimen

Therefore, the final solution of the linear system is

$$\boldsymbol{u} = \boldsymbol{u}^{(i+1)} = \boldsymbol{u}^{(i)} + \boldsymbol{z}^{(i+1)} \tag{5-19}$$

The iterative procedure is applied in the FDM to obtain the sensitivities of SIF with respect to the crack length, and poisson's ratio. The comparisons of relative errors of the sensitivities dK_I / da and $dK_I / d\upsilon$ computed by the FDM with or without the iterative procedure are shown in Figure 5.10 and Figure 5.11, respectively. Two figures show that the iterative procedure improved the accuracy of the sensitivities of SIF computed by FDM in a certain range. Out of this range, because of the subtraction error, the sensitivities are not accurate.

Generally, comparing the sensitivities computed by the SACVM with by other three methods, the sensitivities computed by the SACVM are more consistent, accurate and not sensitive to the perturbation size. The ill-conditioned linear system doesn't affect the accuracy of the sensitivities computed by the SACVM and the SAFDM, while it causes the oscillation of the sensitivities computed by the FDM. The sensitivities computed by SAFDM are sensitive to the small perturbation size because of the subtraction error. The sensitivities computed by the

SACVM are as accurate as those computed by the CVM. However, the computation time of the SACVM are much less than the CVM, and is comparable with the SAFDM.

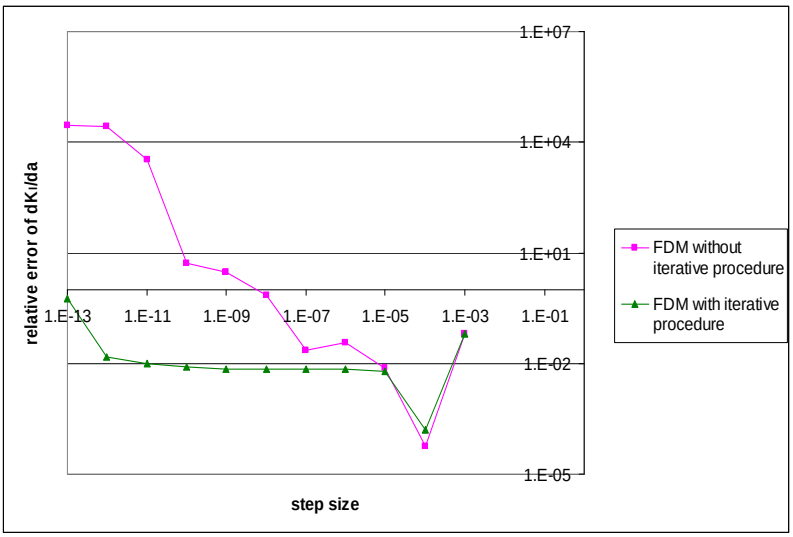

Figure 5.10 Relative error of dK_I/da via perturbation size with or without iterative procedure in CCT specimen

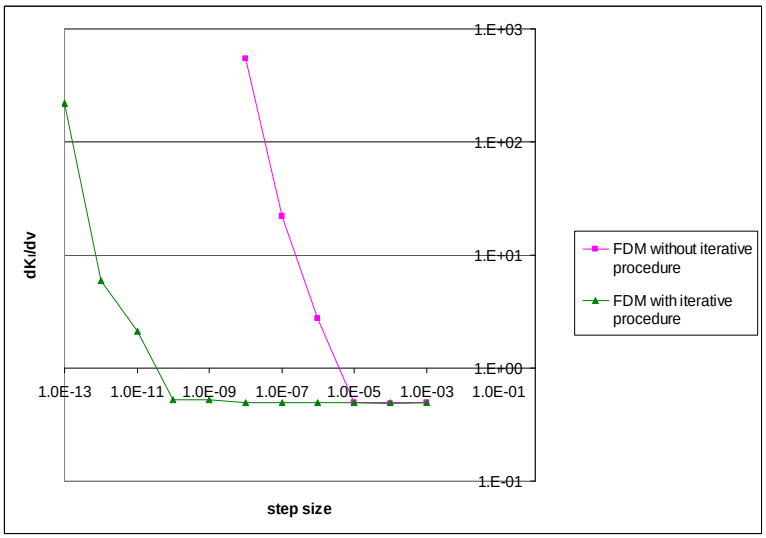

Figure 5.11 dK_I/dv via perturbation size with or without iterative procedure in CCT specimen

5.4.2 Reliability analysis of CCT specimen

The crack size, tensile stress and Poisson's ratio are treated as normally-distributed independent random variables, $a = N(1\text{m}, 0.05\text{m})$, $\sigma = N(100\text{MPa}, 5\text{MPa})$ and

$\nu = \boldsymbol{N}(0.3, 0.01)$, respectively. The reliability index is computed by using sensitivity-based FORM.

The limit state function is defined as

$$\boldsymbol{p} = \boldsymbol{K_I} - 190 \tag{5-20}$$

where 190 $\mathrm{MPa}\sqrt{\mathrm{m}}$ is the maximum allowable value of $\boldsymbol{K_I}$.

At different perturbation size, the reliability index β as well as needed iterations $\boldsymbol{N}$ and computation time $\boldsymbol{T}$ computed by the FD-SFEM, SAFD-SFEM, SACV-SFEM and CV-SFEM are listed in Table 5.4.

Table 5.4 shows the SACV-SFEM and the CV-SFEM can always obtain stable reliability index when the perturbation size is equal or less than 10^{-4}. However, to obtain the same accurate reliability index, the computation time of the CV-SFEM is 5.8 times than that of the SACV-SFEM. When the perturbation size is less than 10^{-8}, the FD-SFEM is not able to obtain the accurate reliability index because the sensitivities of SIF with respect to the crack length and poisson's ratio are far away from the real values. Furthermore, the FD-SFEM needs 3.4 times more computation time than the SACV-SFEM. The SAFD-SFEM has comparable computation time with the SACV-SFEM, however it is not suitable for the small perturbation sizes. When the perturbation size is equal or less than 10^{-12}, the SAFDM can not obtain the accurate reliability index.

5.5 Reliability Analysis of Single Edge Notched Tension (SENT) Specimen

Consider a single edge notched tension specimen (SENT) with width $\boldsymbol{W} = 5$ m, length $\boldsymbol{L} = 10$ m and crack length $\boldsymbol{a} = 1$ m, subjected to a far-field tensile stress, $\sigma = 100$ MPa, as shown in Figure 5.12. The elastic modulus and Poisson's ratio ν are 10^7 MPa and 0.3, respectively. In this case the plane strain condition is studied.

Table 5.4 Reliability analysis of CCT specimen by four methods

		Perturbation size			
		$\varepsilon = 10^{-4}$	$\varepsilon = 10^{-6}$	$\varepsilon = 10^{-8}$	$\varepsilon = 10^{-12}$
FD-SFEM (without iterative procedure)	Reliability Index	0.2772	0.2767	0.2095	-
	Iterations	5	5	61	-
	Compu. Time (s)	2100	2100	24370	-
SAFD-SFEM	Reliability Index	0.2788	0.2772	0.2772	0.2795
	Iterations	5	5	5	8
	Compu. Time (s)	610	610	610	910
SACV-SFEM	Reliability Index	0.2772	0.2772	0.2772	0.2772
	Iterations	5	5	5	5
	Compu. Time (s)	610	610	610	610
CV-SFEM	Reliability Index	0.2772	0.2772	0.2772	0.2772
	Iterations	5	5	5	5
	Compu. Time (s)	3560	3560	3560	3560

"-"represents not convergent.

Due to the symmetry of this specimen, half model is used to do the finite element analysis. Same mesh is generated with CCT specimen in section 5.4 Figure 5.5. The half model consists of 1544 nodes and 495 elements. The displacement distribution of the half model is shown in Figure 5.13.

5.5.1 Sensitivity analysis of SENT specimen

One of the polynomial formulas of SENT specimen is given by [78, 79]

$$\boldsymbol{K_I} = \sigma\sqrt{\boldsymbol{W}}\frac{\left[2\tan\left(\frac{\pi \boldsymbol{a}}{2\boldsymbol{W}}\right)\right]^{1/2}}{\cos\left(\frac{\pi \boldsymbol{a}}{2\boldsymbol{W}}\right)}\left[0.752 + 2.02\left(\frac{\boldsymbol{a}}{\boldsymbol{W}}\right) + 0.37\left(1-\sin\frac{\pi \boldsymbol{a}}{2\boldsymbol{W}}\right)^3\right] \qquad (5\text{-}21)$$

From the equation (5-20), the sensitivity of SIF with respect to the crack length $\boldsymbol{dK_I}/\boldsymbol{da}$ at $\boldsymbol{W} = 5$ m and $\sigma = 100$ MPa is $200.7546\ \text{MPa}\sqrt{\text{m}}$. The sensitivity of SIF with respect to the tensile stress $\boldsymbol{dK_I}/\boldsymbol{d\sigma}$ at $\boldsymbol{W} = 5$ m and $\boldsymbol{a} = 1$ m is 2.4233.

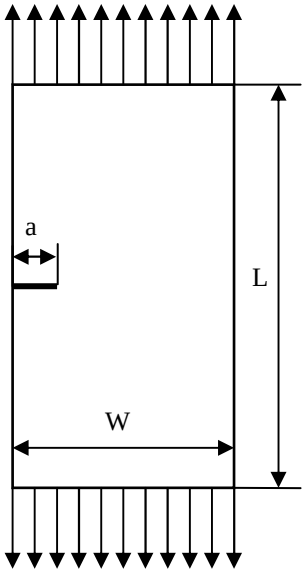

Figure 5.12 Single edge notched tension (SENT) specimen

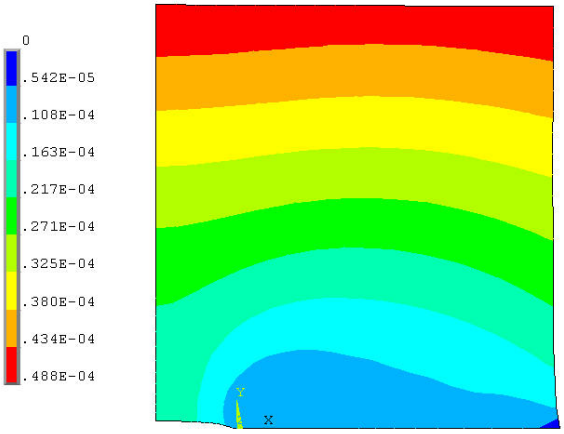

Figure 5.13 Displacement distribution of ½ SENT specimen

The sensitivities of SIF with respect to the crack size, tensile stress and poisson's ratio computed by the FDM, the SAFDM, the SACVM and the CVM are shown in Table 5.5, Table 5.6 and Table 5.7.

At different perturbation size, the relative errors of the sensitivities of SIF with respect to crack length $\boldsymbol{a}$, tensile stress σ computed by the FDM, the SAFDM, the SACVM and the CVM are shown in Figure 5.14 and Figure 5.15, respectively. The sensitivities of SIF with respect to poisson's ration ν computed by four methods are shown in Figure 5.16.

Table 5.5 Sensitivity of SIF with respect to the crack size, dK_I / da in SENT specimen

Perturbation size	FD	SAFD	SACV	CV
10^{-3}	195.9124	-64.4837	201.1314	204.0425
10^{-4}	203.4683	176.9602	204.2964	204.3255
10^{-5}	204.1058	201.5865	204.3280	204.3284
10^{-6}	204.1403	204.0541	204.3284	204.3284
10^{-7}	195.4949	204.3009	204.3284	204.3284
10^{-8}	330.6749	204.3252	204.3284	204.3284
10^{-9}	346.6641	204.3172	204.3284	204.3284
10^{-10}	-17558.88	204.2557	204.3284	204.3284
10^{-11}	17458.61	204.4942	204.3284	204.3284
10^{-12}	-189870.3	196.9624	204.3284	204.3284

The iterative procedure which has been applied in Section 5.4.1 is applied in the FDM to obtain more accurate sensitivities of SIF with respect to the crack length, and poisson's ratio. The comparisons of relative errors of the sensitivities dK_I / da and $dK_I / d\upsilon$ computed by the FDM with or without the iterative procedure are shown in Figure 5.17 and Figure 5.18, respectively.

Generally, comparing the sensitivities computed by the FDM with the other three methods, the sensitivities computed by the SACVM are more consistent, accurate and not sensitive to the perturbation size. The ill-conditioned linear system which causes the oscillation of the sensitivities computed by the FDM doesn't affect the accuracy of the sensitivities computed by the SACVM and SAFDM. The sensitivities computed by the SAFDM are sensitive to small perturbation size because of the subtraction error. However, the sensitivities computed by the SACVM are not sensitive to perturbation size at all. The sensitivities computed by the SACVM are as accurate as those computed by the CVM. However, the computation time of the SACVM is much less than the CVM, and is comparable with the SAFDM.

Table 5.6 Sensitivity of SIF with respect to the tensile stress, $dK_I / d\sigma$ in SENT specimen

Perturbation size	FD	SAFD	SACV	CV
10^{-3}	2.4244	2.4244	2.4244	2.4244
10^{-4}	2.4244	2.4244	2.4244	2.4244
10^{-5}	2.4244	2.4244	2.4244	2.4244
10^{-6}	2.4244	2.4243	2.4244	2.4244
10^{-7}	2.4244	2.4243	2.4244	2.4244
10^{-8}	2.4244	2.4243	2.4244	2.4244
10^{-9}	2.4244	2.4243	2.4244	2.4244
10^{-10}	2.4247	2.4247	2.4244	2.4244
10^{-11}	2.4272	2.4274	2.4244	2.4244
10^{-12}	2.4727	2.4158	2.4244	2.4244

Table 5.7 Sensitivity of SIF with respect to the Poisson's ratio, $dK_I / d\nu$ in SENT specimen

Perturbation size	FD	SAFD	SACV	CV
10^{-3}	0.4752	-0.8742	0.4813	0.4741
10^{-4}	0.4642	0.34	0.4742	0.4741
10^{-5}	0.3462	0.4607	0.4741	0.4741
10^{-6}	-1.3823	0.4727	0.4741	0.4741
10^{-7}	-2.0674	0.4738	0.4741	0.4741
10^{-8}	-189.9566	0.4753	0.4741	0.4741
10^{-9}	-1305.79	0.4756	0.4741	0.4741
10^{-10}	-14693.27	0.3629	0.4741	0.4741
10^{-11}	106917.7	-1.2193	0.4741	0.4741
10^{-12}	-665888	4.2917	0.4741	0.4741

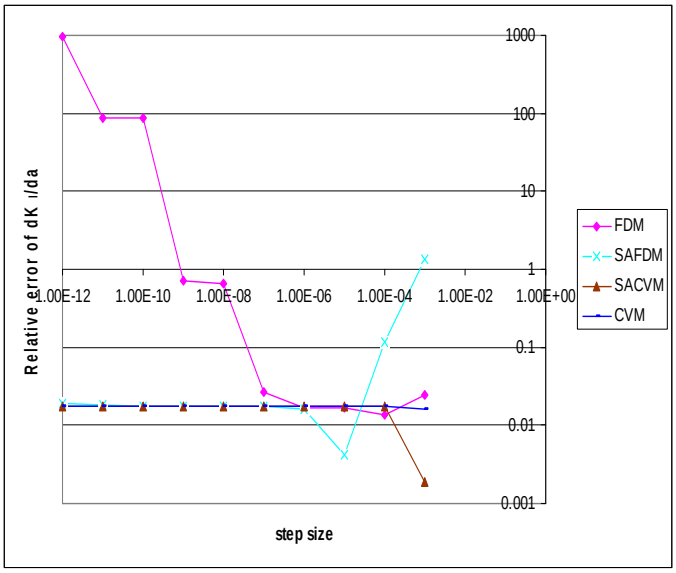

Figure 5.14 Relative error of dK_I / da via perturbation size in SENT specimen

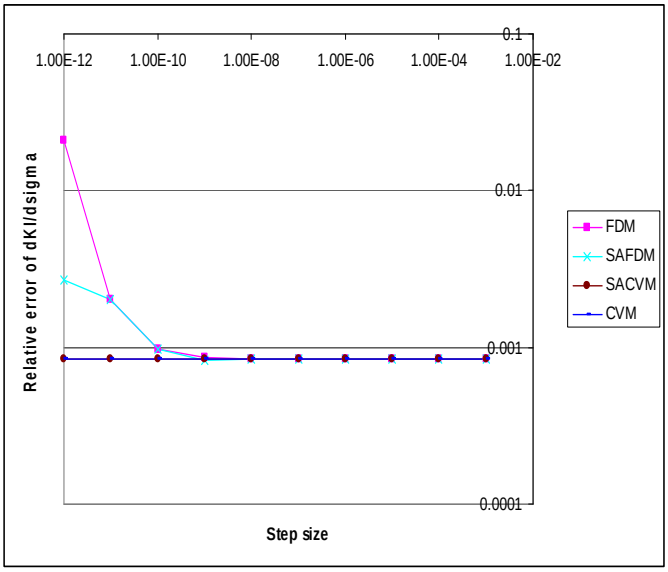

Figure 5.15 Relative error of $dK_I / d\sigma$ via perturbation size in SENT specimen

5.5.2 Reliability analysis of SENT specimen

Similar to Section 5.4.2, the crack size, tensile stress and poisson's ratio are treated as normally-distributed independent random variables, $a = N(1\text{m}, 0.05\text{m})$,

$\sigma = (100\text{MPa}, 5\text{MPa})$ and $\nu = \boldsymbol{N}(0.3, 0.01)$, respectively. The reliability index is computed using sensitivity-based FORM.

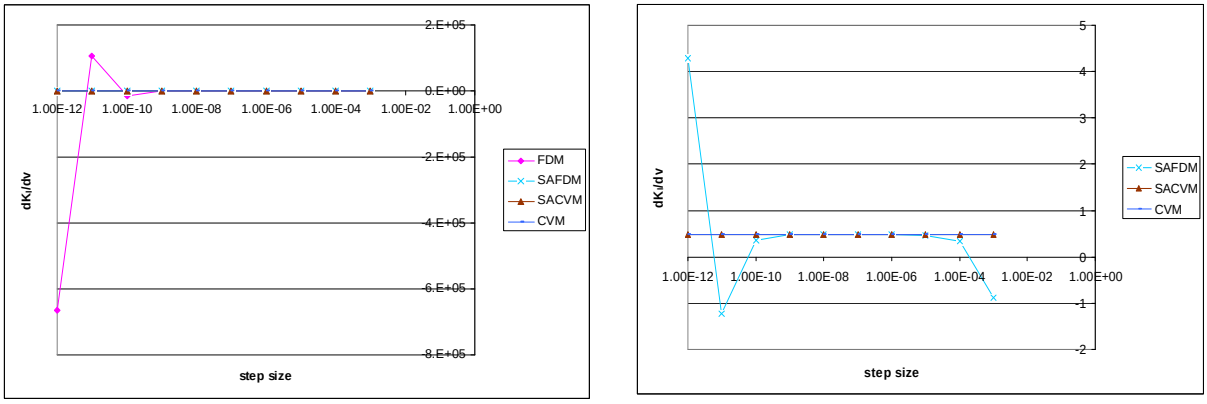

(a) (b)

Figure 5.16 $\boldsymbol{dK_I / d\nu}$ via perturbation size in SENT specimen, (a) Comparison of four methods, (b) Comparison of three methods

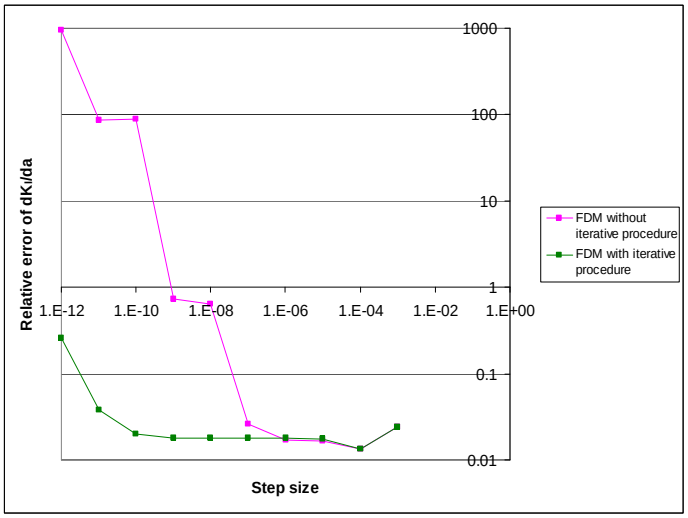

Figure 5.17 Relative error of $\boldsymbol{dK_I / da}$ via perturbation size with or without iterative procedures in SENT specimen

The limit state function is defined as

$$\boldsymbol{p} = \boldsymbol{K_I} - 230 \tag{5-22}$$

where 230 $\text{MPa}\sqrt{\text{m}}$ is the maximum allowable value of $\boldsymbol{K_I}$.

At different perturbation size, the reliability index β as well as needed iterations N and computation time T computed by the FD-SFEM, SAFD-SFEM, SACV-SFEM, and CV-SFEM are listed in Table 5.8.

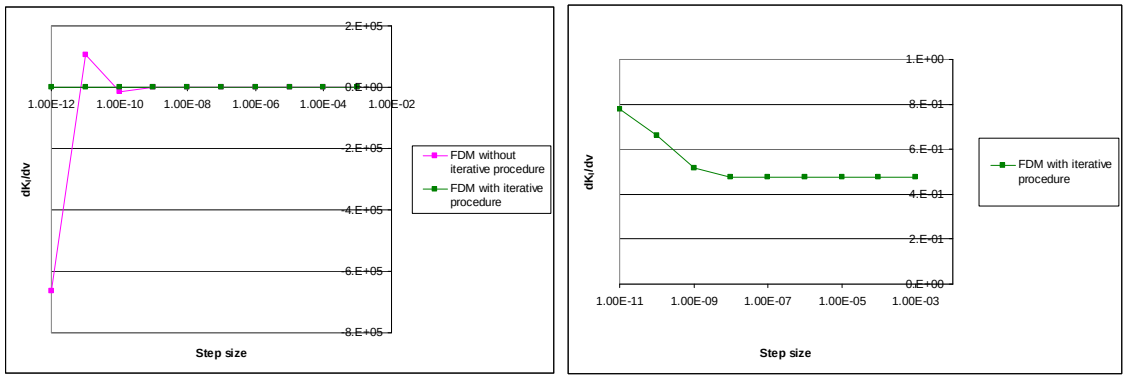

(a) (b)

Figure 5.18 dK_I/dv via perturbation size (a) without and with iterative procedure, (b) with iterative procedure, in SENT specimen

Table 5.8 Reliability analysis of SENT specimen by four methods

		Perturbation size			
		$\varepsilon = 10^{-4}$	$\varepsilon = 10^{-6}$	$\varepsilon = 10^{-8}$	$\varepsilon = 10^{-12}$
FD-SFEM (without iterative procedure)	Reliability Index	0.3774	0.3775	0.3782	-
	Iterations	6	6	5	-
	Computation Time (s)	2500	2500	2090	-
SAFD-SFEM	Reliability Index	0.3774	0.3775	0.3775	0.3774
	Iterations	5	6	6	6
	Computation Time (s)	840	840	840	840
SACV-SFEM	Reliability Index	0.3775	0.3775	0.3775	0.3775
	Iterations	6	6	6	6
	Computation Time (s)	840	840	840	840
CV-SFEM	Reliability Index	0.3775	0.3775	0.3775	0.3775
	Iterations	6	6	6	6
	Computation Time (s)	4250	4250	4250	4250

Table 5.8 shows that the SACV-SFEM and the CV-SFEM can always obtain stable reliability index when the perturbation size is equal or less than 10^{-4}. However, the computation time of the CV-SFEM is five times more than that of the SACV-SFEM. The SAFD-SFEM has comparable computation time with the SACV-SFEM and obtained correct reliability index even if the sensitivities of SIF are inaccurate, which readily mislead people to believe that the SAFD-SFEM can always obtain reliable solution, or whether the response sensitivity is accurate will not affect the final reliability index. The reliability indexes computed by the FD-SFEM vary with the perturbation. When the perturbation size is 10^{-12}, convergent reliability index can not be obtained because the sensitivities of SIF with respect to the crack length and poisson's ratio are far away from the real values. The computation cost of the FD-SFEM is 3 times more than the SACV-SFEM.

5.6 Reliability Analysis of Double Edge Notched Tension (DENT) Specimen

Consider a double edge notched tension specimen (DENT) with width $\boldsymbol{W} = 10$ m, length $\boldsymbol{L} = 10$ m and crack length $\boldsymbol{a} = 1$ m at both edges, subjected to a far-field tensile stress, $\sigma = 100$ MPa, as shown in Figure 5.19. The elastic modulus and Poisson's ratio ν are 10^7 MPa and 0.3, respectively. The plane strain condition is studied.

Due to the double symmetry of the DENT specimen, quarter model is used to do the finite element analysis. Same mesh is generated with CCT specimen in section 5.4 Figure 5.5. The quarter model consists of 1544 nodes and 495 elements. The displacement distribution of the quarter model is shown in Figure 5.20.

5.6.1 Sensitivity analysis of DENT specimen

One of the polynomial formulas of DENT specimen is given by [78, 79]

$$\boldsymbol{K_I} = \frac{\sigma\sqrt{\pi \boldsymbol{a}}}{\sqrt{\left(1-\frac{\boldsymbol{a}}{\boldsymbol{W}}\right)}}\left[1.122 - 0.561\left(\frac{\boldsymbol{a}}{\boldsymbol{W}}\right) - 0.205\left(\frac{\boldsymbol{a}}{\boldsymbol{W}}\right)^2 + 0.471\left(\frac{\boldsymbol{a}}{\boldsymbol{W}}\right)^3 + 0.190\left(\frac{\boldsymbol{a}}{\boldsymbol{W}}\right)^4\right] \quad (5\text{-}23)$$

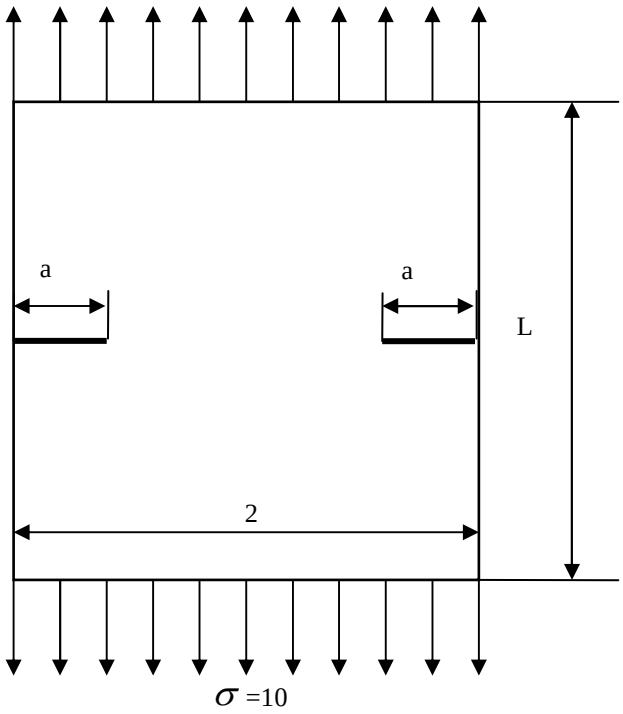

Figure 5.19 Double edge notched tension (DENT) specimen

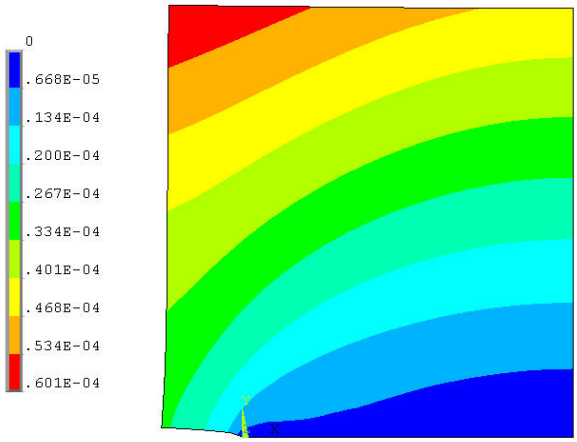

Figure 5.20 Displacement distribution of ¼ DENT specimen

From the equation (5-23), the sensitivity of SIF with respect to the crack length, dK_I / da at $2W = 10$ m and $\sigma = 100$ MPa is 100.3148. The sensitivity of SIF with respect to the tensile stress, $dK_I / d\sigma$ at $2W = 10$ and $a = 1$ is 1.9731.

The sensitivities of SIF with respect to the crack size, tensile stress and poisson's ratio are shown in Table 5.9, Table 5.10 and Table 5.11.

At different perturbation size, the relative errors of the sensitivities of SIF with respect to crack length a, tensile stress σ are shown in Figure 5.21 and Figure 5.22, respectively. The sensitivities of SIF with respect to poisson's ration ν are shown in Figure 5.23.

Table 5.9 Sensitivity of SIF with respect to the crack size, dK_I / da in DENT specimen

Perturbation size	FD	SAFD	SACV	CV
10^{-3}	111.9904	108.1984	116.6965	119.1434
10^{-4}	118.6471	96.2238	119.3658	119.3903
10^{-5}	119.5451	117.0717	119.3925	119.3928
10^{-6}	120.5269	119.1607	119.3928	119.3928
10^{-7}	120.1621	119.3696	119.3928	119.3928
10^{-8}	239.2935	119.3901	119.3928	119.3928
10^{-9}	1402.559	119.3841	119.3928	119.3928
10^{-10}	12429.45	119.3385	119.3928	119.3928
10^{-11}	73078.16	119.5559	119.3928	119.3928
10^{-12}	9.975E5	113.5732	119.3958	119.3928

Table 5.10 Sensitivity of SIF with respect to the tensile stress, $dK_I / d\sigma$ in DENT specimen

Perturbation size	FD	SAFD	SACV	CV
10^{-3}	0.4815	-0.6811	0.4857	0.4795
10^{-4}	0.4915	0.3641	0.4796	0.4795
10^{-5}	0.6415	0.4680	0.4795	0.4795
10^{-6}	0.8295	0.4783	0.4795	0.4795
10^{-7}	5.7987	0.4793	0.4795	0.4795
10^{-8}	253.8486	0.4797	0.4795	0.4795
10^{-9}	1438.017	0.4755	0.4795	0.4795
10^{-10}	12607.29	0.3874	0.4795	0.4795
10^{-11}	129644.5	-0.7304	0.4795	0.4795
10^{-12}	1.2172E6	-5.5422	0.4795	0.4795

Table 5.11 Sensitivity of SIF with respect to the Poisson's ratio, $dK_I / d\nu$ in DENT specimen

Perturbation size	FD	SAFD	SACV	CV
10^{-3}	2.0873	2.0873	2.0873	2.0873
10^{-4}	2.0873	2.0873	2.0873	2.0873
10^{-5}	2.0873	2.0873	2.0873	2.0873
10^{-6}	2.0873	2.0873	2.0873	2.0873
10^{-7}	2.0873	2.0873	2.0873	2.0873
10^{-8}	2.0873	2.0873	2.0873	2.0873
10^{-9}	2.0874	2.0874	2.0873	2.0873
10^{-10}	2.0870	2.0884	2.0873	2.0873
10^{-11}	2.0918	2.0918	2.0873	2.0873
10^{-12}	2.1601	2.1601	2.0873	2.0873

The iterative procedure which has been applied in Section 5.4.1 is applied in the FDM to obtain more accurate sensitivities of SIF with respect to the crack length, and poisson's ratio. The comparisons of relative errors of the sensitivities dK_I / da and $dK_I / d\upsilon$ computed by the FDM with or without the iterative procedure are shown in Figure 5.24 and Figure 5.25, respectively.

Generally, comparing the sensitivities computed by the FDM with the other three methods, the sensitivities computed by the SACVM are more accurate and not sensitive to the perturbation size. The ill-conditioned linear system which causes the oscillation of the sensitivities computed by the FDM doesn't affect the accuracy of the sensitivities computed by the SACVM and the SAFDM. The sensitivities computed by the SAFDM are sensitive to the perturbation size because of the subtraction error. However, the sensitivities computed by the SACVM are not sensitive to the perturbation size at all. The sensitivities computed by the SACVM are as accurate as those computed by the CVM. However, the computation time of the SACVM is much less than the CVM, and is comparable with the SAFDM.

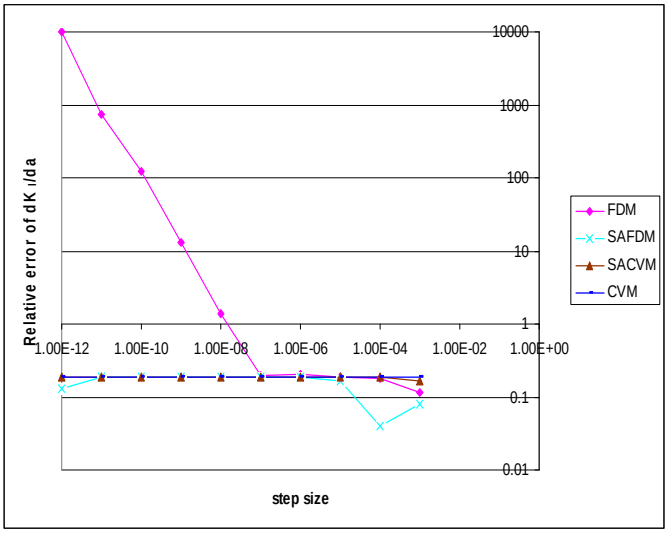

Figure 5.21 Relative error of dK_I / da via perturbation size in DENT specimen

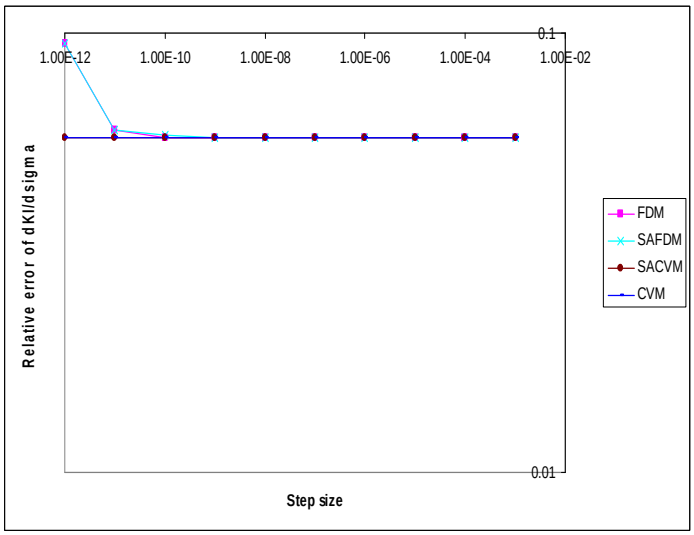

Figure 5.22 Relative error of $dK_I / d\sigma$ via perturbation size in DENT specimen

5.6.2 Reliability analysis of DENT specimen

Similar to Section 5.4.2, the crack size, tensile stress and poisson's ratio are treated as normally-distributed independent random variables, $a = N(1\text{m}, 0.05\text{m})$, $\sigma = (100\text{MPa}, 5\text{MPa})$ and $\nu = N(0.3, 0.01)$, respectively. The reliability index is computed using sensitivity-based FORM.

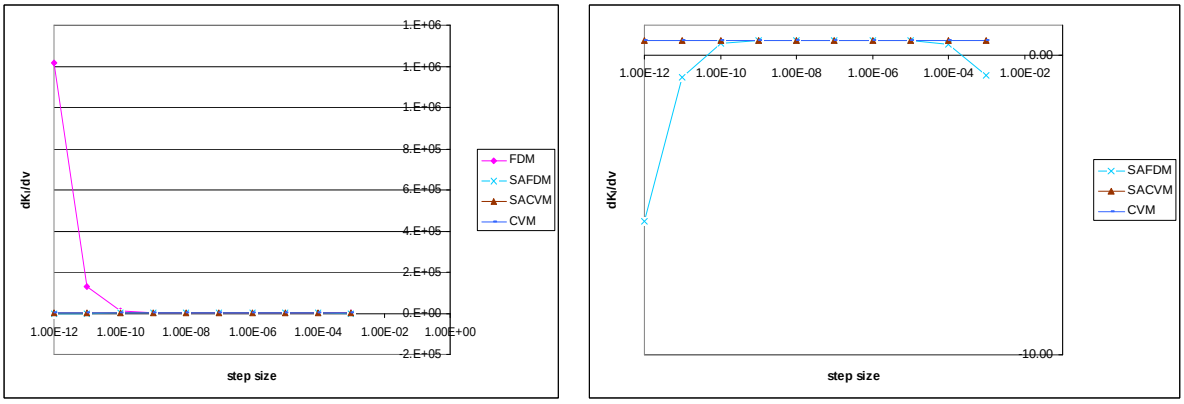

(a) (b)

Figure 5.23 dK_I / dv via perturbation size in DENT specimen, (a) comparison of four methods, (b) comparison of three methods

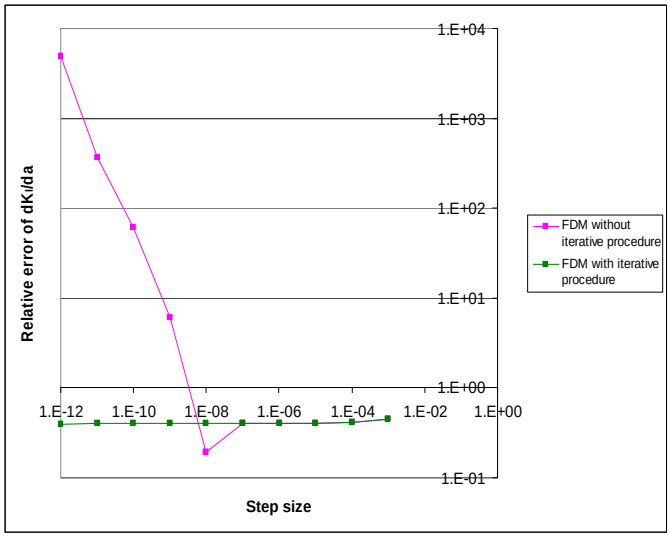

Figure 5.24 Relative error of dK_I / da via perturbation size without or with iterative procedure in DENT specimen

The limit state function is defined as

$$p = K_I - 200 \tag{5-24}$$

where 200 $\mathrm{MPa}\sqrt{\mathrm{m}}$ is the maximum allowable value of K_I.

At different perturbation size, the reliability index β as well as needed iterations N and computation time T computed by the FD-SFEM, the SAFD-SFEM, the SACV-SFEM, and the CV-SFEM are listed in Table 5.12.

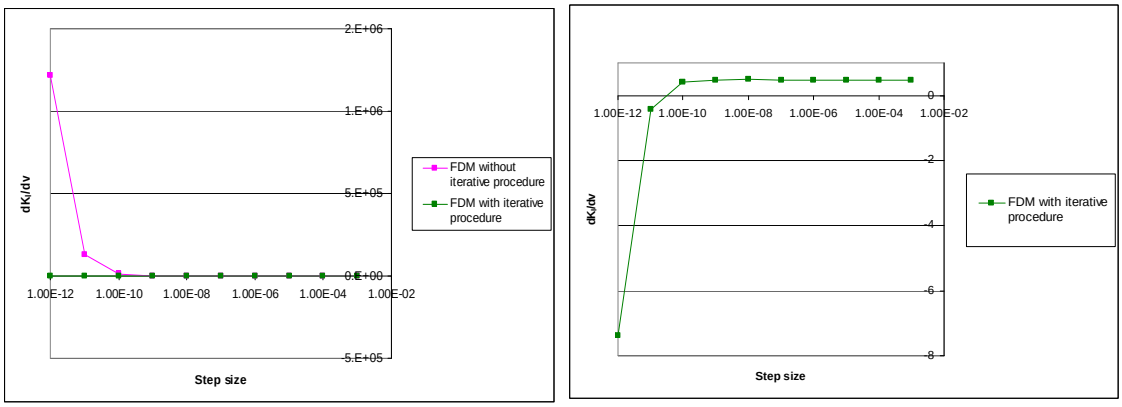

(a) (b)

Figure 5.25 dK_I / dv via perturbation size (a) without and with iterative procedure, (b) with iterative procedure, in DENT specimen

Table 5.12 Reliability analysis of DENT specimen by four methods

		Perturbation size			
		$\varepsilon = 10^{-4}$	$\varepsilon = 10^{-6}$	$\varepsilon = 10^{-8}$	$\varepsilon = 10^{-12}$
FD-SFEM (without iterative procedure)	Reliability Index	0.3625	0.3625	0.3609	0.00017
	Iterations	3	3	8	1
	Computation Time (s)	1230	1230	2090	500
SAFD-SFEM	Reliability Index	0.3625	0.3625	0.3625	0.3625
	Iterations	3	3	3	4
	Computation Time (s)	402	402	402	507
SACV-SFEM	Reliability Index	0.3625	0.3625	0.3625	0.3625
	Iterations	3	3	3	3
	Computation Time (s)	401	401	401	401
CV-SFEM	Reliability Index	0.3625	0.3625	0.3625	0.3625
	Iterations	3	3	3	3
	Computation Time (s)	2185	2185	2185	2185

Table 5.12 shows that the SACV-SFEM and CV-SFEM can always obtain stable reliability index as long as the perturbation size is equal or less than 10^{-4}. However, the computation time cost of the CV-SFEM is 5.4 times than that of the SACV-SFEM. The SAFD-

SFEM has comparable computation time with the SACV-SFEM and obtained correct reliability index when the perturbation size is bigger than 10^{-12}. The reliability indexes computed by the FD-SFEM vary with the perturbation. When the perturbation size is smaller than 10^{-8}, wrong reliability index is obtained because the sensitivities of SIF with respect to the crack length and poisson's ratio are far away from the real values. The computation cost of the FD-SFEM is 3 times more than the SACV-SFEM.

5.7 Conclusions

The SACV-SEFM is applied to linear-elastic fracture mechanics where the limit state function depends on the stress intensity factor. The SACVM is used to compute the sensitivities of stress intensity factors in homogeneous, isotropic, and linear-elastic 2D geometries subject to mode-I loading conditions. Three geometries are considered: a center cracked tension (CCT) specimen, a single edge notched tension (SENT) specimen and double edge notched tension (DENT) specimen. The quarter-point isoparametric elements which can easily represent the specific stress singularities exist at crack tips are used to compute the stress intensity factor of the crack tip.

The sensitivities of SIF with respect to load, poisson's ratio and crack size for three specimens computed by the SACVM are compared with results computed by the FDM, the SAFDM and the CVM. The result shows when the perturbation size is smaller than 10^{-4}, the SACVM can always obtain accurate sensitivities and the sensitivities are not sensitive to the perturbation size. The sensitivities computed by the FDM oscillate with the perturbation size because of ill-conditioned global stiffness matrix. The extra iterative procedure has to be added to decrease the effect from the ill-conditioned matrix. The FDM with iterative procedure and the SAFDM can not obtain accurate sensitivities when the perturbation size is smaller than 10^{-10} because of subtraction error. The CVM can always obtain accurate sensitivities, however its

computation cost is several times than the cost of the other three methods. The SACVM and the SAFDM have almost same computation cost and shows most efficient among four methods.

Based on the sensitivities, the FORM algorithm based SFEM is applied to predict the reliability of cracked structures with material, load and shape uncertainties. The reliability obtained from the SACV-SFEM are compared with the FD-SFEM, SAFD-SFEM and CV-SFEM.

The results of reliability analysis show that the SACV-SFEM can always obtain consistent and accurate reliability index and be computation efficiency. The ill-conditioned global stiffness matrix doesn't affect the accuracy of the SACV-SFEM. However, it causes FD-SFEM without iterative procedure not able to obtain correct reliability index at some perturbation sizes because of oscillation of sensitivities. The SAFD-SFEM has comparable computation time with the SACV-SFEM and sometimes obtained correct reliability index even if the sensitivities of SIF are inaccurate, which readily mislead people to believe that the SAFD-SFEM can always obtain reliable solution, or whether the response sensitivity is accurate will not affect the final reliability index. The CV-SFEM can always obtain right reliability index, however, the computation time of the CV-SFEM is over 5 times than that of the SACVM. And the computation time of the FD-SFEM is about 3 times more than the SACV-SFEM.

Therefore, the SACV-SFEM provides an consistent, accurate and efficient way for reliability analysis in linear elastic fracture mechanics. It computes sensitivities of SIF with respect to material, load and shape random variables without any subtractive cancellation errors. The accuracy of the sensitivities and reliability index computed by the SACV-SFEM is not affected by the ill-conditioned global stiffness matrix which is caused by quarter-point isoparametric elements. Furthermore, the SACV-SFEM takes advantage of the benefits of the semi-analytical method, and obtains the reliability indexes of cracked structures very efficiently.

CHAPTER 6

APPLICATION OF THE SACV-SFEM TO NONLINEAR PROBLEMS

6.1 Introduction

Material and geometric nonlinearity are two common sources of nonlinearity. Material nonlinearity comes from the nonlinear constitutive behavior of the material of the system. Therefore material properties of the body must be updated during the solution process. Geometric nonlinearity comes from geometric consideration of the system, such as the nonlinear strain-displacement relations. Therefore, geometric changes are significant and the geometry of the body must be updated during the deformation process. Evaluating sensitivities and reliability of a nonlinear problem will be more complicated than computing sensitivities of a linear problem. The present chapter will focus on the sensitivity and reliability analysis of the material nonlinearity of a heat conduction problem and the geometric nonlinearity of Euler-Bernoulli beam.

About the sensitivity analysis of the nonlinear heat conduction, Dowding and Blackwell [51] derived the sensitivity equation for the temperature-dependent parameters and presented demonstration calculations. Emery and Fadale [81] presented a formulation for nonlinear heat conduction. Nicolai and De Baedermaeker [42, 43] treated thermal properties as random field parameters. The numerical example illustrated in [51] will be computed by our own finite element codes to test the accuracy. The benchmark problem illustrated in Chapter 4 will be added temperature dependent thermal conductivity to test the consistency, accuracy and efficiency of the SACV-SFEM by comparing solutions computed by the FD-SFEM, the SAFD-SFEM and the CV-SFEM.

The classic nonlinear bending of Euler-Bernoulli beam [82] will be used as the numerical example to test the performance of the SACV-SFEM when it is used in geometric nonlinear problems.

6.2 Verification of the SACV and FD Codes for Nonlinear Steady State Heat Conduction

A slab of unit thickness, $\boldsymbol{L} = 1\,\mathrm{m}$, with temperature-dependent thermal conductivity is considered. The boundary temperatures are maintained at $\boldsymbol{T_L} = 0^{\mathrm{o}}\boldsymbol{C}$ and $\boldsymbol{T_R} = 100^{\mathrm{o}}\boldsymbol{C}$. Conductivity is represented by two piecewise linear segments interpolating between conductivity values at three temperature: $\boldsymbol{k}_1 = 1.0\mathrm{W/m}\cdot^{\mathrm{o}}\mathrm{C}$ at $\boldsymbol{T}_1 = 0^{\mathrm{o}}\boldsymbol{C}$, $\boldsymbol{k}_2 = 2.0\mathrm{W/m}\cdot^{\mathrm{o}}\mathrm{C}$ at $\boldsymbol{T}_2 = 50^{\mathrm{o}}\boldsymbol{C}$, and $\boldsymbol{k}_3 = 6.0\mathrm{W/m}\cdot^{\mathrm{o}}\mathrm{C}$ at $\boldsymbol{T}_2 = 100^{\mathrm{o}}\boldsymbol{C}$. The two piecewise linear segment is

$$\boldsymbol{k}(\boldsymbol{T}) = \begin{cases} \boldsymbol{k}_1\left(1 - \dfrac{\boldsymbol{T}-\boldsymbol{T}_1}{\boldsymbol{T}_2-\boldsymbol{T}_1}\right) + \boldsymbol{k}_2\left(\dfrac{\boldsymbol{T}-\boldsymbol{T}_1}{\boldsymbol{T}_2-\boldsymbol{T}_1}\right), & \boldsymbol{T}_1 \le \boldsymbol{T} \le \boldsymbol{T}_2 \\ \boldsymbol{k}_2\left(1 - \dfrac{\boldsymbol{T}-\boldsymbol{T}_2}{\boldsymbol{T}_3-\boldsymbol{T}_2}\right) + \boldsymbol{k}_3\left(\dfrac{\boldsymbol{T}-\boldsymbol{T}_2}{\boldsymbol{T}_3-\boldsymbol{T}_2}\right), & \boldsymbol{T}_2 \le \boldsymbol{T} \le \boldsymbol{T}_3 \end{cases} \tag{6-1}$$

The analytical solution of this problem is [51]

$$\boldsymbol{T} = \begin{cases} \dfrac{\beta_1}{2}\boldsymbol{T}^2 + (\boldsymbol{k}_1 - \beta_1\boldsymbol{T}_1)\boldsymbol{T} + \boldsymbol{C}_1 & \boldsymbol{T}_1 \le \boldsymbol{T} \le \boldsymbol{T}_2 \\ \dfrac{\beta_2}{2}\boldsymbol{T}^2 + (\boldsymbol{k}_2 - \beta_2\boldsymbol{T}_2)\boldsymbol{T} + \boldsymbol{C}_2 & \boldsymbol{T}_2 \le \boldsymbol{T} \le \boldsymbol{T}_3 \end{cases} \tag{6-2}$$

where $\beta_{\boldsymbol{i}} = \left(\dfrac{\boldsymbol{k}_{\boldsymbol{i}+1} - \boldsymbol{k}_{\boldsymbol{i}}}{\boldsymbol{T}_{\boldsymbol{i}+1} - \boldsymbol{T}_{\boldsymbol{i}}}\right), \qquad \boldsymbol{i} = 1,2$ (6-3)

$$\begin{aligned} \boldsymbol{C}_1 = &-\left[\frac{\beta_1}{2}\boldsymbol{T}_{\boldsymbol{L}}^2 + (\boldsymbol{k}_1 - \beta_1\boldsymbol{T}_1)\boldsymbol{T}_{\boldsymbol{L}}\right]\left(1 - \frac{\boldsymbol{x}}{\boldsymbol{L}}\right) \\ &+ \left\{\frac{(\beta_2 - \beta_1)}{2}\boldsymbol{T}_2^2 + \left[(\boldsymbol{k}_2 - \beta_2\boldsymbol{T}_2) - (\boldsymbol{k}_1 - \beta_1\boldsymbol{T}_1)\boldsymbol{T}_2\right]\right\}\frac{\boldsymbol{x}}{\boldsymbol{L}} \\ &- \left[\frac{\beta_2}{2}\boldsymbol{T}_{\boldsymbol{R}}^2 + (\boldsymbol{k}_2 - \beta_2\boldsymbol{T}_2)\boldsymbol{T}_{\boldsymbol{R}}\right]\frac{\boldsymbol{x}}{\boldsymbol{L}} \end{aligned} \tag{6-4}$$

and

$$C_2 = -\left[\frac{\beta_1}{2}T_L^2 + (k_1 - \beta_1 T_1)T_L\right]\left(1 - \frac{x}{L}\right)$$
$$+\left\{\frac{(\beta_2 - \beta_1)}{2}T_2^2 + [(k_2 - \beta_2 T_2) - (k_1 - \beta_1 T_1)T_2]\right\}\left(\frac{x}{L} - 1\right) \quad (6\text{-}5)$$
$$-\left[\frac{\beta_2}{2}T_R^2 + (k_2 - \beta_2 T_2)T_R\right]\frac{x}{L}$$

Two finite element models are used to compute the temperatures and sensitivities of the temperatures with respect to thermal conductivities k_1, k_2 and k_3. The coarse mesh model has 24 nodes and 24 elements, as shown in Figure 6.1 (a). The fine mesh model has 1212 nodes and 2202 elements, as shown in Figure 6.1 (b).

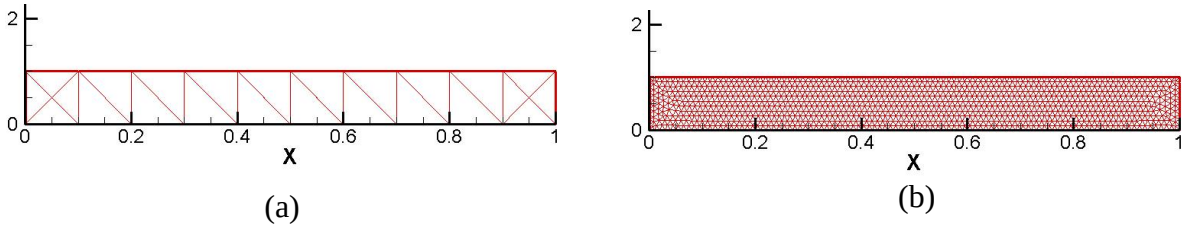

(a) (b)

Figure 6.1 Two FE models of the slab, (a) coarse mesh, (b) fine mesh

The comparison of temperatures obtained from FE coarse mesh model, fine mesh model and analytical formula is shown in Figure 6.2. The SACVM codes are used to compute the sensitivities of temperatures with respect to thermal conductivities k_1, k_2 and k_3 along the length of slab for both coarse mesh and fine mesh. The comparison of sensitivities obtained from the SACVM codes with those obtained from the analytical formula is shown in Figure 6.3. The perturbation size used in the SACVM codes is 10^{-10}.

Figure 6.2 shows temperatures obtained from our finite element codes match the analytical solution well. Therefore, the FE codes used here can be used for other nonlinear heat conduction problems without analytical solutions. Figure 6.3 shows the sensitivities computed from SACVM codes agree well with the analytical solutions. Therefore, the whole procedure and codes of SACVM are reliable to do other sensitivities analysis in nonlinear heat conduction

problems. The sensitivities obtained from coarse mesh FE model is less accurate than from fine mesh FE model because of the discretization error.

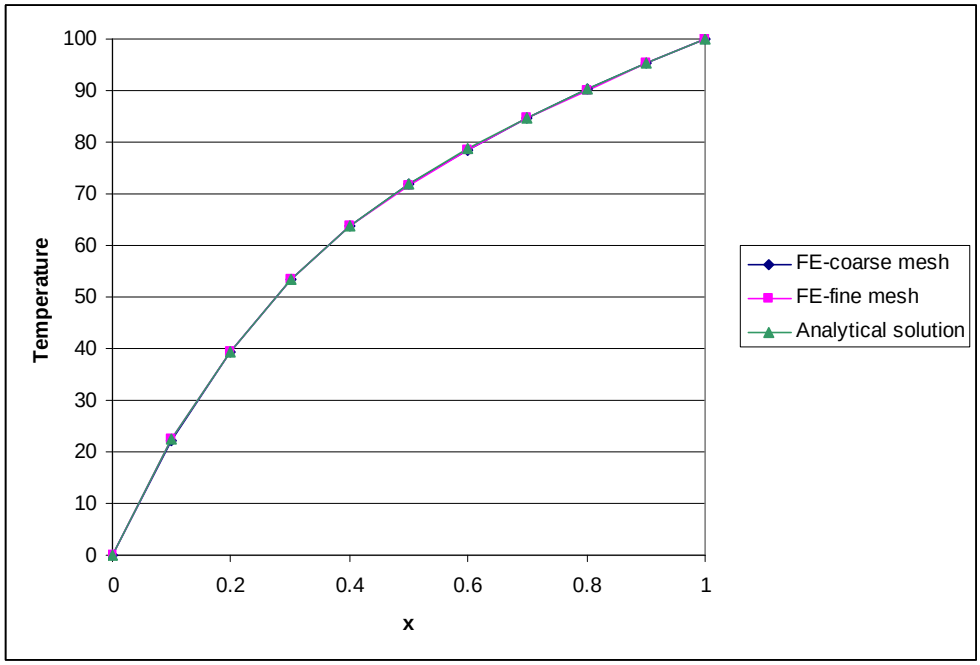

Figure 6.2 Temperatures obtained from FE and analytical formula

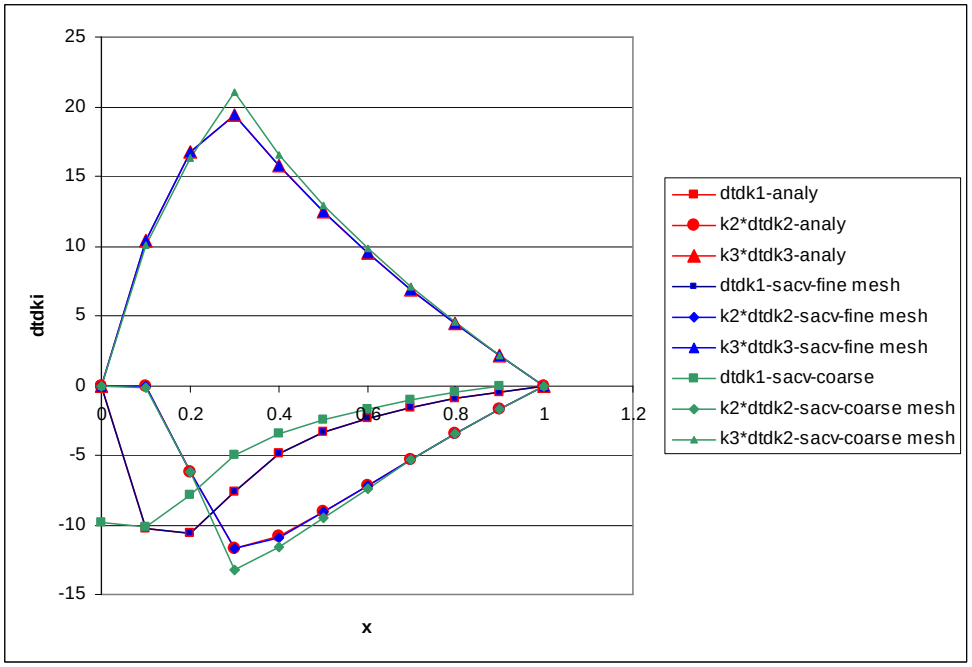

Figure 6.3 Sensitivities obtained from SACV FE codes and analytical formula

6.3 Application of the SACV-SFEM to Benchmark Plate in Nonlinear Heat Conduction

From linear heat conduction analyis, we know the SACV-SFEM always performs consistent, accurate and efficient. In this section, the performance of the SACV-SFEM in the nonlinear heat conduction problem will be tested.

Consider the benchmark problem demonstrated in section 4.3.3. Assume the thermal conductivity for the area $\boldsymbol{y} \geq 0$ in the plate, k_1, is dependent on the temperature as follows,

$$\boldsymbol{k}_1 = \boldsymbol{C} + 0.02 * \boldsymbol{T} \tag{6-6}$$

where, $\boldsymbol{T}$ is the temperatures of each node on the plate, C is a normally-distributed constant, $\boldsymbol{C} = \boldsymbol{N}\left(10\text{W/m}\cdot^{\text{o}}\text{C},\ 1\text{W/m}\cdot^{\text{o}}\text{C}\right)$.

The rest of the parameters are same with those in section 4.3.3. The temperature on the square edge is $\boldsymbol{T}_1 = 100°\boldsymbol{C}$ and the temperature on the circle edge is $\boldsymbol{T}_2 = 10°\boldsymbol{C}$. The thermal conductivity of the area $y < 0$ is a normally-distributed random variable, $\boldsymbol{k}_2 = \boldsymbol{N}\left(20\ \text{W/m}\cdot^{\text{o}}\text{C}, 2\ \text{W/m}\cdot^{\text{o}}\text{C}\right)$. The uniform heat source is a normally-distributed random variable, $\boldsymbol{Q} = \boldsymbol{N}\left(1000\text{W/m}^2, 100\text{W/m}^2\right)$. And the edge of the plate is a normally-distributed random $\boldsymbol{a} = \boldsymbol{N}\left(10\text{m}, 1\text{m}\right)$.

The Picard method is employed to solve this nonlinear heat conduction problem. The scheme is given by

$$\boldsymbol{K}\left(\boldsymbol{T}^{\boldsymbol{n}}\right)\boldsymbol{T}^{\boldsymbol{n}+1} = \boldsymbol{F} \tag{6-7}$$

where n is the iteration number. $\boldsymbol{T}^{\boldsymbol{n}}$ which is computed from the previous iteration is substituted into $\boldsymbol{K}$ to solve $\boldsymbol{T}^{\boldsymbol{n}+1}$. The whole procedure is repeated until the root-mean-square value of the difference between the solution vectors at two consecutive iterations is reduced to a values less than the defined tolerance, $\boldsymbol{\delta}$

$$\frac{\left(\boldsymbol{T}^{n+1}-\boldsymbol{T}^{n}\right)\left(\boldsymbol{T}^{n+1}-\boldsymbol{T}^{n}\right)}{\left(\boldsymbol{T}^{n+1}\right)^{T}\left(\boldsymbol{T}^{n+1}\right)}<\delta^{2} \tag{6-8}$$

Where the value of δ^2 is defined as 10^{-6}.

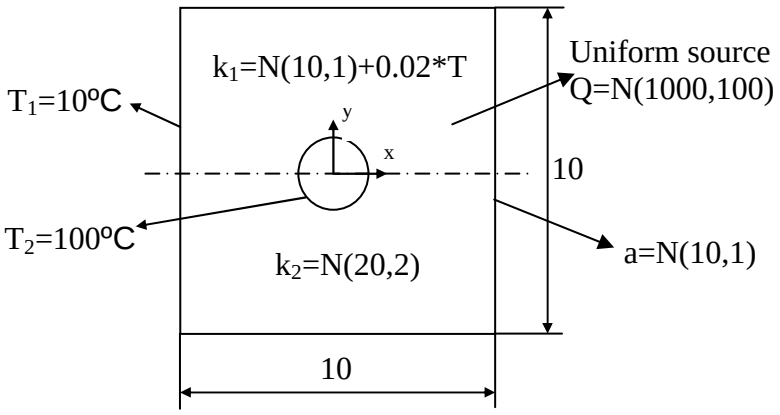

Figure 6.4 Parameters of the nonlinear benchmark plate

When the random variables are at the mean values, such that the thermal conductivities $\boldsymbol{k}_1 = 10 + 0.02\boldsymbol{T}$ W/m·°C , $\boldsymbol{k}_2 = 20$ W/m·°C , heat source $\boldsymbol{Q} = 1000$ W/m^2 and the edge of the plate $a = 10$ m, temperature distribution of this nolinear heat conduction plate is shown in Figure 6.5.

The flowchart of using the SACV-SFEM to compute the sensitivities of heat flux along the circle with respect to input parameters, $\boldsymbol{dGflux}/\boldsymbol{dx}$, is shown in Figure 6.6.

The criteria of the limit state function is defined as

$$\boldsymbol{f} = \boldsymbol{Gflux} - 35000 \tag{6-9}$$

where $\boldsymbol{Gflux}$ is the normal heat flux across the circular boundary, and 35000 W/m°C represents the limited value of the normal heat flux across the circular boundary.

In this nonlinear problem, there are 3 sub-iterations to obtain convergent temperature $\boldsymbol{T}$ and sensitivities of every random variable in each loop of reliability evaluation. By the SACV-SEFM, the reliability index of the limit state function is $\boldsymbol{\beta} = 1.2169$. The computation time and

needed iterations for solving the nonlinear benchmark problem by the SACV-SFEM, CV-FEM, FD-SFEM and SAFD-SFEM are listed in Table 6.1.

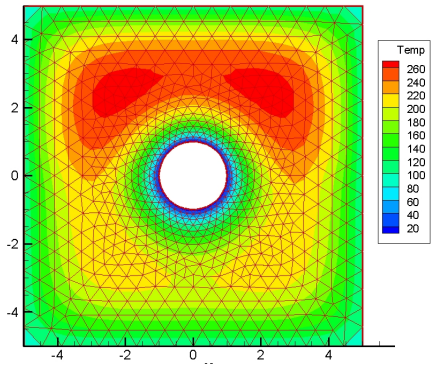

Figure 6.5 Temperature distribution of the nonlinear benchmark plate

Table 6.1 Computation Time and Needed Iterations of Four Methods

Perturba-tion	FD-SFEM		SAFD-SFEM		CV-SFEM		SACV-SFEM	
	Compu. Time	Iter.	Compu. Time	Iter.	Compu. Time	Iter.	Compu. Time	Iter.
10^{-1}	244	6	X		736	5	219	5
10^{-2}	207	5	218	5				
10^{-3}	207	5	218	5				
10^{-6}	207	5	218	5				
10^{-8}	207	5	218	5				
10^{-10}	1217	29	X					

"X" represents not convergent

When the perturbation size is between 10^{-2} and 10^{-8}, the computation time of the FD-SFEM, the SAFD-SFEM and the CV-SFEM are comparable. When the perturbation size is out of this range, the SAFD-SFEM and the FD-SFEM can not converge or need more iteration to evaluate the reliability because of the subtraction error. The SACV-SFEM can always obtain the consistent, accurate reliability index with same iterations that the CV-SFEM needs. Also it is not sensitive to the perturbation size at all. Furthermore, it needs less than 3 times computation

time than the CV-SFEM. Therefore, the SACV-SFEM shows the most consistent, accurate and computational efficiency.

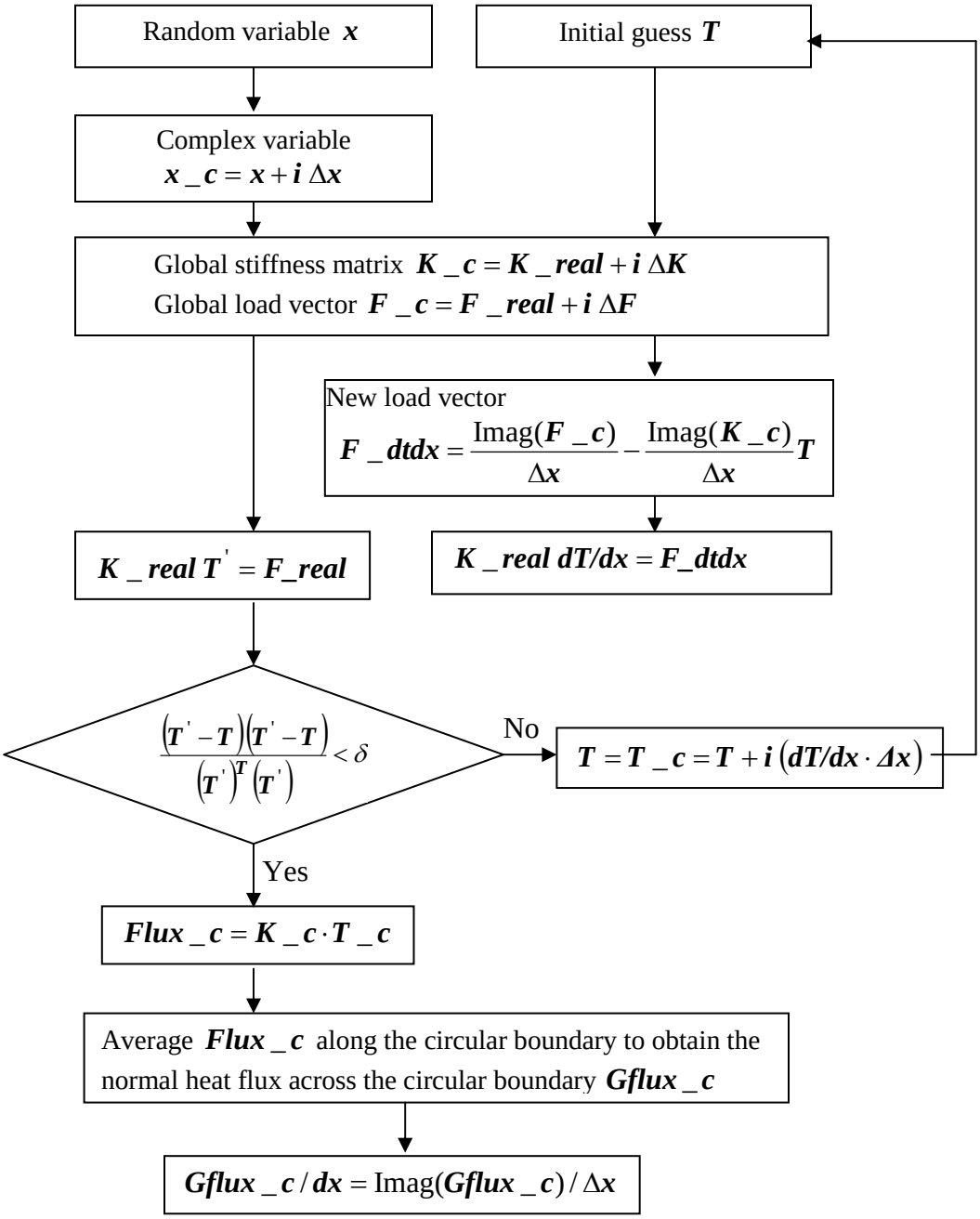

Figure 6.6 Flowchart of computing sensitivities in nonlinear benchmark plate using the SACVM

6.4 Application of the SACV-SFEM to Geometric Nonlinear Bending of Clamped-clamped Euler-Bernoulli beam

The classical Euler-Bernoulli beam theory is based on the Euler-Bernoulli hypothesis that plane sections perpendicular to the axis of the beam before deformation remain 1) plane; 2) rigid (not deform); and 3) rotate such that they remain perpendicular to the deformed axis after deformation. It neglects the Poisson effect and transverse shear strains.

Reddy [82] introduced the nonlinear formulation of straight Euler-Bernoulli beams which is based on assumptions of large transverse displacements, small strains and moderate rotations. The nonlinearity in the formulation comes solely from the inclusion of the inplane forces that are proportional to the square of the rotation of the transverse normal to the beam axis. The von Karman strains is used to represent the strain-displacement relations in axial direction as follows,

$$\varepsilon_{xx} = \frac{\boldsymbol{du}}{\boldsymbol{dx}} + \frac{1}{2}\left(\frac{\boldsymbol{dw}}{\boldsymbol{dx}}\right)^2 - \frac{\boldsymbol{d}^2\boldsymbol{w}}{\boldsymbol{dx}^2} \tag{6-10}$$

where $\boldsymbol{u}$ and $\boldsymbol{w}$ denotes the axial and transverse displacement of a point on the neutral axis.

The study of this section will focus on the sensitivity and reliability analysis of a clamped-clamped nonlinear bending Euler-Bernoulli beam. The length of the beam is $\boldsymbol{L} = 100\,\boldsymbol{in.}$. The cross sectional dimensions is $1\,\boldsymbol{in.} \times 1\,\boldsymbol{in.}$. It is made of steel (Young's modulus $\boldsymbol{E} = 30\boldsymbol{msi}$) and subjected to uniformly distributed load of intensity $\boldsymbol{q} = 10\,\boldsymbol{lb/in}$, as shown in Figure 6.7.

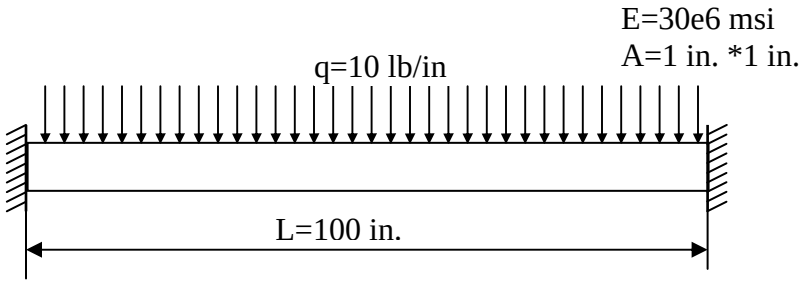

Figure 6.7 Clamped-clamped beam

Using the symmetry about $x = L/2$, one half of the domain is built as the computational domain. The geometric boundary conditions are

$$u(0) = w(0) = \left.\frac{dw}{dx}\right|_{x=0} = u\left(\frac{L}{2}\right) = \left.\frac{dw}{dx}\right|_{x=\frac{L}{2}} = 0 \tag{6-11}$$

Four beam elements are used in half length finite element model. One-point Guass quadrature is used to evaluate all nonlinear stiffness coefficients and two-point Guass quadrature is used to evaluate the linear stiffness coefficients. When the beam becomes increasing stiff with an increase in load, the numerical scheme might not yield convergent. Therefore, the large load is divided into several smaller load increment such that

$$F = \sum_{i=1}^{n} \Delta F_i \tag{6-12}$$

In each load step, an iterative procedure is needed to compute the displacement vector which is based on the displacement vector obtained from previous load step. The flow chart for the nonlinear bending of Euler-Bernoulli beam analysis is shown in Figure 6.8.

The nonlinear system of equations is solved using direct iteration procedure. The convergent criterion is given in Equation (6-8).

The maximum transverse displacements at each load step obtained from the finite element codes are shown in Figure 6.9. These results comparing with results listed in [82] is shown in Table 6.2. The results computed by our FE codes agree well with the results listed in [82].

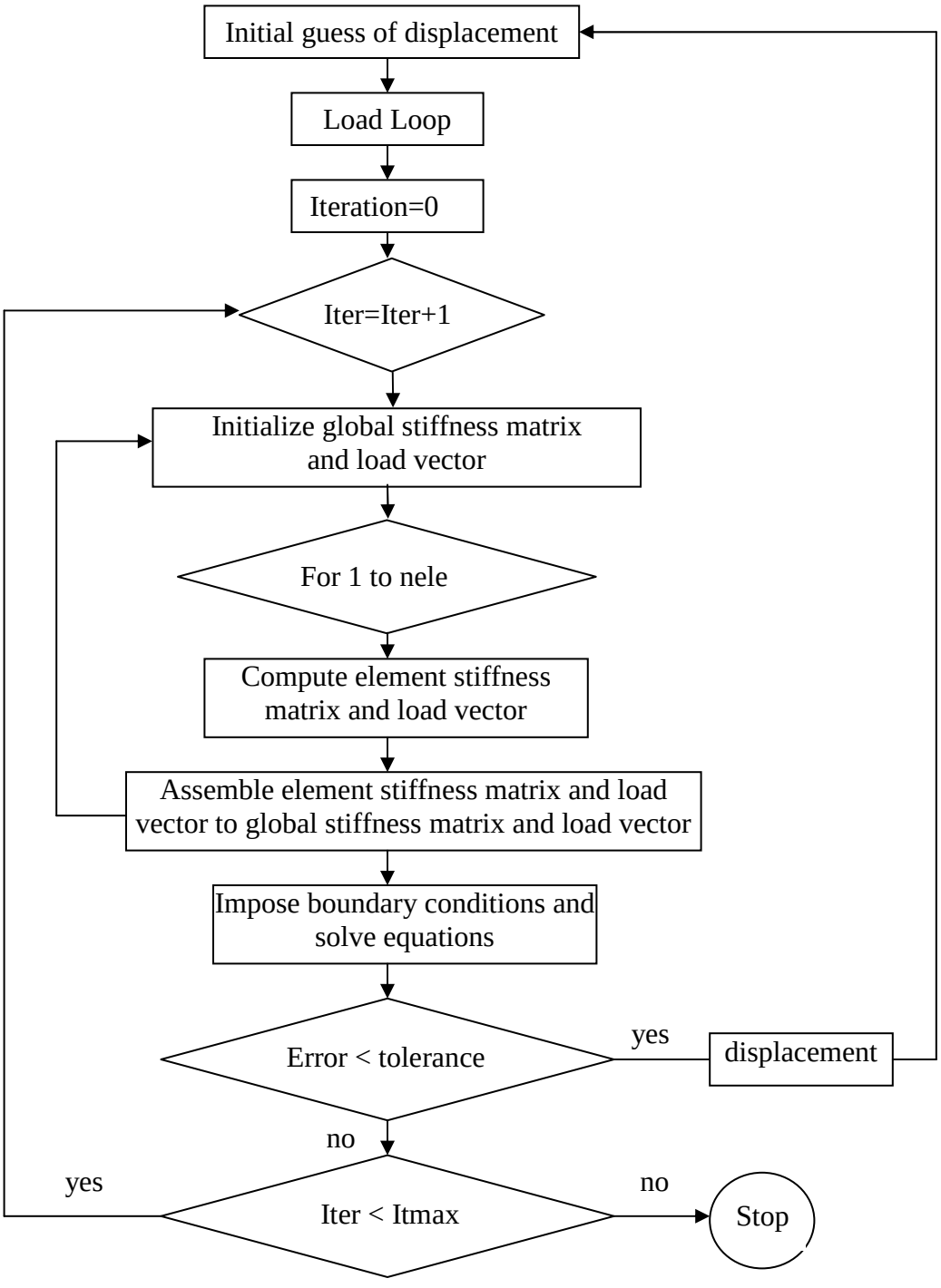

Figure 6.8 Flow chart of nonlinear bending of Euler-Bernoulli beam analysis

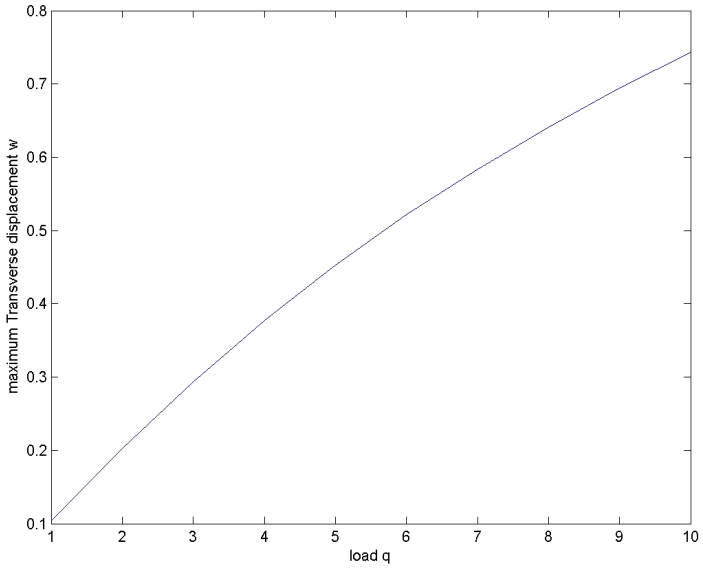

Figure 6.9 Load versus maximum transverse displacement for nonlinear bending of clamped-clamped Euler-Bernoulli beam

Table 6.2 Maximum Transverse Displacement of the Nonlinear Bending of Clamped-clamped Euler-Bernoulli Beam

Load	FEM codes	Reference [82]
1.0	0.1034	0.1033
2.0	0.2022	0.2022
3.0	0.2938	0.2938
4.0	0.3773	0.3773
5.0	0.4528	0.4529
6.0	0.5214	0.5213
7.0	0.5839	0.5840
8.0	0.6413	0.6412
9.0	0.6943	0.6945
10.0	0.7435	0.7433

6.4.1 Sensitivity analysis of the nonlinear bending of clamped-clamped Euler-Bernoulli beam

The sensitivities of the maximum transverse displacement with respect to the Young's modulus $\boldsymbol{dw}_{\max} / \boldsymbol{dE}$, beam length $\boldsymbol{dw}_{\max} / \boldsymbol{L}$ and uniform load $\boldsymbol{dw}_{\max} / \boldsymbol{dq}$ are studied. The

FDM, SAFDM, SACVM and CVM are used to evaluate the sensitivities at different perturbation sizes, as listed in Table 6.3, 6.4 and 6.5.

Table 6.3 $\boldsymbol{dw}_{\max} / \boldsymbol{dE}$ at different perturbation size computed by four methods

Perturbation size	FD	SAFD	SACV	CV
10^{4}	-1.5848e-8	-1.5867e-8	-1.5848e-8	-1.5848e-8
10^{3}	-1.5848e-8	-1.6041e-8	-1.5848e-8	-1.5848e-8
10^{2}	-1.5848e-8	-1.7772e-8	-1.5848e-8	-1.5848e-8
10^{1}	-1.5848e-8	-3.5088e-8	-1.5848e-8	-1.5848e-8
10^{0}	-1.5848e-8	-2.0824e-8	-1.5848e-8	-1.5848e-8
10^{-1}	-1.5848e-8	-1.9398e-6	-1.5848e-8	-1.5848e-8
10^{-2}	-1.5847e-8	-1.9255e-5	-1.5848e-8	-1.5848e-8
10^{-3}	-1.6886e-8	-1.9241e-4	-1.5848e-8	-1.5848e-8
10^{-4}	-7.8826e-9	-0.0019	-1.5848e-8	-1.5848e-8

Table 6.4 $\boldsymbol{dw}_{\max} / \boldsymbol{dL}$ at different perturbation size computed by four methods

Perturbation size	FD	SAFD	SACV	CV
10^{-1}	0.038	0.0378	0.038	0.038
10^{-2}	0.038	0.038	0.038	0.038
10^{-3}	0.038	0.0378	0.038	0.038
10^{-4}	0.038	0.0361	0.038	0.038
10^{-5}	0.038	0.0188	0.038	0.038
10^{-6}	0.038	-0.1544	0.038	0.038
10^{-7}	0.038	-1.8859	0.038	0.038
10^{-8}	0.038	-19.2013	0.038	0.038
10^{-9}	0.0381	-192.355	0.038	0.038
10^{-10}	0.0382	-1.9239e3	0.038	0.038
10^{-12}	0.0653	-1.9239e5	0.038	0.038

Table 6.3, 6.4 and 6.5 show that the SACVM and CVM can always obtain accurate sensitivities without being sensitive to the perturbation size. While the FDM and the SAFDM are

sensitive to the perturbation size. Especially for the SAFDM, the range of perturbation size which can be used to obtain accurate sensitivities are much smaller than such range of the FDM. The FDM requires run all load steps twice to obtain one sensitivity value, once for without parameter perturbation, and once for with parameter perturbation. The CVM requires run all load steps once to obtain the imaginary part of the displacement, however it computes results in complex field. The computation cost of the CVM is more expensive than the FDM. The SAFDM and the SACVM only need run all load steps once to obtain the final stiffness matrix and displacement. Based on these final stiffness matrix and displacement, only the last load step is repeated to compute one more time to obtain the sensitivities of the displacement with respect to the parameter. Therefore, the SAFDM and SACVM show more computational efficiency than the FDM and the CVM.

Table 6.5 $\boldsymbol{dw}_{\max} / \boldsymbol{dq}$ at different perturbation size computed by 4 methods

Perturbation size	FD	SAFD	SACV	CV
10^{-1}	0.04601	0.0468	0.04755	0.04728
10^{-2}	0.04738	0.0475	0.04755	0.04754
10^{-3}	0.04753	0.0475	0.04755	0.04755
10^{-4}	0.04754	0.0474	0.04755	0.04755
10^{-5}	0.04755	0.0456	0.04755	0.04755
10^{-6}	0.04755	0.0283	0.04755	0.04755
10^{-7}	0.04755	-0.1448	0.04755	0.04755
10^{-8}	0.04755	-1.8764	0.04755	0.04755
10^{-9}	0.04755	-19.1918	0.04755	0.04755
10^{-10}	0.0476	-192.3455	0.04755	0.04755
10^{-12}	0.05042	-1.9239e4	0.04755	0.04755

6.4.2 Reliability analysis of the nonlinear bending of clamped-clamped Euler-Bernoulli beam

The Young's modulus, beam length and uniform pressure are treated as normally-distributed independent random variables, $\boldsymbol{E} = \boldsymbol{N}\left(3\times10^{7}\,\text{psi}, 30\times10^{3}\,\text{psi}\right)$,

$\boldsymbol{L} = (50\,\text{in.}, 1\,\text{in.})$ and $\boldsymbol{q} = \boldsymbol{N}(10\,\text{lb/in}, 1\,\text{lb/in})$, respectively. The reliability index is computed by FORM algorithm.

The limit state function is defined as

$$\boldsymbol{p} = \boldsymbol{w}_{\max} - 0.8 \tag{6-13}$$

where $\boldsymbol{w}_{\max}$ is the maximum transverse displacement of the beam, and 0.8 in. is the maximum allowable value of $\boldsymbol{w}_{\max}$.

At different perturbation size, the reliability index β and needed iterations $\boldsymbol{N}$ computed by finite difference based the FD-SFEM, SAFD-SFEM, SACV-SFEM and CV-SFEM are listed in Table 6.6.

Table 6.6 Reliability Analysis of Nonlinear Bending of Clamped-clamped Euler-Bernoulli Beam by Four Methods

		Perturbation size			
		$\varepsilon_{\boldsymbol{E}} = 10^{-3}$ $\varepsilon_{\boldsymbol{L}} = 10^{-3}$ $\varepsilon_{\boldsymbol{q}} = 10^{-3}$	$\varepsilon_{\boldsymbol{E}} = 10^{-6}$ $\varepsilon_{\boldsymbol{L}} = 10^{-6}$ $\varepsilon_{\boldsymbol{q}} = 10^{-6}$	$\varepsilon_{\boldsymbol{E}} = 10^{-1}$ $\varepsilon_{\boldsymbol{L}} = 10^{-1}$ $\varepsilon_{\boldsymbol{q}} = 10^{-1}$	$\varepsilon_{\boldsymbol{E}} = 10^{3}$ $\varepsilon_{\boldsymbol{L}} = 10^{-3}$ $\varepsilon_{\boldsymbol{q}} = 10^{-3}$
FD-SFEM	β	0.9321	X	0.9321	0.9321
	Iterations	3	-	5	4
SAFD-SFEM	β	X	X	-	0.9321
	Iterations	-	-	-	3
SACV-SFEM	β	0.9321	0.9321	0.9321	0.9321
	Iterations	3	3	3	3
CV-SFEM	β	0.9321	0.9321	0.9321	0.9321
	Iterations	3	3	3	3

"X" represents not convergent

Table 6.6 shows the SACV-SFEM and the CV-SFEM can always obtain stable reliability index. However, to obtain the same accurate reliability index, the computation time cost of the CV-SFEM is about 1.5 times than the cost of the SACV-SFEM. When the perturbation size is 10^{-6} or 10^{-3}, both the FD-SFEM and the SAFD-SFEM or either of them are not able to

converge because of the inaccurate sensitivities of $\boldsymbol{w}_{\max}$. The SACV-SFEM has comparable computation time with the SAFD-SFEM and is more efficient than the FD-SFEM and the CV-SFEM. Therefore, the SACV-SFEM exhibits consistent, accurate and efficient, and shows great advantages than other three methods.

6.5 Conclusions

The semi-analytical complex variable based stochastic finite element method (SACV-SFEM) is applied to material and geometrical nonlinear problems to test its consistency, accuracy and efficiency.

A slab with temperature-dependent thermal conductivity is used to test the nonlinear heat conduction finite element codes. The results shows temperatures and sensitivities obtained from finite element codes match the analytical solution very well. Therefore, the finite element codes can be used for other nonlinear heat conduction problems without analytical solutions.

Further study of material nonlinearity focuses on the benchmark square plate in nonlinear steady-state heat conduction field. The thermal conductivity of the plate is dependent on the temperature. Comparing with the FD-SFEM, the SAFD-SFEM and the CV-SFEM, the SACV-SFEM is applied to get the reliability index of an implicit limit state function. The results reveal that the SACV-SFEM and the CV-SFEM can always obtain accurate reliability index. However the FD-SFEM and the SAFD-SFEM doesn't work for the relatively big or small perturbation size. The SACV-SFEM has the comparable computation time with the SAFD-SFEM and the FD-SFEM, and save 3 times computation time than the CV-SFEM.

The nonlinear bending of an Euler-Bernoulli beam is a classical geometrical nonlinear problem. The SACV-SFEM is used to compute the reliability of this beam system with considering Young's modulus, beam length and uniform load as random variables. The results verify again that the SACV-SFEM can always obtain consistent, accurate and efficient reliability index. While the FD-SFEM and the SAFD-SFEM are sensitive to the perturbation size and the CV-SFEM costs more computation time.

CHAPTER 7

CONCLUSIONS

Stochastic finite element methods (SFEM) allows the analyst to define material, load, and geometry parameters as random variables to represent uncertainties, then estimates probabilities of exceeding specified performance thresholds. A necessary ingredient for such analysis is consistent, accurate and efficient algorithms for computing finite element response sensitivities.

The semi-analytical complex variable method (SACVM) provides a powerful, robust and attractive approach to evaluate the response sensitivity consistently, accurately and efficiently. It incorporates the semi-analytical algorithm (SAM) with the complex variable method (CVM), takes advantages of the consistency and accuracy of the CVM and efficiency of the SAM. The SACVM can be applied to any finite element code with a few modifications. The response sensitivity can be computed semi-analytically as

$$\boldsymbol{K}\frac{\partial \boldsymbol{u}}{\partial \boldsymbol{X}} = \frac{\partial \boldsymbol{f}}{\partial \boldsymbol{X}} - \frac{\partial \boldsymbol{K}}{\partial \boldsymbol{X}}\boldsymbol{u} \tag{7-1}$$

where $\boldsymbol{K}$ is global stiffness matrix, $\boldsymbol{f}$ is the load vector, $\boldsymbol{u}$ is the finite element response, and $\partial \boldsymbol{u} / \partial \boldsymbol{x}$ is response sensitivity.

The SACVM avoids the subtractive cancellation errors that plague the FDM. The sensitivities obtained from the SACVM don't involve any subtraction of two functions, and are as accurate, consistent as the sensitivities obtained from the CVM. In the SACVM algorithm, the response $\boldsymbol{u}$ is computed in the deterministic finite element formulation where float point variables are declared as real variables. And the LU decomposition of global stiffness matrix $\boldsymbol{K}$ is also calculated using the deterministic finite element method. The sensitivities $\partial \boldsymbol{f_e} / \partial \boldsymbol{X}$

and $\partial \boldsymbol{K}_{\boldsymbol{e}} / \partial \boldsymbol{X}$ can be readily computed by taking a complex perturbation in imaginary part of element stiffness matrix and load vector where floating point variables are declared as complex variables. The right side of Equation (7-1) will be computed in element level, and then assembled as a global vector $\boldsymbol{FF} = \frac{\partial \boldsymbol{f}}{\partial \boldsymbol{X}} - \frac{\partial \boldsymbol{K}}{\partial \boldsymbol{X}} \boldsymbol{u}$. On the left side of Equation (7-1), the global stiffness matrix $\boldsymbol{K}$ has already been done for computing the response $\boldsymbol{u}$. Since the most time consuming computation about LU decomposition of global stiffness matrix is computed only once using real variable declaration, and the computation of $\boldsymbol{FF}$ in the element level in complex variable field takes a little time, the SACVM does not require much more time or memory than traditional SAM, and is much faster than the finite difference method (FDM) and CVM.

To date, there is no paper in the open literature that can get more efficient and accurate response sensitivity than the SACVM. This research introduces the SACVM for sensitivity analysis, and further applies it into the FORM algorithm based SFEM.

The semi-analytical complex variable based stochastic finite element method (SACV-SFEM) provides a novel perspective for the application, development, and evaluation of reliability analysis. The SACV-SFEM incorporates the SAVCM with the SFEM to transform a deterministic FEM approach into one that can consistently, efficiently and accurately incorporate uncertainties in the input parameters. The SACV-SFEM can readily compute the reliability of the system whether the limit state function is explicit or implicit. It computes first-order derivative of the limit state function with respect to the input random variables consistently and accurately without any subtractive cancellation errors. Also it takes advantage of the benefits of the SAM algorithm to decrease the computation time. In the FORM algorithm for searching new design points for $\boldsymbol{n}$ random variables in each iteration, the LU decomposition of global stiffness matrix is computed only once for obtaining sensitivities of all $\boldsymbol{n}$ design variables. Comparing to the FDM, the SACV-SFEM saves n times computation time of LU decomposition in each iteration.

The applications of the SACV-SFEM to beam bending and thin plate bending problems reveal that the sensitivity analysis by the SACVM eliminates the drawback of extra computational cost in the CVM and the sensitivity to the perturbation size choice in the SAFDM. The SACV-SFEM can always get as accurate results as Monte Carlo method, with the same computational efficiency as the SAFD-SFEM. However, the SAFD-SFEM obtained correct reliability index in thin plate problem even if the response sensitivities are inaccurate, which readily mislead people to believe that the SAFD-SFEM can always obtain reliable solution, or whether the response sensitivity is accurate will not affect the final reliability index. The application of the SAFD-SFEM in beam bending problem obtained a totally wrong reliability index because of the inaccurate response sensitivity. The SAFDM is not safe enough to obtain the response sensitivity in a general purpose SFEM code.

The SACV-SFEM is applied to linear steady-state heat conduction to test its performance. For an infinitely long hollow cylinder, the results computed by the SACVM codes match well with the analytical solution. Therefore, the SACVM codes of heat conduction can be used for similar heat conduction problems without analytical solutions. Four cases of the benchmark square plate were computed by SACV-SFEM to get the reliability index of the implicit limit state function. Comparing to the FD-SFEM, SAFD-SFEM and CV-SFEM, the SACV-SFEM is not sensitive to the relatively big or small perturbation size which however can not be used in the FD-SFEM or the SAFD-SFEM to obtain the right or convergent reliability index. The computation time of the SACV-SFEM is comparable to the SAFD-SFEM and much faster than the FD-SFEM and the CV-SFEM. Further application of the SACV-SFEM to electronic BGA packaging problem shows that the SACV-SFEM can always obtain the accurate reliability index without considering the big difference between the values of input random variables. However, the FD-SFEM and the SAFD-SFEM can not obtain convergent correct reliability index by using only one perturbation size for all the variables. The computation time of the SACV-SFEM is much faster than that of the CV-SFEM and the FD-SFEM.

The SACV-SEFM is then employed into linear-elastic fracture mechanics where the limit state function builds on the stress intensity factor in homogeneous, isotropic, and linear-elastic 2D geometries subject to mode-I loading conditions. Three geometries are considered: a center cracked tension (CCT) specimen, a single edge notched tension (SENT) specimen and double edge notched tension (DENT) specimen. The quarter-point isoparametric elements are used to compute the stress intensity factor of the crack tip. The results show that the SACV-SFEM can always obtain consistent and accurate reliability index and be computational efficiency. The ill-conditioned global stiffness matrix doesn't affect the accuracy of the SACV-SFEM. However, it causes FD-SFEM without iterative procedure not able to obtain correct reliability index at some perturbation sizes because of oscillation of sensitivities. The SAFD-SFEM shows not safe enough for reliability analysis of SENT specimen. The computation time of the SACV-SFEM is 1/5 times of the CV-SFEM, and 1/3 of the SACV-SFEM.

The SACV-SFEM is further applied to material and geometrical nonlinear problems. The temperatures and response sensitivities obtained from SACVM codes in a slab with temperature-dependent thermal conductivity match the analytical solution very well. The results computed by the SACV-SFM in the benchmark square plate in nonlinear steady-state heat conduction field reveal that the SACV-SFEM can always obtain accurate reliability index. However the FD-SFEM and SAFD-SFEM doesn't work for the relatively big or small perturbation size. The SACV-SFEM has the comparable computation time with the SAFD-SFEM, and save 3 times computation time than the CV-SFEM. In the geometrical nonlinear bending of Euler-Bernoulli beam, the SACV-SFEM can always obtain consistent, accurate reliability index. And the SACV-SFEM is more efficient than the FD-SFEM and the CV-SFEM because it computes sensitivities without repeating all the load steps. However the FD-SFEM and SAFD-SFEM are sensitive to the perturbation size, and the FD-SFEM and CV-SFEM spend more computation time for repeating all the load steps required to obtain the sensitivities.

REFERENCES

[1] Handa, A. and Andersson, K., 1981, “Application of finite element methods in the statistical analysis of structures,” in Proc. 3rd Int. Conf. Struc. Safety and Reliability, ICOSSAR’81, 409-420.

[2] Hisda, T. and Nakagiri, S., 1981, “Stochastic finite element method developed for structural safety and reliability,” in Proc. 3rd Int. Conf. Struc. Safety and Reliability, ICOSSAR’81, 395-408.

[3] Hisda, T. and Nakagiri, S., 1985, “Role of stochastic finite element method in structural safety and reliability,” in Proc. 4th Int. Conf. Struc. Safety and Reliability, ICOSSAR’85, 385-395.

[4] Baecher, G. B. and Ingra, T. S., 1981, “Stochastic finite element method in settlement predictions,” J. Geotech. Eng. Div., ASCE, 107, 4, 449-463.

[5] Phoon, K., Quek, S., Chow, Y., and Lee, S., 1990, “Reliability analysis of pile settlements,” J. Geotech., Eng., ADCE, 116, 11, 1707-1735.

[6] Ghanem, R. G., and Spanos, P. D., 1991, “Stochastic finite elements – a spectral approach” , Dover Publication, Inc.

[7] Ghanem, R. G. and Kruger, R., 1996, “Numerical solution of spectral stochastic finite element systems,” Comp. Meth. Appl. Mech. Eng., 129, 3, 289-303.

[8] Ghanem, R. G. and Spanos, P. D., 1990, “Polynomial chaos in stochastic finite elements,” J. App. Mech. ASME, 197-202.

[9] Ghanem, R. G. and Spanos, P. D., 1991, “Spectral stochastic finite element formulation for reliability analysis,” J. Eng. Mech. 117, 10, 2351-2372.

[10] Cornell, C. A., 1969, “A probability-based structural code,” Journal of the American Concrete Institute, 66, 12, 974-985.

[11] Hasofer, A. M. and Lind, N. C., 1974, “Exact and invariant second moment code format,” Journal of the Engineering Mechanics Division, ASCE, 100(EM1), 111-121.

[12] Rackwitz, R., and Fiessler, B., 1978, “Structural reliability under combined random load sequences,” Computers and Structures, 9, 5, 484-494.

[13] Chen, X., and Lind, N. C., 1983, “Fast probability integration by three-parameter normal tail approximation,” Structural Safety, 1, 269-276.

[14] Der Kiureghian, A., Liu, P. L., 1986, “Structural reliability under incomplete probability information,” J. Eng. Mech., ASCE, 112, 1, 85-104.

[15] Liu, P. L., and Der Kiureghian, A., 1986, “Multivariate distribution models with prescribed marginals and covariances,” Prob. Eng. Mech., 1, 2, 105-112

[16] Ditlevsen, O. and Madsen, H., 1996, Structural reliability methods, J. Wiley and Sons, Chichester.

[17] Sudret, B. and Der Kiureghian A., 2000, “ Stochastic finite element methods and reliability a state-of-the-art report,” Report No. UCB/SEMM-2000/08.

[18] Breitung, K., 1984, “Asymptotic approximation for multinormal integrals,” J. Eng. Mech., ASCE, 110, 3, 357-366

[19] Der Kiureghian, A., and Liu, P. L., 1987, “Second order reliability approximations,” J. Eng. Mech., ASCE, 113, 8, 1208-1225.

[20] Der Kiureghian, and de Stefano, M., 1991, “Efficient algorithms for second algorithms for second order reliability analysis,” J. Eng. Mech., ASCE, 117, 12, 2906-2923.

[21] Grandhi, R. V. and Wang, L., 1999, “Higher-order failure probability calculation using non linear approximations,” Comp. Meth. Appl. Mech. Eng., 168, 185-206.

[22] Gill, P. E. Murray, W., and Wright, M. H., Practical Optimization, Academic Press, San Diego, California, Chapter 2, pp 11-12.

[23] Liu, P. L., and Der Kiureghian, A., 1989, “Finite element reliability methods for geometrically non linear stochastic structures,” Tech. Rep. No. UCB/SEMM/89-05, University of California, Berkeley.

[24] Zhang, Y. and Der Kiureghian, A., 1993, “Dynamic response sensitivity of inelastic structures,” Comp. Meth. Appl. Mech. Eng., 108, 23-26.

[25] Zhang, Y. and Der Kiureghian, A., 1997, “Finite element reliability methods for inelastic structures,” Tech. Rep. UCB/SEMM-91/05, University of California, Berkeley Dpt of Civil Engineering

[26] Barthelemy, B., Haftka, R. T., 1988, “Accuracy of the semi-analytical method for shape sensitivity calculations,” Proc. AIAA/ASMA/ASCE/ASC 29th Structures Structural Dynamics and Materials Conf. Part 1, 562-581.

[27] Olhoff, N., Rasmussen, J., 1991, “Study of inaccuracy in semi-analytical sensitivity analysis-a model problem.” Structural Optimization, 3, 203-213.

[28] Cheng, G., Gu, Y., Wang, X., 1990, “Improvement of semi-analytic sensitivity analysis and MCADS,” Proc. Int. Conf. Eng. Optim. in Design Processes, Berlin, Heidelberg, New York: Springer.

[29] Cheng, G., Olhoff, N., 1991, “New method of error analysis and detection in semi-analytical sensitivity analysis Optimization of large structural systems,” Proc. NATO/DFDASI, Berchtesgaden, 361-383.

[30] Mlejned, H. P., 1992, “Accuracy of semi-analytical sensitivities and its improvement by the natural method,” Structural Optimization, 4, 128-131.

[31] Oral, S., 1996, “An improved semianalytical method for sensitivity analysis,” Structural Optimization, 11, 67-69.

[32] E. Parente Jr., and Vaz, L. E., 2001, “Improvement of semi-analytical design sensitivities of non-linear structures using equilibrium relations,” International Journal for Numerical Methods., 50, 2127-2142.

[33] http://www.efunda.com/formulae/solid_mechanics/plates/calculators/SSSS_PUniform.cfm

[34] Lyness, J. N., and Moler, C. B., 1967, “Numerical differentiation of analytic functions,” SIAM Journal of Numerical Analysis, 4, 2 (June), 202-210.

[35] Lyness, J. N., 1967, “Numerical algorithms based on the theory of complex variables,” Proc. ACM 22nd National Conference, Thomas Book Co., Washington, D. C., 124-134.

[36] Squire, W. and Trapp, G., 1998, “Using complex variables to estimate derivatives of real functions,” SIAM review, 10, 1, 110-112.

[37] Martins, J. R .R. A., Sturdza P., and Alonso, J. J., 2003, “The complex-step derivative approximation,” ACM Transa. on Mathe. Software, 29, 3, 245-262.

[38] Martins, J. R. R. A., Kroo, I. M., and Alonso, J. J., 2000, “An automated method for sensitivity analysis using complex variables,” 38th Aerospace Science Meeting and Exhibit, AIAA paper, AIAA-2000-0689, 1-12.

[39] Anderson, W. K., Newman, J. C., Whitfield D. L., and Nielsen E. J., 1999, “Sensitivity analysis for the Navier-Stokes equations on unstructured meshes using complex variables,” AIAA paper, AIAA-99-3294, 381-389.

[40] Rodriguez, D. L., 2000, “A multidisciplinary optimization method for designing inlets using complex variables,” AIAA paper, AIAA-2000-4875, 1-10.

[41] Wang, B. P., and Apte, A. P., 2006, “Complex variable method for eigensolution sensitivity analysis,” AIAA Journal, 44, 12, 2958-2961.

[42] Nicolai, B. M. and De Baerdemaeker J., 1997, “Finite element perturbation analysis of non-linear heat conduction problems with random field parameters,” International Journal of Numerical Methods for Heat & Fluid Flow, 7, 5.

[43] Nicolai, B. M. and De Baerdemaeker J., 1993, “Compuation of heat conduction in materials with random variable thermophysical properties,” International Journal for Numerical Methods in Engineering, 36, 523-535.

[44] Nicolaï, B.M., 1994, "Modeling and uncertainty propagation analysis of thermal food processes", PhD thesis, K.U. Leuven, Leuven.

[45] Hien, T.D., Kleiber, M., 1997, “Stochastic finite element modeling in linear transient heat transfer,” Computer. Methods in Applied Mechanical and Engineering, 144, 111–124.

[46] Hien, T.D., Kleiber, M., 1998, “On solving nonlinear transient heat transfer problems with random parameters,” Computer. Methods in Applied Mechanical and Engineering, 151, 287–299.

[47] Xiu, Dongbin and Karniadakis, G. E., 2003, “A new stochastic approach to transient heat conduction modeling with uncertainty,” International Journal of Heat and Mass Transfer, 46, 4681-4693.

[48] Blackwell, B. F. and Dowding, K. J., 2002, “Sensitivity and uncertainty analysis for thermal problems,” 4th International Conference on Inverse Problems in Engineering, Brazil.

[49] Dems, K. and Rousselet, R., 1999, “Sensitivity analysis for transient heat conduction in a solid body,” Structural Optimization, 17, 36-45.

[50] Fadale, T. D. and Emery, A.F., “Transient effects of uncertainties on the sensitivities of temperatures and heat fluxs using stochastic finite elements,” Transactions of the ASME.

[51] Dowding, K. J. and Blackwell, B. F., 2001, “Sensitivity analysis for nonlinear heat conduction,” Journal of Heat Transfer, 123.

[52] Incropera, F. P. and DeWitt D. P., 2002, “Fundamentals of heat and mass transfer,” John Wiley & Sons, Inc.

[53] Ghosh, S., 2006, “Finite element analysis of moisture and thermal induced stress in flip chip packages,” Master of Science in Mechanical Engineering Thesis, University of Texas at Arlington.

[54] Yuan, T. D., Pan H. Y. and Li, Y., “Thermal Interface Material (TIM) design Guidance for flip chip BGA package thermal performance”, http://www.altera.com/literature/cp/cp-01020.pdf.

[55] Chang, K. C., Li, Y., Lin, C. Y., and Lii M. J., “Design guidance for the mechanical reliability of low-K flip chip BGA package”, http://www.altera.com/literature/cp/cp-01018.pdf.

[56] Eghan, A., Do, H., Zheng, L. L., Lan, H., and Pan, S., “Flip chip BGA bump & board level reliability: power & thermal cycling compared”, http://www.optimalcorp.com/support_downloads /TechPapers/FLIPCHIP_powercycle_paper.pdf

[57] Desmond, Y.R., Chong, R. K., and Sun A.Y.S., “Reliability assessment of a high performance flip-chip BGA package (organic substrate based) using finite element analysis”, http://ieeexplore.ieee.org/stamp/stamp.jsp?arnumber=01216278.

[58] Provan, W. J. 1987, “Probabilistic fracture mechanics and reliability,” Dordrecht, The Netherland: Martinus Nijhoff Publishers.

[59] Grigoriu, M., Saif, M.T.A, El-Borgi, S. and Ingraffea, A., 1990, “Mixed-mode fracture initiation and trajectory prediction under random stresses,” International Journal of Fracture, 45, 19-34.

[60] Chen, G. F., Rahman, S. and Park, Y. H., 2001, “Shape sensitivity and reliability analyses of linear-elastic cracked structures,” International Journal of Fracture, 112, 223-246.

[61] Rahman, S. and Chen, G. F., 2005, “Continuum shape sensitivity and reliability analyses of nonlinear cracked structures,” International Journal of Fracture, 131, 189-209.

[62] Rahman,S., 2001, “Probabilistic fracture mechanics: J-estimation and finite element methods,” Engineering Fracture Mechanics, 68, 107-125.

[63] Tarcoco, E., 2000, “Shape sensitivity analysis in linear elastic fracture mechanics,” Computational Methods in Applied Mechanical Engineering, 188, 697-712.

[64] Puatatsananon, W. and Saouma, V. E., 2006, “Reliability analysis in fracture mechanics using the first-order reliability and Monte Carlo simulation,” Fatigue and Fracture of Engineering materials and structures, 29, 959-975, 2006

[65] Besterfield, G. H., Lawrence, M. A., and Belytschko, T., 1990, “Brittle fracture reliability by probabilistic finite elements,” ASCE Journal of Engineering Mechanics, 116, 642-659.

[66] Besterfield, G. H., Liu, W. K., Lawrence, M. A. and Belytschko, T., 1991, “Fatigure crack growth reliability by probabilistic finite elements,” Computer Methods in Applied Mechanics and Engineering, 86, 297-230

[67] Feijoo, R.A., Padra, C., Saliba, R., Taroco, E., and Venere, M. J., 2000, “Shape sensitivities analysis for energy release rate evaluations and its application to the study of three dimensional

cracked bodies," Computational Methods in Applied Mechanics and Engineering, 188, 649-664.

[68] Barsoum, R. S., 1976, "On the use of isoparametric finite elements in linear fracture mechanics," International journal for numerical methods in engineering, 10, 25-37.

[69] Barsoum, R. S., 1977, "Triangular quarter-point elements as elastic and perfectly-plastic crack tip elements," International journal for numerical methods in engineering, 11, 85-98.

[70] Henshell, R. D., AND Shaw, K. G., 1975, "Crack tip finite elements are unnecessary," International Journal for Numerical Methods in Engineering, 9, 495-507.

[71] Bloom, J. M., 1975, "An evaluation of a new crack tip element-- the distorted 8-node isoparametric element," International Journal of Fracture, 11, 705-707.

[72] Freese, C. E. and Tracey, D. M., 1976, "The natural isoparametric triangle versus collapsed quadrilateral for elastic crack analysis," International Journal of fracture, 12, 767-770.

[73] Shih, C. F., deLorenzi, H. G. and German, M. D., 1976, "Crack extension modeling with singular quadratic isoparametric elements," International Journal of fracture, 12, 647-651.

[74] Lim, I. L., Johnson, I. W. and Choi, S. K., 1992, "Comparison between various displacement-based stress intensity factor computation techniques," International Journal of Fracture, 58, 193-210.

[75] Banks-sills, L. and Sherman, D., 1986, "Comparison of methods for calculating stress intensity factors with quarter-point elements," International Journal of Fracture, 32, 127-140.

[76] Release 11.0, documentation for ANSYS.

[77] Paris, P. C. and Sih, G. C., 1965, "Stress analysis of cracks, Fracture toughness and testing and its applications," American Society for Testing and Materials, Philadelphia, STP 381, 30-83.

[78] Tada, H., Paris, P. C. and Irwin, G. R., 1973, "The stress analysis of cracks handbook," Dei Research Corporation, Hellertown, Pennsylvania.

[79] Anderson, T. L., 1995, "Fracture mechanics fundamentals and applications," CRC Press.

[80] Engeln- Mullges, G., Uhlig, F., 1996, "Numerical Algorithms with C," Springer.

[81] Emery, A. FL., and Fadale, T. D., 1997, “Handling temperature dependent properties and boundary conditions in stochastic finite element analysis,” Numerical Heat transfer, Part A, 31, 37-51.

[82] Reddy, J. N., 2004, “An introduction to nonlinear finite element analysis,” Oxford University Press: Oxford, U.K.

BIOGRAPHICAL INFORMATION

Weiya Jin is a Ph. D candidate of the University of Texas at Arlington. She completed a Bachelor of Science degree in mechanical engineering at the Zhejiang University of Technology in China in 1995. In 1998, she received a master degree of mechanical engineering in the same university. From 1998 to 2005, she was an assistant professor and lecturer in the Zhejiang University of Technology. She had teaching experiences and research experiences in structural analysis and assessment about pressure vessels, heat exchangers and so on. She has published one book, Reliability Engineering (in Chinese), and over 10 papers. Her current research interests are focused on applying finite element methods to fluid & solid mechanics, heat transfer, combining reliability analysis and optimization methods with finite element method to solve realistic engineering problems with uncertainties.